AWARD NUMBER: W81XWH-15-1-0529

TITLE: A Model for Understanding the Genetic Basis for Disparity in Prostate Cancer Risk

PRINCIPAL INVESTIGATOR: Dr. Vijayasaradhi Setalyr

CONTRACTING ORGANIZATION: The Board of Regents of the University of Wisconsin System (UW-Madison)
MADISON, WI 53715

REPORT DATE: DECEMBER 2019

TYPE OF REPORT: FINAL

PREPARED FOR: U.S. Army Medical Research and Development Command
Fort Detrick, Maryland 21702-5012

REPORT DOCUMENTATION PAGE

Form Approved
OMB No. 0704-0188

1. REPORT DATE	2. REPORT TYPE	3. DATES COVERED
DECEMBER 2019	FINAL	21SEP2015 - 20SEP2019

4. TITLE AND SUBTITLE

A Model for Understanding the Genetic Basis for Disparity in Prostate Cancer Risk

5a. CONTRACT NUMBER

5b. GRANT NUMBER
W81XWH-15-1-0529

5c. PROGRAM ELEMENT NUMBER

6. AUTHOR(S)

Dr. Vijayasaradhi Setalyr

E-Mail: vsetaluri@dermatology.wisc.edu

5d. PROJECT NUMBER

5e. TASK NUMBER

5f. WORK UNIT NUMBER

7. PERFORMING ORGANIZATION NAME(S) AND ADDRESS(ES)

The Board of Regents of the University
21 N. Park Street, Suite 6401
of Wisconsin System Madison, WI
537151218

8. PERFORMING ORGANIZATION REPORT NUMBER

9. SPONSORING / MONITORING AGENCY NAME(S) AND ADDRESS(ES)

U.S. Army Medical Research and Development Command
Fort Detrick, Maryland 21702-5012

10. SPONSOR/MONITOR'S ACRONYM(S)

11. SPONSOR/MONITOR'S REPORT NUMBER(S)

12. DISTRIBUTION / AVAILABILITY STATEMENT

Approved for Public Release; Distribution Unlimited

13. SUPPLEMENTARY NOTES

14. ABSTRACT

Prostate cancer is the most commonly diagnosed cancer in men. Among African American men, the incidence of prostate cancer is approximately 60% higher and the mortality rate in this population is 2 to 3 times greater compared with European American men. The reasons for this disparity are not completely understood. Current tools in hand to study these differences, such as genetically altered mouse models, are useful for dissecting roles of specific genes and signaling pathways in intact animal, but have limited utility for understanding differences in disease susceptibility in humans.

The overall objective of this application is to model prostate epithelial cells to understand the molecular basis for the disparities in prostate cancer risk between white Caucasian and black African-American men. The specific aims are: 1) to establish conditions that promote differentiation of human neonatal foreskin skin fibroblast-derived iPSC into cells with characteristics of prostate epithelium, 2) identify differences in gene expression and epigenetic signatures between prostate epithelial cells derived from iPSC of Caucasian and African-American foreskin fibroblasts and 3) compare and establish methods to transform differentiated prostate epithelial cells to identify differences in susceptibility to transformation.

15. SUBJECT TERMS: NONE LISTED

16. SECURITY CLASSIFICATION OF:			17. LIMITATION OF ABSTRACT	18. NUMBER OF PAGES	19a. NAME OF RESPONSIBLE PERSON
a. REPORT	b. ABSTRACT	c. THIS PAGE			USAMRMC
Unclassified	Unclassified	Unclassified	Unclassified	77	19b. TELEPHONE NUMBER *(include area code)*

Standard Form 298 (Rev. 8-98)
Prescribed by ANSI Std. Z39.18

TABLE OF CONTENTS

1. INTRODUCTION

Prostate cancer is the most commonly diagnosed cancer in men in Europe and the United States. Numerous studies have indicated genetics to have a major role in the etiology of this disease; as much as 42% of the risk may be explained by heritable factors. Moreover, among African American men, the incidence of prostate cancer is approximately 60% higher and the mortality rate in this population is 2 to 3 times greater compared with European American men The reasons for this disparity are not completely understood. Since no clear patterns were observed for association with dietary factors or life style factors such as physical activity, occupational history, sexual behavior and other health conditions), it is likely that inherent genetic and epigenetic differences, presumably both germ-line and prostate-cell specific, contribute to this disparity in prostate cancer risk. Efforts are ongoing to identify molecular mechanism and common risk alleles for prostate cancer risk using genome-wide association studies. While identification of individuals/population at risk is important, additional in-depth studies are needed to understand the genetic and molecular mechanisms responsible for the differences in susceptibility of prostate epithelial cells to malignant transformation. However, limited access to human prostate tissue prior to onset of age-related or malignant changes has hampered analyses of genetic and epigenetic mechanisms intrinsic to prostate epithelial cells. More recent strategies to study prostate development, maturation and carcinogenesis included differentiation of human embryonic stem cells (hESC) using rodent mesenchyme. Studies using hESC also have many limitations including ongoing ethical debate and the number of available cell lines, especially that represent different genetic ancestry. Induced pluripotent stem cells (iPSC) offer a useful alternative to hESC. For example, recently, in vivo regeneration potential of human iPSC has been documented. The proposed project is aimed to test the hypothesis that differentiation of neonatal foreskin fibroblasts-derived iPSC to prostate epithelial cells is a unique and powerful strategy to investigate the genetic and molecular basis for the disparities in prostate cancer risk among men of different genetic ancestry.

2. KEYWORDS:

Induced Pluripotent cells, Directed differentiation, Prostate Cancer, Disparity in Cancer Risk, African-American

3. ACCOMPLISHMENTS:

- **What were the major goals of the project?**
    - To establish culture conditions that promote differentiation of human neonatal foreskin skin fibroblast-derived iPSC into cells with characteristics of prostate epithelium.
    - Identify differences in gene expression and epigenetic signatures between prostate epithelial cells derived from iPSC of Caucasian and African-American foreskin fibroblasts.
    - Compare and establish methods to transform differentiated prostate epithelial cells to identify differences in susceptibility to transformation
- **What was accomplished under these goals?**

    See below

Optimization of reprogramming neonatal human skin fibroblasts

We reprogrammed neonatal human primary fibroblasts to induced pluripotent stem cells (**Figure 1A**). Fibroblasts were transduced with three lentiviruses containing OCT4-SOX2, KLF4-cMYC and NANOG-LIN28 reprogramming factors. Five days after transduction, cells were plated on MEF feeders with reprogramming stem cell medium. The medium was supplemented with a chemical cocktail previously shown to enhance iPSC reprogramming (Hou et al., 2013) (SEE APPENDIX FOR REFERENCES CITED). This cocktail consists valproic acid (VPA, a HDAC inhibitor) CHIR-99021 (a GSK-3α/β inhibitor), forskolin (FSK, an activator of adenylyl cyclase/cAMP pathway), tranylcypromine (TCP, a histone lysine specific demethylase 1 inhibitor) and RepSox (an inhibitor of the TGFβR-1/ALK5 pathway). One week after iPSC induction, granular colonies were visible indicative of early reprograming. Three weeks after induction, colonies with iPSC morphology appeared and expressed the stem cell marker alkaline phosphatase (AP). Total number and AP-positive colonies were quantitated (**Figure 2A-B**). AP-Positive colonies were selected for expansion with stem cell maintenance medium. Expression of reprogramming factors was verified by Western blot (WB) (**Figure 2C**).

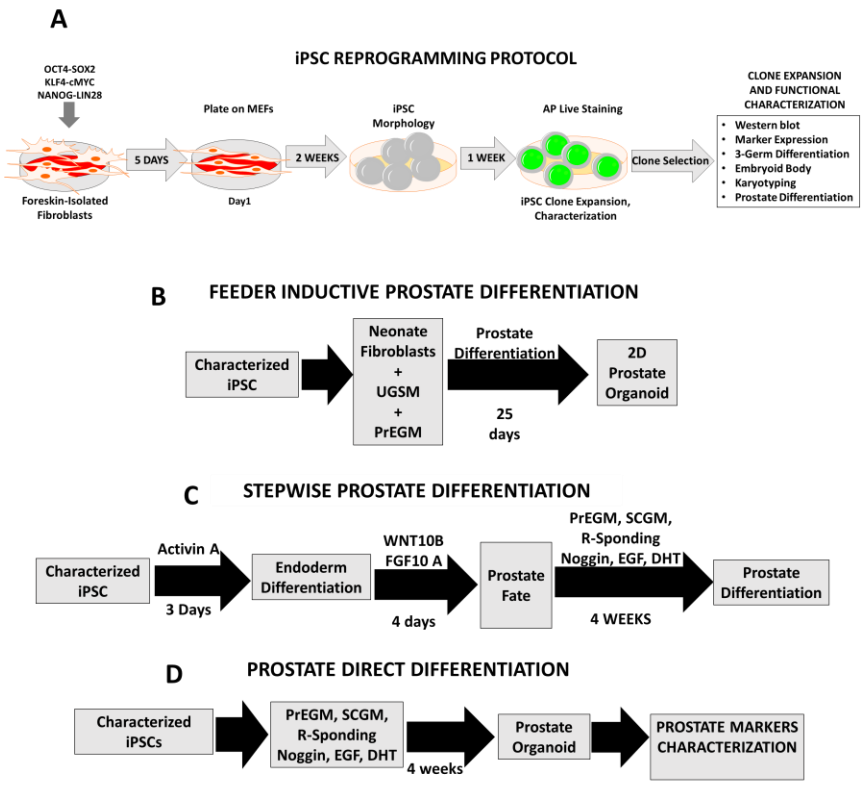

FIGURE 1

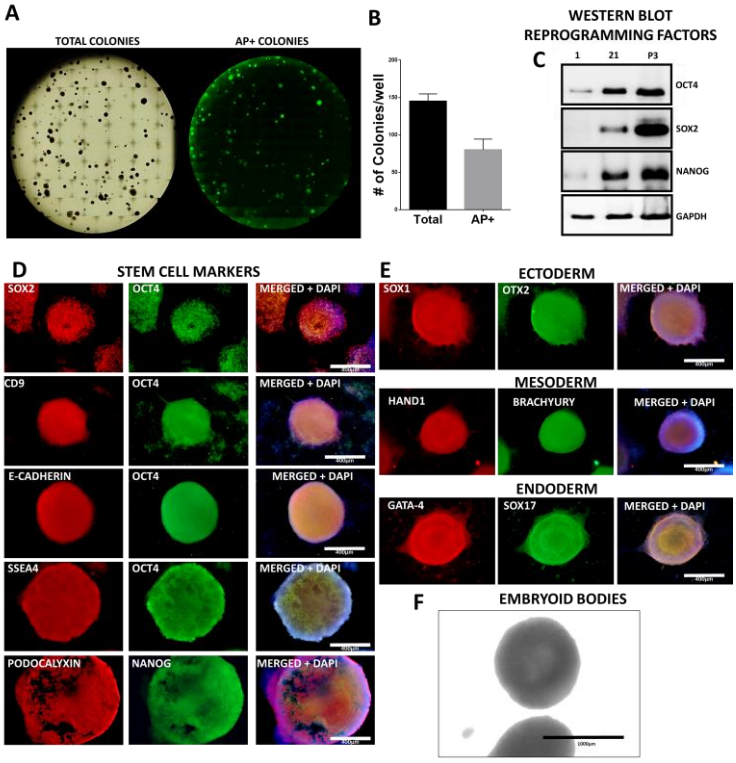

FIGURE 2

Characterization of iPS cells

We determined the expression of reprogramming factors at day 1 (Day 5 post-transduction), and day 21 of iPSC induction and at passage 3 (P3) by WB (**Figure 2C**) and noted progressively increasing expression of the reprogramming factors OCT4, SOX2 and NANOG through day 21 and P3. Immunofluorescence analysis (**Figure 2D**) showed co-expression of reprogramming factors OCT4 or NANOG and stem cell surface markers CD9, E-cadherin, SSEA4 and podoclyxin.

Pluripotency of iPSC clones was determined using *in vitro* differentiation assays and immuno-fluorescence staining for early markers specific for the three germ layers (Deshpande et al., 2017;

Shinozawa et al., 2017). Differentiation of iPSC to ectoderm, mesoderm and endoderm was verified by expression, respectively of SOX1 and OTX2, and HAND1 and Brachyury, and GATA4 and SOX17 (**Figure 2E)**. Furthermore, in embryoid body (EB) formation assay by the hanging drop method (**Figure 2F**), iPSC clones exhibited the ability to form EBs.

Optimization for *in vitro* differentiation of prostate organoids

We employed three different protocols for differentiation of iPSC to prostate organoids. The first method (**Figure 1B**) was based on inductive differentiation by co-culture of iPSC with neonatal mouse urogenital sinus mesenchymal (UGSM) cells and neonatal human dermal fibroblasts. The second method (**Figure 1C**) involved stepwise differentiation with growth factors and differentiation factors first to endoderm followed by commitment to prostate lineage and finally to prostate differentiation (Calderon-Gierszal and Prins, 2015). The third protocol (**Figure 1D**) involved direct differentiation with growth and differentiation factors.

Co-culture with UGSM feeder cells

Previous reports have shown that mouse UGSM, stromal cells (human fibroblasts) and extracellular matrix (ECM) have an inductive effect for prostate differentiation of hESC *in vivo* using xenografts models (Taylor et al., 2006). Fibroblasts secrete components of the ECM and basement membrane that have inductive roles for prostate growth, development and differentiation (Olumi et al., 1999). Additionally, it is well known that the prostate development and differentiation rises from the embryonic UGSM bud (Taylor et al., 2006). Induced pluripotent cells were co-cultured with human dermal fibroblasts and UGSM cells in prostate epithelial growth media (PrEGM™ BulletKit™, LONZA) (**Figure 3A-D**). This resulted in organization of cells to structures with prostate-like features including acinar-like morphology (**Figure 3B**) and expression of prostate specific antigen (PSA), p63 and androgen receptor (AR), markers associated to prostate cells (**Figure 3C-D**). The protocol is somewhat time consuming with variable efficiency of differentiation that is affected by several factors such as quality and passage of the UGSM and fibroblasts.

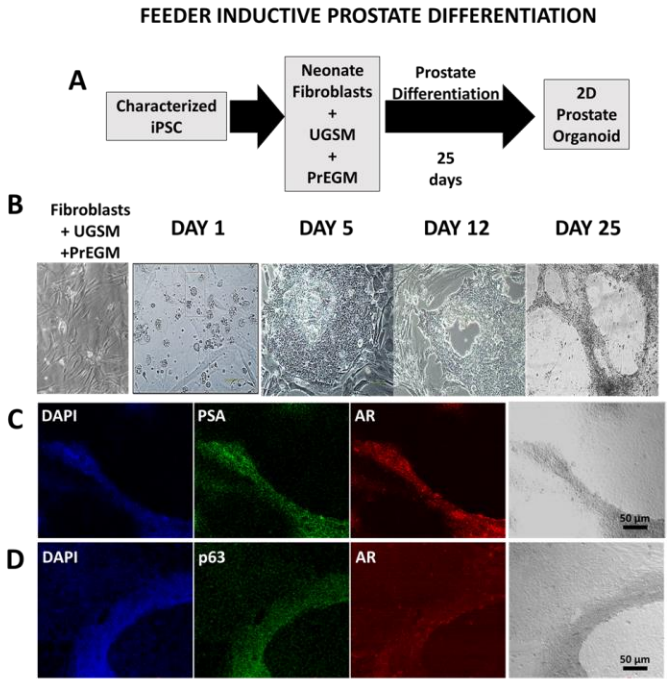

FIGURE 3

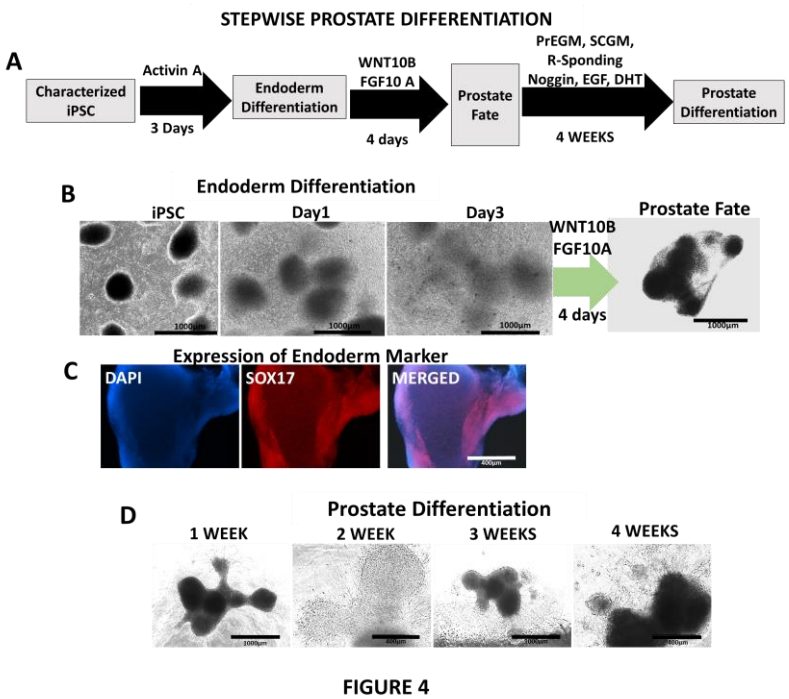

FIGURE 4

Stepwise Differentiation

For stepwise directed differentiation, we employed a modified method (Calderon-Gierszal and Prins, 2015) (**Figure 4A-D**). First, iPS cells were differentiated into definitive endoderm with Activin A and endoderm differentiation was verified by expression of SOX17, as determined by immunofluorescence (**Figure 4B-C**). Endoderm-differentiated cells were treated with WNT10B and FGF10A for 4 days to promote prostate fate (**Figure 4B**) and finally cultured in prostate differentiation

medium (**Figure 4D**) (1:1 PrEGM-Bullet kit:SCGM Stromal Cell Bullet Kit) supplemented with 15 mM HEPES, 1x B27, Noggin, EGF, R-Spondin1, dihydrotestosterone (DHT) and 2 mM Glutamax. After four weeks, morphological changes such as formation of outgrowth and buds. However, these organoids did not exhibit internal duct formation.

Direct Differentiation

The third approach involved the direct differentiation of iPS cells in prostate differentiation medium PrEGM:SCGM and growth/differentiation factors, as described above, but without endoderm and prostate fate differentiation steps (**Figure 5A**). This protocol was performed in 2D and 3D. For 2D organoids, iPS cells were suspended as single cells and plated in Matrigel-coated wells. For 3D organoids, 5-8 iPS cell colonies were isolated and manually plated in Matrigel-coated wells. After one week, cells started to differentiate and organize into multiple acinar-like shaped structures in 2D, while 3D organoids formed small outgrowths. By second and third week, acinar-like structures and internal ducts were prominent in both 2D cultures and 3D organoids (**Figure 5B**). After 4 weeks in culture, in addition to acinar-like structures exhibiting branching internal ducts, presence of spheroid-like structures inside the lumen (**Figure 5C**). These spheroids produced by 2D and 3D organoids are similar to prostaspheres reported in prostate organoid models from healthy and prostate cancer adult tissues samples from human and rodents (Chua et al., 2014; Huang et al., 2015). Time-lapse microscopy of 2D organoids confirmed that prostate organoids were generation and release of prostasphere in the lumen (**Figure 5D**).

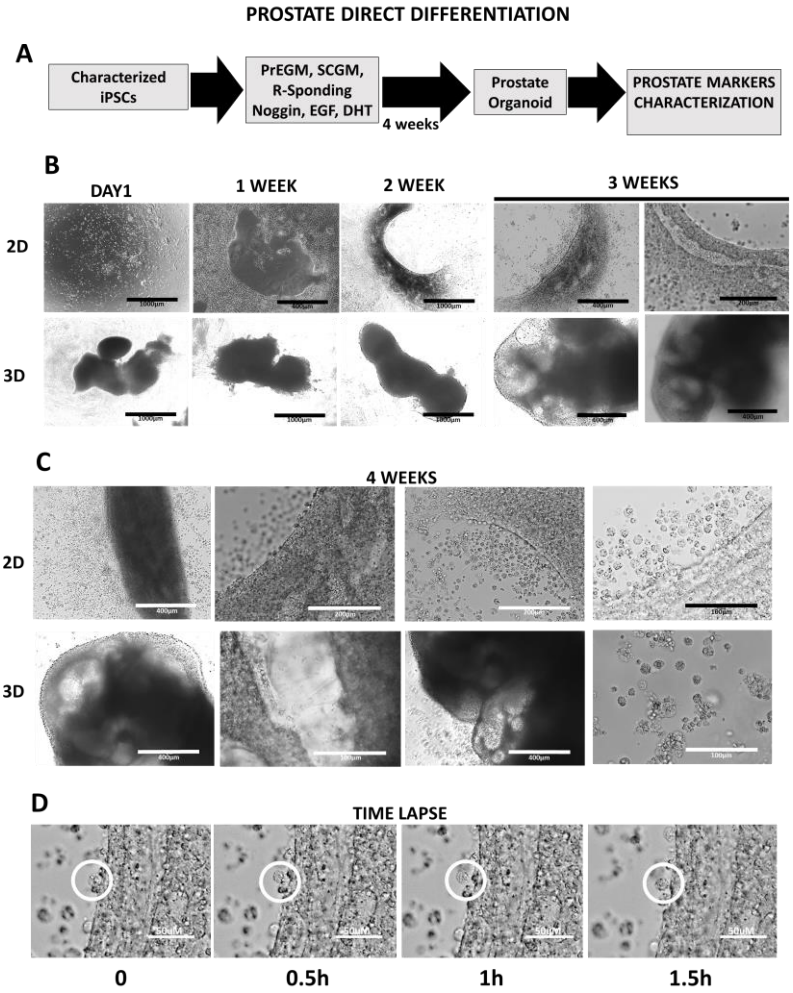

FIGURE 5

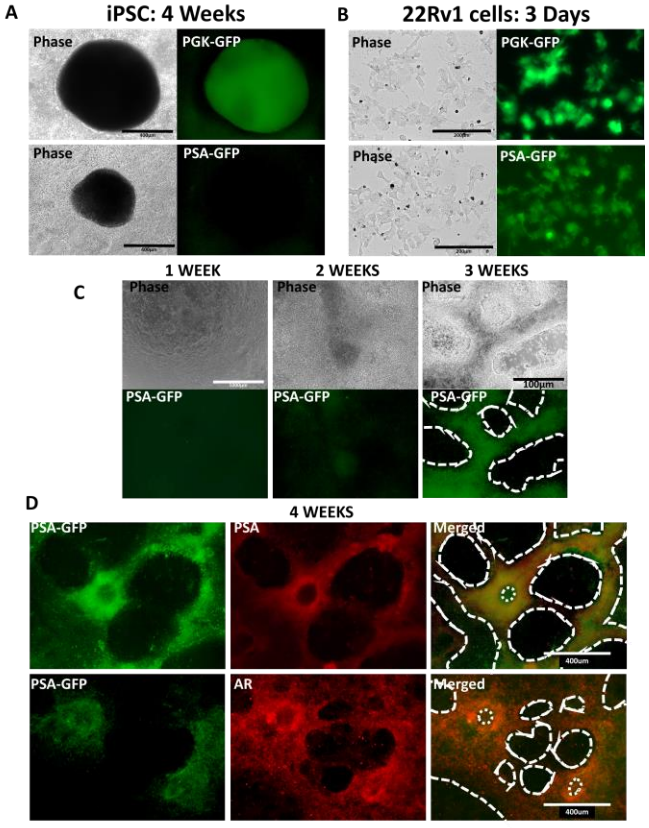

FIGURE 6

Organoids express prostate differentiation

To monitor the progress of prostate-like differentiation, we generated a lentivirus for human PSA-promoter GFP-reporter plasmid. To verify the specificity of the PSA-GFP reporter, we transduced iPS cells and 22Rv1 human prostate cancer cells with lentivirus for either ubiquitous phosphoglycerate kinase-promoter GFP-reporter (PGK-GFP) or with PSA-GFP reporter. Four weeks of transduction, PGK-GFP reporter transduced iPS cells, but not the PSA-GFP lentivirus transduced cells, expressed the GFP reporter (**Figure 6A**). In contrast, 22Rv1 prostate

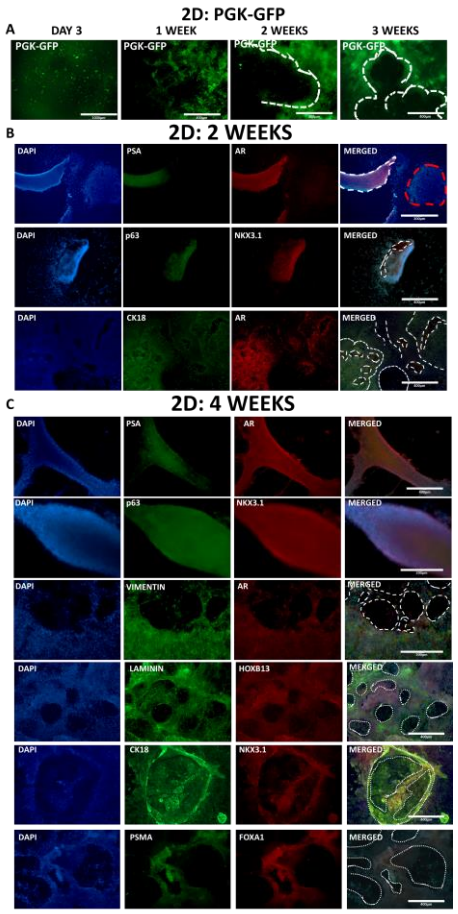

FIGURE 7

cancer cells expressed both, PGK-GFP and PSA-GFP reporters just three days after transduction (**Figure 6B**). For evaluation of prostate lineage specificity during prostate differentiation, iPS cells were transduced with either PSA-GFP or with PGK-GFP reporter lentiviruses at day 1 in prostate differentiation medium. Medium was replaced with fresh prostate differentiation medium 24 h after transduction and GFP expression was monitored for 4 weeks. In PGK-GFP-reporter lentivirus transduced iPSC, GFP expression was detectable as early as three days post-transduction in all areas of the organoids including areas with low prostate-like morphology (**Figure 7A**). In contrast, PSA-GFP reporter transduced iPSC, GFP expression was detectable only two weeks after prostate differentiation prominently in areas of the organoids with acinar-like morphology (**Figures 6C-D**). We asked if expression of the PSA-GFP reporter was consistent with expression of endogenous prostate markers PSA and AR. As shown in **Figure 6D (top panels**), GFP reporter expression was co-localized with expression of endogenous PSA and enriched in acinar-like structures. In contrast, while AR expression was detectable throughout the organoid, there was limited co-localization with PSA-promoter driven GFP expression (**Figure 6D, bottom panels**). In addition to PSA and AR, two weeks after induction of prostate differentiation, the organoids also exhibited expression of p63, NKX3.1 and cytokeratin 18 (**Figure 7B**). Importantly, expression of prostate markers is localized to areas with enriched prostate-like differentiation, such as acinar-like structures. For instance, not all cells with nuclear staining (DAPI) show staining for PSA or AR (**Figure 7B, top panels, red dashed circle**) indicating specificity of expression of prostate markers. By 4 weeks, expression of other prostate-related markers, including vimentin, cytokeratin 5 (CK5), laminin, HOXB13, PSMA and FoxA1, was also prominent in morphologically distinctive areas of the organoids.

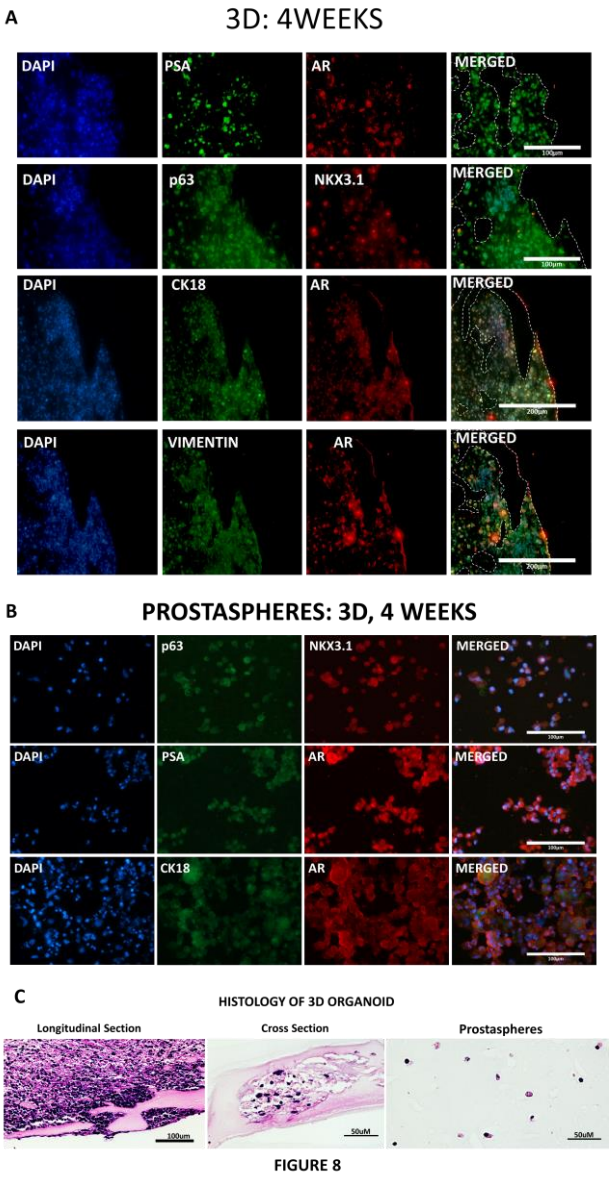

FIGURE 8

Prostate organoids exhibit stromal cell features and prostate-like function

After 4 weeks of prostate differentiation, 3D organoids were fixed, sectioned and analyzed by immunofluorescence staining for expression of prostate markers PSA, AR, p63, NKX3.1, CK18 and vimentin (**Figure 8A**). Furthermore, we collected supernatant from 3D organoid cultures and pelleted to harvest prostatspheres and prepared them for staining of prostate markers (Chua et al., 2014; Huang et al., 2015). These structures also showed expression of prostate markers PSA, AR, p63, NKX3.1 and CK18 (**Figure 8B**). These data show that iPSC-derived organoids exhibit some features

similar to prostate organoids derived from adult prostate tissues (Drost et al., 2016; Huang et al., 2015). Moreover, 3D organoids exhibited histological features of stromal-like with internal branched ducts (**Figure 8C, left panel**). Cross sections also indicate that the organoids may form internal zones with a primitive lumen-like morphology surrounded by stromal basal structure (**Figure 8C, middle panel**). Additionally, hematoxylin-eosin staining of prostaspheres collected from 3D organoids showed a cellular architecture in these structure (**Figure 8C, right panel**) (Chua et al., 2014).

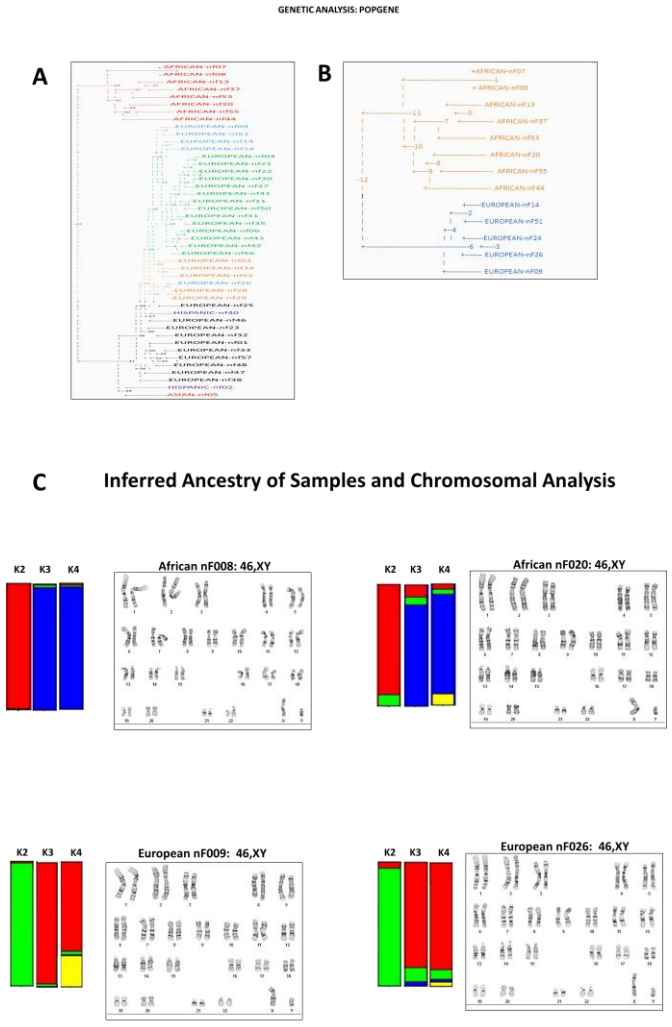

FIGURE 9

Selection of African- and European fibroblasts for iPSC reprogramming

Having established the conditions for iPSC reprogramming and prostate differentiation, we set out to select and reprogram skin fibroblasts derived from African- and European-American individuals from a collection of fibroblasts (UW Skin Disease Research Center, Cell Culture Core). Among 45 selected with self-identified (by the parent of the newborn) race- 34 white Caucasian, 8 African-American, 2 Hispanic-American and 1 Asian-American. At passage 3, we isolated total DNA from these fibroblasts and analyzed for 39 SNPs ancestral informative markers (AIM). AIM SNP data was analyzed using POPGENE to determine the genetic diversity of the samples and STRUCTURE to determine the genetic ancestry or admixture for each individual. Selection of samples was based on two criteria: self-identification of samples by race at the moment of skin collection (African-American and European-American) and ancestry confirmation by 39 SNP-AIMs genetic analysis to determine individual gene admixture. POPGENE analysis showed that samples collected are admixed and highly polymorphic (**Figure 9A**) as observed by the multiple clusters by the genetic distance-based UPGMA dendrogram (Nei's, 1972, modified from NEIGHBOR procedure of PHYLIP Version 3,5). However, all self-identified African-American samples clustered together and separated from other samples. Pooled gene admixture estimates determined by STRUCTURE based on K=2, K=3 and K=4 analyses, confirmed that fibroblast DNA from self-identified African-American exhibited high genetic homology (averaging 90% - 93% shown in red for K=2 and blue for K=3 and K=4) with low admixture levels (averaging 7% - 10% for all Ks analyzed) shown mostly in red, green and

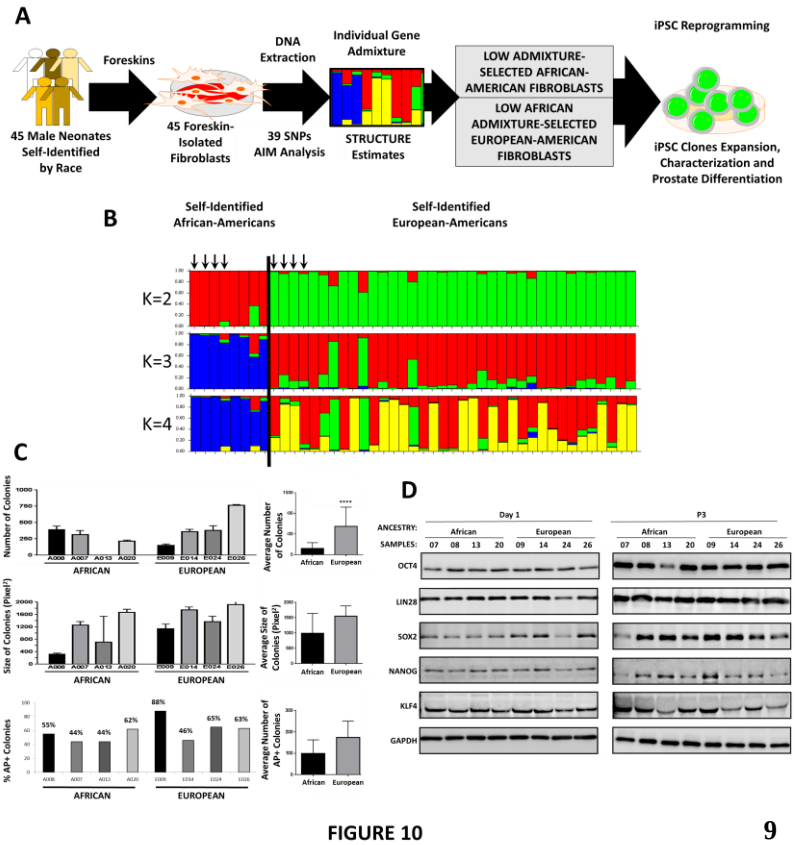

FIGURE 10

yellow. Thus, self-identified African-American samples appear to be genetically different from other self-identified races/populations (**Figure 10B**). Based on these data, we selected four African-American fibroblasts (nF007, nF008, nF013 and nF020, **Figure 10B, arrows**) with high percentage of African ancestry markers [averaging 93.1% (red) for K=2; 89.9% (blue) for K=3; and 89.8% (blue) for K=4] and low percentage of markers of other races/populations. Additionally, we selected four European-American fibroblasts (nF009, nF014, nF024 and nF026, **Figure 10B, arrows**) with very low percentage of African genes [averaging 4.3% (red) for K=2; 1.8% (blue) for K=3; and 1.1% (blue) for K=4) and high percentage of genes from European populations. Further analysis by POPGENE of the 8 selected samples demonstrated both groups clustered separated from each other (**Figure 9B**).

Comparison of efficiency of reprogramming of fibroblasts from European and African ancestry

Under identical conditions of reprogramming, European ancestry fibroblasts showed higher efficiency than African ancestry fibroblasts as determined by the number of colonies (**Figure 10C, top panels**). However, the colony size (**Figure 10C, middle panels**) and the percentage of alkaline-positive colonies (**Figure 10C, bottom panels**) were similar for both groups. Expression of reprogramming factors, determined by Western blot analysis, showed that all samples similarly express the reprogramming factors determined at day 1 of reprogramming (5 days after transduction) and iPSC clones at passage 3 (**Figure 10D**). These data suggest that the difference in the efficiency in reprogramming is not due differences in transduction or expression of reprogramming factors.

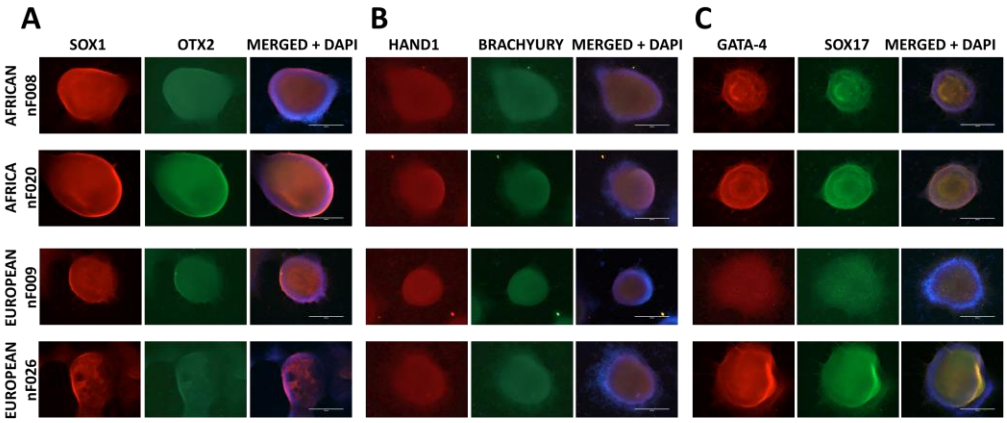

FIGURE 11

European and African ancestry iPSC show pluripotency

Pluripotency of iPSC clones from African- and European-American iPSC were determined using germ layer *in vitro* differentiation assays and staining for early markers (Deshpande et al., 2017; Shinozawa et al., 2017). Ectoderm differentiation was verified by SOX1 and OTX2 expression (**Figure 11A**), mesoderm by the expression of HAND1 and Brachyury (**Figure 11B**) and endoderm by the expression of GATA4 and

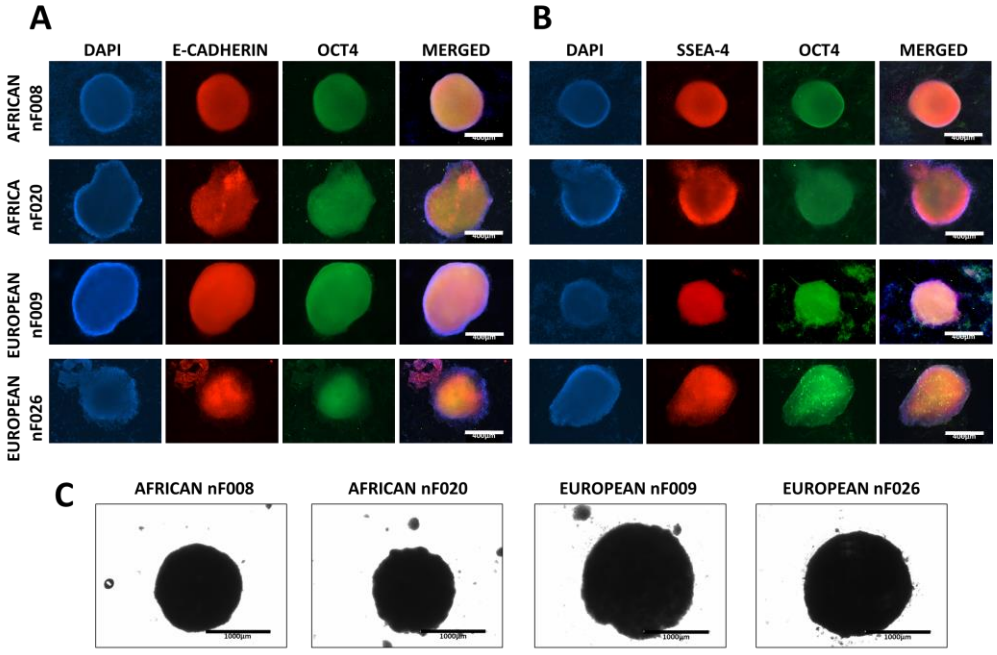

FIGURE 12

SOX17 (**Figure 11C**). Data in **Figure 11A-C** show that all iPSC clones similarly differentiate into precursors of the three embryonic layers.

European- and African- ancestry iPSC express stem cell markers and form EB

Immunofluorescence co-staining of reprogramming factor OCT4 with surface markers demonstrated that all clones similarly co-express stem cell surface markers E-cadherin and SSEA4 (**Figure 12A-B**). Embryoid body (EB) formation assays by the hanging drop method showed that all iPSC clones exhibit the ability to form EBs (**Figure 12C**). Chromosomal analysis (**Figure 9C**) demonstrated that the selected iPSC clones have a normal human male karyotype 46, XY (WiCell, Madison, WI).

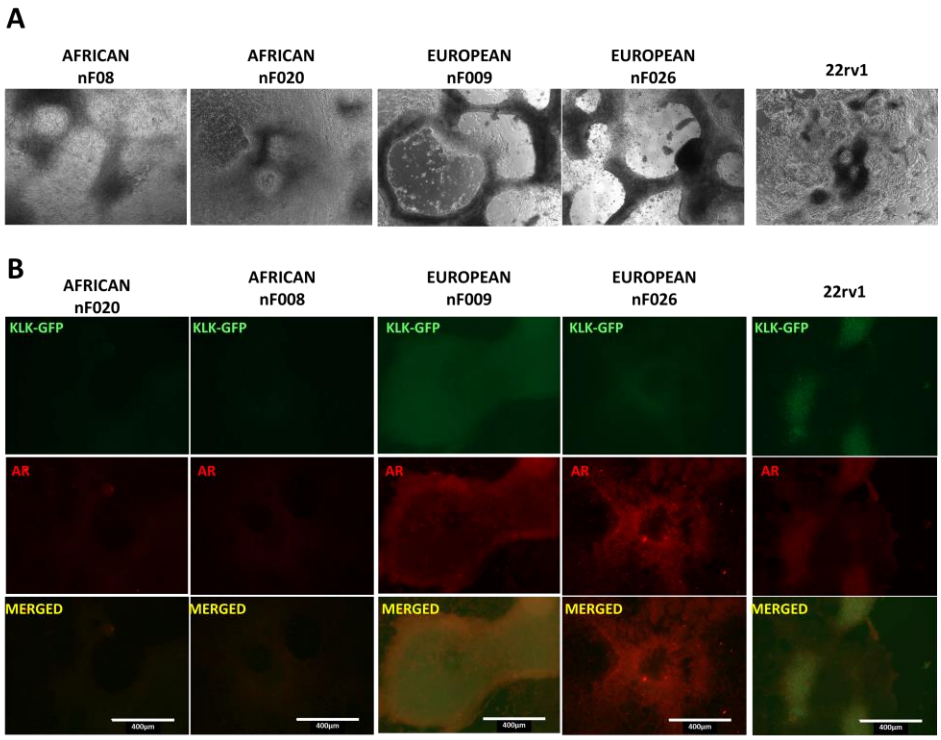

FIGURE 13

Differentiation of European and African ancestry iPSC

We selected 2 African-American (nF008 and nF020) and 2 European-American (nF009 and nF026) iPSC for prostate differentiation (**Figure 9C**) using the prostate direct differentiation protocol (**Figure 1D**). Interestingly, African ancestry iPSC (nF008 and nF020) did not form organoids with acinar-like structures or internal ducts and branching (**Figure 7A**). In contrast, iPSC from European ancestry (nF009 and nF026) efficiently formed organoids with acinar-like structures, internal ducts and branching (**Figure 13A**). We also evaluated PSA-GFP reporter expression. We transduced iPS cells with PSA-GFP reporter lentiviruses on day 1 in prostate differentiation medium and medium was replaced 24 h after transduction. After 4 weeks, in differentiated cells from African-American iPSC, there was no detectable GFP expression. (**Figure 13B**). Co-staining for endogenous AR showed weak expression of this receptor. In contrast, iPS cells from European-American ancestry exhibited PSA-GFP expression and strong staining of endogenous AR (**Figure 13B**). These data suggest differences in the ability of African-American and European ancestry iPSC to differentiate into prostate organoids.

Prostate cancer cell-derived iPSCs and prostate differentiation

We hypothesized that the ability of prostate carcinoma-derived iPSC to differentiate back into

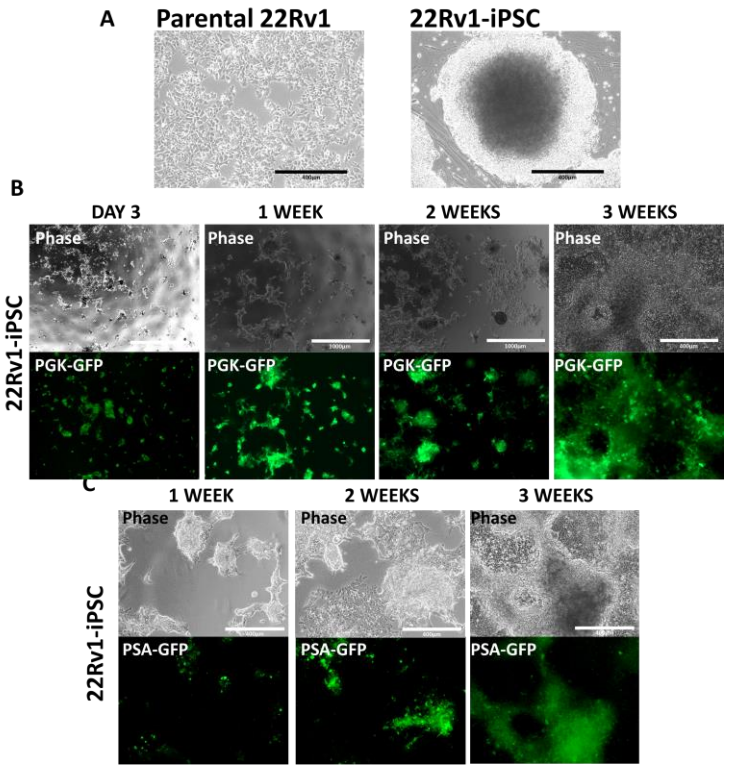

FIGURE 14

prostate organoids could help us to further evaluate the utility of the proposed model. For these experiments, we employed widely used primary 22Rv1 and metastatic LNCaP and PC3, human prostate carcinoma cell lines. We first asked if iPSC could be generated from these cell lines. We found that similar to fibroblasts, 22Rv1 cells generated iPSC colonies (**Figure 14A**). However, LNCaP and PC3 cells did not exhibit iPSC reprogramming. We then asked if 22Rv1-derived iPSC could be differentiated back into prostate-like organoids as described above with fibroblasts-derived iPS cells. 22Rv1-derived iPSCs were subjected to prostate differentiation using the direct protocol described above with PGK-GFP and PSA-GFP reporters. Results indicated that similar to fibroblasts-derived iPS cells, PGK1-GFP reporter showed expression three days after induction of prostate differentiation; PGK-GFP expression increased after a week and remained steadily high during the progression of the experiment (**Figure 14B**). PSA-GFP reporter from 22Rv1-derived iPS cells showed expression one week after prostate differentiation (**Figure 14C**), a week earlier than prostate differentiation from fibroblasts-derived iPS cells (**Figure 6C-D**). Although, PSA-GFP reporter expression in organoids from 22Rv1-iPSC co-localized with endogenous AR expression (**Figure 14B**), however, organoids did not show prostate-like morphogenesis. Similar to African-American iPSC, 22Rv1-iPSC organoids were less efficient than European-American fibroblasts-iPSC in forming prostate-related structures, including lack of acinar-like structures and internal ducts. These data show that 22Rv1-derived iPS cells fail to re-differentiate back to normal prostate-like organoids.

- What opportunities for training and professional development has the project provided?
  - This project provided the training and professional development of
    - Postdoctoral fellow Dr. Edgardo Castro Perez- he acquired skills in iPSC methodology, 2D and 3D organoids differentiation *in vitro* and learnt concepts in prostate development and cancer.
    - Graduate students Carlos Rodriguez and Dareen Mikheil- acquired skills in maintenance of human iPSC and RT-PCR and western blot analyses of stem cell factors and prostate specific antigens
    - Research Intern Ms. Kirthana Prabhakar and undergraduate students Alexandra McCarthy and Shakir Siddique to understand the concepts in prostate cancer and methods in human iPSC generation and differentiation.
- How were the results disseminated to communities of interest?
  - See the attached published paper and a manuscript being finalized for submission.
- What do you plan to do during the next reporting period to accomplish the goals?
  - Although this is the Final Report, we will continue to pursue this project to generate transcriptome data from iPSC clones and iPSC-derived prostate organoids from European- and African- derived samples and perform experiments on potential genetic susceptibility disparities assays of European- and African- derived iPS cells differentiated into prostate organoids.
  - We leverage the data collected in this project to obtain additional funding to carry out detailed studies including in vivo mouse models.

4. IMPACT:

- What was the impact on the development of the principal discipline(s) of the project?

In this report, we demonstrated for the first time that human iPS cells could be successfully differentiated into prostate-like organoids *in vitro*. Although the three approaches used here generated organoids with prostate-like features, the most efficient method was the third one described as direct differentiation. Direct exposure to prostate differentiation media was sufficient to efficiently generate prostate-like organoids in at least 8 fibroblasts-derived iPSC clones subjected to prostate differentiation. These data is consistent with previous reports of human ESC differentiated into prostate-like organoids *in vivo* in which human ESC were directly exposed to a xenograft rodent mesenchymal-epithelial tissue model *in vivo* (Taylor et al., 2006). However, these results contrast with previous report of human ESC prostate differentiation *in vitro*, in which endoderm and prostate fate steps were required for efficient prostate-like differentiation (Calderon-Gierszal and Prins, 2015). One possibility for the high efficiency of the method reported by us here is the use of dihydrotestosterne (DHT) instead of testosterone. It is well known that in serum, DHT levels are just 10% of testosterone. However, in the prostate gland, DHT levels are 5-10 times fold higher than those of testosterone, due to a more than 90% conversion of testosterone into DHT (Hay and Wass, 2009). Additionally, DHT is a much more potent AR agonist than testosterone, therefore, DHT is more specifically related to prostate tissue than testosterone (Mozayani and Raymon, 2011). However, the *in vitro* studies with human ESC did not compare a direct method and only used testosterone for differentiation so it is not possible to compare (Calderon-Gierszal and Prins, 2015).

Fibroblasts-iPS cell-derived prostate organoids exhibit functional features similar to previously reported prostate organoids derived from healthy adult prostate and prostate cancer tissues (Chua et al., 2014; Drost et al., 2016; Gao et al., 2014). For instance, the organoids reported here exhibited prostate-related morphogenesis such as functional acinar-like structures that generate and release prostasphere-like cells to the lumen-like structures. Additionally, organoids displayed efficient morphogenesis of internal ducts with branching morphogenesis. The PSA-GFP reporter used during prostate differentiation supports these results, in which GFP expression was only observed in areas with enriched differentiation and prostate-related morphogenesis. Although prostate differentiation induced strong PSA-GFP reporter expression in 22Rv1-iPSC cells, GFP expression was not specific, since 22Rv1-iPSC prostate differentiation failed to generate prostate-like morphogenesis. This expression pattern suggests that PSA-GFP expression in 22Rv1-iPSC derived organoids is intrinsically related to their cancer nature. Interestingly, features of 22Rv1-iPSC differentiated in prostate differentiation medium are consistent with prostate cancer histology, in which the prostate de-differentiate losing acinar organization and internal ducts (Eggener et al., 2015). Furthermore, comparison of prostate organoids derived from African- and European-American iPSC showed that genetic ancestry background may affect prostate differentiation in African-American derived iPSC. We propose to use these organoids as models to study genetic disparities in prostate cancer. Ongoing experiments are aimed at identifying the genetic and epigenetic risk alleles for African-American men to prostate cancer.

- What was the impact on other disciplines?
    - Although many cancers are thought to arise from a specific cell type, recently, this concept has come under scrutiny. This project opened the possibility of utilizing iPSC strategy to investigate the cell of origin of cancer, especially for cancer for which the normal cell counterpart is uncertain or not readily accessible.
- What was the impact on technology transfer?
    - Nothing to Report
- What was the impact on society beyond science and technology?
    - In the long-term, we expect to identify the genetic factors that predispose African-American men to prostate cancer and reduce prostate cancer burden and heath care costs to the society.

5. Changes/problems:

- **Changes in approach and reasons for change**

  During the period when Prostate Medium (PrGEM) was unavailable form Lonza, Dr. Castro-Perez leveraged the iPSC generated from fibroblasts to investigate their ability to other cell types, specifically melanocytes, and their relationship to cell differentiated from melanoma-derived iPSC (see attached paper). Subsequently, this strategy was used to compare the European- and African-American iPSC-derived prostate organoids to primary and metastatic human prostate cancer cells. Thus, the change necessitated by the delay in acquiring prostate growth medium has allowed us to optimize methods to reprogram human cancer cells.

- Actual or anticipated problems or delays and actions or plans to resolve them
  - In October 2018, Dr. Castro-Perez announced that he will be leaving the laboratory abruptly as we were planning to complete the RNA-seq analyses. We currently have frozen pellets, DNA and total RNA from the European- African-American prostate organoids. These samples need to be sent for sequencing. Unfortunately, with the departure of Dr. Castro-Perez and lack of other personnel to continue this project, completion of this project is delayed. We are seeking additional funding opportunities to complete this analysis.
- Changes that had a significant impact on expenditures
  - As described in the previous progress report, the delay in obtaining the media has negative impact on the available funds for the project. In the previous Progress Report, I requested request supplemental funding, if possible, to complete the final stage of the project, i. e., DNA and RNA sequencing.
- Significant changes in use or care of human subjects, vertebrate animals, biohazards, and/or select agents
  - Nothing to Report.
- Significant changes in use or care of human subjects
  - None
- Significant changes in use or care of vertebrate animals.
  - None
- Significant changes in use of biohazards and/or select agents
  - None

6. PRODUCTS:

- **Publications, conference papers, and presentations**.

  Journal publications.

  Castro-Pérez, E., Rodriguez, C. I., Mikheil, D., Newton, M. A., Siddique, A., McCarthy, A., and **Setaluri, V.** (2019) Melanoma Tumor Progression Inhibits Pluripotency and Melanoma-Derived iPSC Differentiate Predominantly to Neural-like Cells. *Stem Cell Reports* 13:177-192

Castro-Perez E, Prabhakar, K., Jayanthy A, Setaluri V. **In vitro Differentiation of iPS Cells into Prostate-like Organoids under Defined Conditions as a Model to Study Genetic Disparity in Prostate Cancer** (To be submitted to Stem Cell Research)

- Books or other non-periodical, one-time publications.
    - Nothing to Report.
- Other publications, conference papers, and presentations.
    - Nothing to report
- Website(s) or other internet site(s).
    - Nothing to Report
- Technologies or techniques.
    - Nothing to report

7. PARTICIPATION & OTHER COLLABORATING ORGANIZATIONS

- What individuals have worked on the project?

Name:	**Project Role:**	**Researcher Identifier**	**Nearest person month worked:**	**Contribution to Project:**	**Funding Support:**
Vijayasaradhi Setaluri	PI	None	1.2	Overall project administration	This grant
Nihal Ahmad	Co-Investigator	None	0.36	Contributor, supplies PCa cell lines	This grant
Rupa Sridharan	Co-Investigator	None	0.6	Contributor, iPSC characterization: has provided guidance in reprogramming protocols	This grant
Edgardo Castro Perez	Postdoctoral researcher	None	12	Performed most of experiments to date	This grant
Kirthana Prabhakar	Postdegree intern	None	3	Experimental support to Dr. Perez	This grant
Murray Brilliant	PI, Marshfield Clinical Research Foundation subaward	None	0.18	Project oversight: genotyping of fibroblasts	This grant
Lynn Ivacic	Research Associate	None	0.3	Performed genotyping experiments to date	This grant
Terrie Kitchner	Research Coordinator	None	0.12	Coordinated institutional regulatory matters	This grant

- Has there been a change in the active other support of the pd/pi(s) or senior/key personnel since the last reporting period?
    - Nothing to Report
- What other organizations were involved as partners?
    - **Organization Name:** Marshfield Clinic Research Foundation
    - **Location of Organization:** Marshfield, WI
- Partner's contribution to the project
    - **Financial support:** NA
    - **In-kind support**: NA
    - **Facilities**: NA
    - **Collaboration**: Genetic ancestry analyses
- Personnel exchanges: na
    - **Other.**
- Inventions, patent applications, and/or licenses
    - Nothing to Report.
- Other products
    - Nothing to report.
- **SPECIAL REPORTING REQUIREMENTS**
    - NONE
        - **COLLABORATIVE AWARDS:** *For collaborative awards, independent reports are required from BOTH the Initiating PI and the Collaborating/Partnering PI. A duplicative report is acceptable; however, tasks shall be clearly marked with the responsible PI and research site. A report shall be submitted to https://ers.amedd.army.mil for each unique award.*
        - **QUAD CHARTS:** *If applicable, the Quad Chart (available on https://www.usamraa.army.mil) should be updated and submitted with attachments.*
- **APPENDICES**

Castro-Pérez, E., Rodriguez, C. I., Mikheil, D., Newton, M. A., Siddique, A., McCarthy, A., and Setaluri, V. (2019) Melanoma Tumor Progression Inhibits Pluripotency and Melanoma-Derived iPSC Differentiate Predominantly to Neural-like Cells. Stem Cell Reports 13:177-192

Castro-Perez E, Prabhakar, K., Jayanthy A, Setaluri V. In vitro Differentiation of iPS Cells into Prostate-like Organoids under Defined Conditions as a Model to Study Genetic Disparity in Prostate Cancer (To be submitted to Stem Cell Research)

In vitro Differentiation of iPS Cells into Prostate-like Organoids under Defined Conditions as a Model to Study Genetic Disparity in Prostate Cancer

Edgardo Castro-Pérez[1,2], Kirthana Prabhakar[1,2], Ashika Jayanthy[1], and Vijayasaradhi Setaluri[1,2*]

[1]*Department of Dermatology, University of Wisconsin-Madison School of Medicine and Public Health,* Madison, WI 53706, USA.

[2]*William S. Middleton Memorial Hospital,* Madison, WI 53705, USA.

**Corresponding author*

Running Title: Prostate Differentiation of iPS Cells

*Corresponding author:

Vijayasaradhi Setaluri, PhD

Department of Dermatology

1300 University Avenue, B25

University of Wisconsin-Madison

Madison, WI 53706

Tel: (608) 263-5362

E-mail: setaluri@wisc.edu

Keywords: Prostate cancer, prostate differentiation, iPS cells, PSA-promoter-GFP reporter.

Abstract

The incidence of prostate cancer in African-American men is nearly 60% higher with a corresponding 2-3 times higher mortality rate than in Caucasian-American males. The reasons for this disparity are not understood. Most studies aimed at understanding the genetic basis for susceptibility to prostate cancer have focused on GWAS and mouse models. Although very powerful, however, these studies do not provide insight into the reasons for these disparities. We propose to use iPSC-derived from African- and European-American neonates and differentiate them into prostate organoids *in vitro*. We have established here a new method to differentiate iPSC into prostate-like organoids. Organoids express PSA as determined by immunofluorescence and PSA-GFP reporter. Organoids express prostate-related markers including AR, p63, NKX3.1, CK18, vimentin, PSMA, FOXA1 and HOXB13. Morphological changes associated with prostate organoids such as the formation of acinar-like structures, internal ducts, branching and the generation of prostasphere-like cells were evident in organoids. These features correlate with prostate organoids derived from adult prostate tissues. Comparison of prostate organoids derived from African- and European-American iPSC showed that African-American iPSCs are less efficient than European-American iPSC forming prostate organoids. We propose to use these organoids as models to study genetic disparities in prostate cancer.

INTRODUCTION

Prostate cancer is the most commonly diagnosed cancer in men in Europe and the United States. Up to 42% of prostate cancer risk may be explained by heritable factors suggesting contribution of genetic factors in the etiology of this disease. Moreover, among African-American men, the incidence of prostate cancer is approximately 60% higher and the mortality rate in this population is 2 to 3 times greater compared with European-American men (Cotter et al., 2002; Hoffman et al., 2001; Thompson et al., 2001; Zullig et al., 2012). The reasons for this disparity are not completely understood. Since no clear patterns were observed for association with dietary or life style factors such as physical activity, occupational history, sexual behavior and other health conditions, it is likely that inherent genetic and epigenetic differences, presumably both germ-line and prostate-cell specific, contribute to this disparity in prostate cancer risk (Mordukhovich et al., 2011). Efforts are ongoing to identify molecular mechanism and common risk alleles for prostate cancer risk using genome-wide association studies (Farrell et al., 2013; Gudmundsson et al., 2012; Ricks-Santi et al., 2012). While identification of individuals/populations at risk is important, additional in-depth studies are needed to understand the genetic and molecular mechanisms responsible for the differences in susceptibility of prostate cells to malignant transformation. However, limited access to adult, juvenile and embryonic human prostate tissues prior to the onset of age-related or malignant changes has hampered analyses of genetic and epigenetic mechanisms intrinsic to prostate cells. Genetically altered mouse models, although very powerful for dissecting roles of specific genes and signaling pathways in intact animal have limited utility for understanding differences in disease susceptibility in humans (Ellwood-Yen et al., 2003; Mulholland et al., 2011). More recent strategies to study prostate development, maturation and carcinogenesis included differentiation of human embryonic stem cells (hESC) (Calderon-Gierszal

and Prins, 2015; Taylor et al., 2006) also have many limitations including ongoing ethical debate and the number of hESC available cell lines, especially the limited representation of different genetic ancestries. Therefore, novel innovative strategies are needed to model human prostate cells for understanding the genetic and epigenetic basis of differences in susceptibility to prostate cancer. Induced pluripotent stem cells (iPSC) offer a useful alternative to hESC and reprogramming prostate cells into iPSC has been documented (Moad et al., 2013; Zhao et al., 2013).

We hypothesized that differentiation of African- and European-American neonatal fibroblasts-derived iPSCs to prostate cells is a unique and powerful strategy for studies on prostate cancer risk differences of African-American men. iPSC represent a powerful tool model with several advantages including the capacity to recapitulate the developmental process of adult tissues differentiation and organogenesis *in vitro*. Prostate differentiation of iPS cells was also evaluated using a prostate specific gene promoter-GFP reporter. Together with prostate-related marker expression, morphological changes associated with prostate function were evident in both 2D and 3D prostate-like organoids. In particular, the formation of acinar-like structures, internal ducts with branching and the generation of prostasphere-like cells. Time-lapse imaging demonstrated budding of prostaspheres from areas of the organoids with enriched differentiation (acinar structures) and branching ducts (Chua et al., 2014; Drost et al., 2016; Gao et al., 2014). Comparison of prostate organoids derived from African- and European-American iPSC showed that African-American iPSCs are less efficient than European-American iPSC forming prostate organoids. Furthermore, prostate organoid differentiation form prostate carcinoma cells 22Rv1-derived iPSC showed that 22Rv1-iPSC did not differentiate into prostate-like organoids. Thus, human iPSC-derived prostate organoids can serve as models to study risk disparities in aggressive prostate

cancer.

RESULTS

iPS cells were efficiently reprogrammed and exhibit stem cell features

We reprogrammed neonatal human primary fibroblasts to induced pluripotent stem cells (**Figure 1A**). Fibroblasts were transduced with three lentiviruses containing OCT4-SOX2, KLF4-cMYC and NANOG-LIN28 reprogramming factors. Five days after transduction, cells were plated on MEF feeders with reprogramming stem cell medium. The medium was supplemented with a chemical cocktail previously shown to enhance iPSC reprogramming (Hou et al., 2013). This cocktail consists valproic acid (VPA, a HDAC inhibitor) CHIR-99021 (a GSK-3α/β inhibitor), forskolin (FSK, an activator of adenylyl cyclase/cAMP pathway), tranylcypromine (TCP, a histone lysine specific demethylase 1 inhibitor) and RepSox (an inhibitor of the TGFβR-1/ALK5 pathway). One week after iPSC induction, granular colonies were visible indicative of early reprograming. Three weeks after induction, colonies with iPSC morphology appeared and expressed the stem cell marker alkaline phosphatase (AP). Total number and AP-positive colonies were quantitated (**Supplementary Figure 1A-B**). AP-Positive colonies were selected for expansion with stem cell maintenance medium. Expression of reprogramming factors was verified by Western blot (WB) (**Supplementary Figure 1C**).

iPS cells express the reprogramming factors and stem cell markers

We determined the expression of reprogramming factors at day 1 (Day 5 post-transduction), and day 21 of iPSC induction and at passage 3 (P3) by WB (**Supplementary Figure 1C**) and noted progressively increasing expression of the reprogramming factors OCT4, SOX2 and NANOG through day 21 and P3. Immunofluorescence analysis (**Supplementary Figure 1D**) showed co-

expression of reprogramming factors OCT4 or NANOG and stem cell surface markers CD9, E-cadherin, SSEA4 and podoclyxin.

iPS cells exhibit pluripotency into three germ layers and form embryoid bodies

Pluripotency of iPSC clones was determined using *in vitro* differentiation assays and immunofluorescence staining for early markers specific for the three germ layers (Deshpande et al., 2017; Shinozawa et al., 2017). Differentiation of iPSC to ectoderm, mesoderm and endoderm was verified by expression, respectively of SOX1 and OTX2, and HAND1 and Brachyury, and GATA4 and SOX17 (**Supplementary Figure 1E)**. Furthermore, in embryoid body (EB) formation assay by the hanging drop method (**Supplementary Figure 1F**), iPSC clones exhibited the ability to form EBs.

Optimization for *in vitro* differentiation of prostate organoids

We employed three different protocols for differentiation of iPSC to prostate organoids. The first method (**Figure 1B**) was based on inductive differentiation by co-culture of iPSC with neonatal mouse urogenital sinus mesenchymal (UGSM) cells and neonatal human dermal fibroblasts. The second method (**Figure 1C**) involved stepwise differentiation with growth factors and differentiation factors first to endoderm followed by commitment to prostate lineage and finally to prostate differentiation (Calderon-Gierszal and Prins, 2015). The third protocol (**Figure 1D**) involved direct differentiation with growth and differentiation factors.

Co-culture with UGSM feeder cells

Previous reports have shown that mouse UGSM, stromal cells (human fibroblasts) and extracellular matrix (ECM) have an inductive effect for prostate differentiation of hESC *in vivo* using xenografts models (Taylor et al., 2006). Fibroblasts secrete components of the ECM and basement membrane that have inductive roles for prostate growth, development and differentiation

(Olumi et al., 1999). Additionally, it is well known that the prostate development and differentiation rises from the embryonic UGSM bud (Taylor et al., 2006). Induced pluripotent cells were co-cultured with human dermal fibroblasts and UGSM cells in prostate epithelial growth media (PrEGM™ BulletKit™, LONZA) (**Supplementary Figure 2A-D**). This resulted in organization of cells to structures with prostate-like features including acinar-like morphology (**Supplementary Figure 2B**) and expression of prostate specific antigen (PSA), p63 and androgen receptor (AR), markers associated to prostate cells (**Supplementary Figure 2C-D**). The protocol is somewhat time consuming with variable efficiency of differentiation that is affected by several factors such as quality and passage of the UGSM and fibroblasts.

Stepwise Differentiation

For stepwise directed differentiation, we employed a modified method (Calderon-Gierszal and Prins, 2015) (**Supplementary Figure 3A-D**). First, iPS cells were differentiated into definitive endoderm with Activin A and endoderm differentiation was verified by expression of SOX17, as determined by immunofluorescence (**Supplementary Figure 3B-C**). Endoderm-differentiated cells were treated with WNT10B and FGF10A for 4 days to promote prostate fate (**Supplementary Figure 3B**) and finally cultured in prostate differentiation medium (**Supplementary Figure 3D**) (1:1 PrEGM-Bullet kit:SCGM Stromal Cell Bullet Kit) supplemented with 15 mM HEPES, 1x B27, Noggin, EGF, R-Spondin1, dihydrotestosterone (DHT) and 2 mM Glutamax. After four weeks, morphological changes such as formation of outgrowth and buds. However, these organoids did not exhibit internal duct formation.

Direct Differentiation

The third approach involved the direct differentiation of iPS cells in prostate differentiation medium PrEGM:SCGM and growth/differentiation factors, as described above, but without

endoderm and prostate fate differentiation steps (**Figure 2A**). This protocol was performed in 2D and 3D. For 2D organoids, iPS cells were suspended as single cells and plated in Matrigel-coated wells. For 3D organoids, 5-8 iPS cell colonies were isolated and manually plated in Matrigel-coated wells. After one week, cells started to differentiate and organize into multiple acinar-like shaped structures in 2D, while 3D organoids formed small outgrowths. By second and third week, acinar-like structures and internal ducts were prominent in both 2D cultures and 3D organoids (**Figure 2B**). After 4 weeks in culture, in addition to acinar-like structures exhibiting branching internal ducts, presence of spheroid-like structures inside the lumen (**Figure 2C**). These spheroids produced by 2D and 3D organoids are similar to prostaspheres reported in prostate organoid models from healthy and prostate cancer adult tissues samples from human and rodents (Chua et al., 2014; Huang et al., 2015). Time-lapse microscopy of 2D organoids confirmed that prostate organoids were generation and release of prostasphere in the lumen (**Figure 2D**).

Organoids express prostate differentiation

To monitor the progress of prostate-like differentiation, we generated a lentivirus for human PSA-promoter GFP-reporter plasmid. To verify the specificity of the PSA-GFP reporter, we transduced iPS cells and 22Rv1 human prostate cancer cells with lentivirus for either ubiquitous phosphoglycerate kinase-promoter GFP-reporter (PGK-GFP) or with PSA-GFP reporter. Four weeks of transduction, PGK-GFP reporter transduced iPS cells, but not the PSA-GFP lentivirus transduced cells, expressed the GFP reporter (**Figure 3A**). In contrast, 22Rv1 prostate cancer cells expressed both, PGK-GFP and PSA-GFP reporters just three days after transduction (**Figure 3B**). For evaluation of prostate lineage specificity during prostate differentiation, iPS cells were transduced with either PSA-GFP or with PGK-GFP reporter lentiviruses at day 1 in prostate differentiation medium. Medium was replaced with fresh prostate differentiation medium 24 h

after transduction and GFP expression was monitored for 4 weeks. In PGK-GFP-reporter lentivirus transduced iPSC, GFP expression was detectable as early as three days post-transduction in all areas of the organoids including areas with low prostate-like morphology (**Supplementary Figure 4A**). In contrast, PSA-GFP reporter transduced iPSC, GFP expression was detectable only two weeks after prostate differentiation prominently in areas of the organoids with acinar-like morphology (**Figures 3C-D**). We asked if expression of the PSA-GFP reporter was consistent with expression of endogenous prostate markers PSA and AR. As shown in **Figure 3D (top panels**), GFP reporter expression was co-localized with expression of endogenous PSA and enriched in acinar-like structures. In contrast, while AR expression was detectable throughout the organoid, there was limited co-localization with PSA-promoter driven GFP expression (**Figure 3D, bottom panels**).

In addition to PSA and AR, two weeks after induction of prostate differentiation, the organoids also exhibited expression of p63, NKX3.1 and cytokeratin 18 (**Supplementary Figure 4B**). Importantly, expression of prostate markers is localized to areas with enriched prostate-like differentiation, such as acinar-like structures. For instance, not all cells with nuclear staining (DAPI) show staining for PSA or AR (**Supplementary Figure 4B, top panels, red dashed circle**) indicating specificity of expression of prostate markers. By 4 weeks, expression of other prostate-related markers, including vimentin, cytokeratin 5 (CK5), laminin, HOXB13, PSMA and FoxA1, was also prominent in morphologically distinctive areas of the organoids.

Prostate organoids exhibit stromal cell features and prostate-like function

After 4 weeks of prostate differentiation, 3D organoids were fixed, sectioned and analyzed by immunofluorescence staining for expression of prostate markers PSA, AR, p63, NKX3.1, CK18 and vimentin (**Supplementary Figure 5A**). Furthermore, we collected supernatant from 3D

organoid cultures and pelleted to harvest prostatspheres and prepared them for staining of prostate markers (Chua et al., 2014; Huang et al., 2015). These structures also showed expression of prostate markers PSA, AR, p63, NKX3.1 and CK18 (**Supplementary Figure 5B**). These data show that iPSC-derived organoids exhibit some features similar to prostate organoids derived from adult prostate tissues (Drost et al., 2016; Huang et al., 2015). Moreover, 3D organoids exhibited histological features of stromal-like with internal branched ducts (**Supplementary Figure 5C, left panel**). Cross sections also indicate that the organoids may form internal zones with a primitive lumen-like morphology surrounded by stromal basal structure (**Supplementary Figure 5C, middle panel**). Additionally, hematoxylin-eosin staining of prostaspheres collected from 3D organoids showed a cellular architecture in these structure (**Supplementary Figure 5C, right panel**) (Chua et al., 2014).

Selection of African- and European fibroblasts for iPSC reprogramming

Having established the conditions for iPSC reprogramming and prostate differentiation, we set out to select and reprogram skin fibroblasts derived from African- and European-American individuals from a collection of fibroblasts (UW Skin Disease Research Center, Cell Culture Core). Among 45 selected with self-identified (by the parent of the newborn) race- 34 white Caucasian, 8 African-American, 2 Hispanic-American and 1 Asian-American. At passage 3, we isolated total DNA from these fibroblasts and analyzed for 39 SNPs ancestral informative markers (AIM). AIM SNP data was analyzed using POPGENE to determine the genetic diversity of the samples and STRUCTURE to determine the genetic ancestry or admixture for each individual. Selection of samples was based on two criteria: self-identification of samples by race at the moment of skin collection (African-American and European-American) and ancestry confirmation by 39 SNP-AIMs genetic analysis to determine individual gene admixture. POPGENE analysis showed that

samples collected are admixed and highly polymorphic (**Supplementary Figure 6A**) as observed by the multiple clusters by the genetic distance-based UPGMA dendrogram (Nei's, 1972, modified from NEIGHBOR procedure of PHYLIP Version 3,5). However, all self-identified African-American samples clustered together and separated from other samples. Pooled gene admixture estimates determined by STRUCTURE based on K=2, K=3 and K=4 analyses, confirmed that fibroblast DNA from self-identified African-American exhibited high genetic homology (averaging 90% - 93% shown in red for K=2 and blue for K=3 and K=4) with low admixture levels (averaging 7% - 10% for all Ks analyzed) shown mostly in red, green and yellow. Thus, self-identified African-American samples appear to be genetically different from other self-identified races/populations (**Figure 4B**). Based on these data, we selected four African-American fibroblasts (nF007, nF008, nF013 and nF020, **Figure 4B, arrows**) with high percentage of African ancestry markers [averaging 93.1% (red) for K=2; 89.9% (blue) for K=3; and 89.8% (blue) for K=4] and low percentage of markers of other races/populations. Additionally, we selected four European-American fibroblasts (nF009, nF014, nF024 and nF026, **Figure 4B, arrows**) with very low percentage of African genes [averaging 4.3% (red) for K=2; 1.8% (blue) for K=3; and 1.1% (blue) for K=4) and high percentage of genes from European populations. Further analysis by POPGENE of the 8 selected samples demonstrated both groups clustered separated from each others (**Supplementary Figure 6B**).

Comparison of efficiency of reprogramming of fibroblasts from European and African ancestry

Under identical conditions of reprogramming, European ancestry fibroblasts showed higher efficiency than African ancestry fibroblasts as determined by the number of colonies (**Figure 4C, top panels**). However, the colony size (**Figure 4C, middle panels**) and the percentage of alkaline-

positive colonies (**Figure 4C, bottom panels**) were similar for both groups. Expression of reprogramming factors, determined by Western blot analysis, showed that all samples similarly express the reprogramming factors determined at day 1 of reprogramming (5 days after transduction) and iPSC clones at passage 3 (**Figure 4D**). These data suggest that the difference in the efficiency in reprogramming is not due differences in transduction or expression of reprogramming factors.

European and African ancestry iPSC show pluripotency

Pluripotency of iPSC clones from African- and European-American iPSC were determined using germ layer *in vitro* differentiation assays and staining for early markers (Deshpande et al., 2017; Shinozawa et al., 2017). Ectoderm differentiation was verified by SOX1 and OTX2 expression (**Figure 5A**), mesoderm by the expression of HAND1 and Brachyury (**Figure 5B**) and endoderm by the expression of GATA4 and SOX17 (**Figure 5C**). Data in **Figure 5A-C** show that all iPSC clones similarly differentiate into precursors of the three embryonic layers.

European- and African- ancestry iPSC express stem cell markers and form EB

Immunofluorescence co-staining of reprogramming factor OCT4 with surface markers demonstrated that all clones similarly co-express stem cell surface markers E-cadherin and SSEA4 (**Figure 6A-B**). Embryoid body (EB) formation assays by the hanging drop method showed that all iPSC clones exhibit the ability to form EBs (**Figure 6C**). Chromosomal analysis (**Supplementary Figure 6C**) demonstrated that the selected iPSC clones have a normal human male karyotype 46, XY (WiCell, Madison, WI).

Differentiation of European and African ancestry iPSC

We selected 2 African-American (nF008 and nF020) and 2 European-American (nF009 and nF026) iPSC for prostate differentiation (**Supplementary Figure 6C**) using the prostate direct

differentiation protocol (**Figure 1D**). Interestingly, African ancestry iPSC (nF008 and nF020) did not form organoids with acinar-like structures or internal ducts and branching (**Figure 7A**). In contrast, iPSC from European ancestry (nF009 and nF026) efficiently formed organoids with acinar-like structures, internal ducts and branching (**Figure 7A**). We also evaluated PSA-GFP reporter expression. We transduced iPS cells with PSA-GFP reporter lentiviruses on day 1 in prostate differentiation medium and medium was replaced 24 h after transduction. After 4 weeks, in differentiated cells from African-American iPSC, there was no detectable GFP expression. (**Figure 7B**). Co-staining for endogenous AR showed weak expression of this receptor. In contrast, iPS cells from European-American ancestry exhibited PSA-GFP expression and strong staining of endogenous AR (**Figure 7B**). These data suggest differences in the ability of African-American and European ancestry iPSC to differentiate into prostate organoids.

Prostate cancer cell-derived iPSCs and prostate differentiation

We hypothesized that the ability of prostate carcinoma-derived iPSC to differentiate back into prostate organoids could help us to further evaluate the utility of the proposed model. For these experiments, we employed widely used primary 22Rv1 and metastatic LNCaP and PC3, human prostate carcinoma cell lines. We first asked if iPSC could be generated from these cell lines. We found that similar to fibroblasts, 22Rv1 cells generated iPSC colonies (**Supplementary Figure 7A**). However, LNCaP and PC3 cells did not exhibit iPSC reprogramming. We then asked if 22Rv1-derived iPSC could be differentiated back into prostate-like organoids as described above with fibroblasts-derived iPS cells. 22Rv1-derived iPSCs were subjected to prostate differentiation using the direct protocol described above with PGK-GFP and PSA-GFP reporters. Results indicated that similar to fibroblasts-derived iPS cells, PGK1-GFP reporter showed expression three days after induction of prostate differentiation; PGK-GFP expression increased after a week and

remained steadily high during the progression of the experiment (**Supplementary Figure 7B**). PSA-GFP reporter from 22Rv1-derived iPS cells showed expression one week after prostate differentiation (**Supplementary Figure 7C**), a week earlier than prostate differentiation from fibroblasts-derived iPS cells (**Figure 3C-D**). Although, PSA-GFP reporter expression in organoids from 22Rv1-iPSC co-localized with endogenous AR expression (**Figure 7B**), however, organoids did not show prostate-like morphogenesis. Similar to African-American iPSC, 22Rv1-iPSC organoids were less efficient than European-American fibroblasts-iPSC in forming prostate-related structures, including lack of acinar-like structures and internal ducts. These data show that 22Rv1-derived iPS cells fail to re-differentiate back to normal prostate-like organoids.

DISCUSSION

In this report, we demonstrated for the first time that human iPS cells could be successfully differentiated into prostate-like organoids *in vitro*. Although the three approaches used here generated organoids with prostate-like features, the most efficient method was the third one described as direct differentiation. Direct exposure to prostate differentiation media was sufficient to efficiently generate prostate-like organoids in at least 8 fibroblasts-derived iPSC clones subjected to prostate differentiation. These data is consistent with previous reports of human ESC differentiated into prostate-like organoids *in vivo* in which human ESC were directly exposed to a xenograft rodent mesenchymal-epithelial tissue model *in vivo* (Taylor et al., 2006). However, these results contrast with previous report of human ESC prostate differentiation *in vitro*, in which endoderm and prostate fate steps were required for efficient prostate-like differentiation (Calderon-Gierszal and Prins, 2015). One possibility for the high efficiency of the method reported by us here is the use of dihydrotestosterne (DHT) instead of testosterone. It is well known that in serum, DHT levels are just 10% of testosterone. However, in the prostate gland, DHT levels are 5-10 times fold

higher than those of testosterone, due to a more than 90% conversion of testosterone into DHT (Hay and Wass, 2009). Additionally, DHT is a much more potent AR agonist than testosterone, therefore, DHT is more specifically related to prostate tissue than testosterone (Mozayani and Raymon, 2011). However, the *in vitro* studies with human ESC did not compare a direct method and only used testosterone for differentiation so it is not possible to compare (Calderon-Gierszal and Prins, 2015).

Fibroblasts-iPS cell-derived prostate organoids exhibit functional features similar to previously reported prostate organoids derived from healthy adult prostate and prostate cancer tissues (Chua et al., 2014; Drost et al., 2016; Gao et al., 2014). For instance, the organoids reported here exhibited prostate-related morphogenesis such as functional acinar-like structures that generate and release prostasphere-like cells to the lumen-like structures. Additionally, organoids displayed efficient morphogenesis of internal ducts with branching morphogenesis. The PSA-GFP reporter used during prostate differentiation supports these results, in which GFP expression was only observed in areas with enriched differentiation and prostate-related morphogenesis. Although prostate differentiation induced strong PSA-GFP reporter expression in 22Rv1-iPSC cells, GFP expression was not specific, since 22Rv1-iPSC prostate differentiation failed to generate prostate-like morphogenesis. This expression pattern suggests that PSA-GFP expression in 22Rv1-iPSC derived organoids is intrinsically related to their cancer nature. Interestingly, features of 22Rv1-iPSC differentiated in prostate differentiation medium are consistent with prostate cancer histology, in which the prostate de-differentiate losing acinar organization and internal ducts (Eggener et al., 2015). Furthermore, comparison of prostate organoids derived from African- and European-American iPSC showed that genetic ancestry background may affect prostate differentiation in African-American derived iPSC. We propose to use these organoids as models

to study genetic disparities in prostate cancer. Ongoing experiments are aimed at identifying the genetic and epigenetic risk alleles for African-American men to prostate cancer.

MATERIALS AND METHODS

Lentivirus Production

Human Embryonic Kidney (HEK293) cells were plated on 10cm plates with DMEM + 10% FBS without antibiotics and allowed reach 70 – 90 % confluency within 48hrs. Following the Lipofectamine 2000 (Thermo Fisher, #11668019) protocol, cells were then triple co-transfected with plasmids containing packaging (psPAX2, Addgene #12260) and VSV G envelope (pMD2.G, Addgene #12259) and target genes [(OCT4-SOX2, pSIN4-EF2-O2S, Addgene #21162) or KLF4-cMYC (pSIN4-CMV-K2M, Addgene #21164) or NANOG-LIN28 (pSIN4-EF2-N2L, Addgene #21163). After ~15-18 h, the transfection medium was discarded and replaced with fresh medium (DMEM +10% FBS + 1% P/S- antibiotics). The next day, the supernatant-containing lentiviruses was collected and replaced with fresh medium. Supernatant-containing lentiviruses was pelleted and supernatant stored at -80 until use. The process was repeated the next day.

Human fibroblasts transduction and induction into iPSCs

Human fibroblasts were obtained from the UW-Skin Disease Research Center (SDRC) cell bank. Briefly, on day 1, fibroblasts were plated on 6-well plates at a density of $5x10^4$ cells per well in DMEM, 10% FBS and 1% P/S-antibiotics. The next day, fibroblasts were transduced with supernatant-containing lentiviruses containing the reprogramming factors (200µL each) and polybrene (10ug/mL). ~15-18 h after transduction, the medium was replaced with fresh medium without polybrene and cells are allowed to grow for 4-5 days.

Transduced fibroblasts with three reprogramming lentiviruses were then plated at a density of ~$2x10^4$ cells per well of 6 well plates on mouse embryonic fibroblasts (MEFs) feeder cells (WiCell Research Institute) with stem cell reprogramming medium (KO DMEM, 20% KOSR, 1% Glutamax, 1% NEAA, 1% antibiotics, 10ng/mL bFGF, $2x10^{-4}$M of 2-Mercaptoethanol at a density of $2x10^4$ cells per well of 6 well plates. A cocktail of up to five chemicals was used for reprogramming melanoma cells including Forskolin (FSK, 10µM), valproic acid (VPA, 500µM), CHIR99021 (10µM), RepSox (5µM) and Tranylcipromine (5µM). Medium was replaced every 3-4 days for three weeks. After three weeks, colonies were passaged using Versene and ROCK inhibitor Y-27632 on fresh MEFs every two weeks with maintenance stem cell medium, which is the same basal medium as reprogramming's but supplemented only with 4ng/mL bFGF, CHIR99021 (3µM) and PD0325901 (1µM).

Alkaline Phosphatase (AP) live staining

AP staining (ThermoFisher #A14353) was performed after three weeks of reprogramming and after two weeks in passage 1 according to the manufacturer's protocol.

Stem cell markers expression and pluripotency assays

Expression of stem cell markers was performed using the Human Pluripotent Stem Cell Marker Antibody Panel Plus (R&D Systems #SC009). Differentiation of miPSCs to three germ layer was evaluated using the Human Pluripotent Stem Cell Functional Identification Kit (R&D Systems #SC027B). Images were taken using an EVOS™ FL Auto Imaging System (Thermo Fisher).

Embryoid Body Formation

Embryoid bodies (EBs) was performed as reported by (Ohta et al., 2011; Yang et al., 2011) with some modifications. Briefly, EBs were formed from hanging drop culture in EB medium consisting of DMEM/F12 containing 20% KOSR, 1X glutamax, 1X nonessential amino acids (NEAA), $2x10^{-4}$ M 2-mercaptoethanol, and 1% antibiotics in a cell culture dish with sterile PBS in the bottom for 5 days. EBs were then harvested and visualized under the microscope.

Western Blotting

Cells were harvested and lysed using RIPA buffer containing Halt protease inhibitor cocktail (Thermo Fisher, #78410) and phosphatase inhibitor cocktail (Bimake.com, #B15001). Samples were then sonicated, centrifuged for 30 min at 4ºC and the supernatants were collected. Protein concentration was estimated using Pierce BCA Protein Assay Kit (Thermo Fisher, #23227). SDS-PAGE was performed using 20µg of protein and proteins were transferred to a PVDF membrane. The membrane was blocked with 5% nonfat dry milk prepared in TBST buffer. After incubation overnight with primary antibodies at optimized dilutions (Supplementary Tables), membranes were washed and incubated with HRP conjugated secondary antibodies. Protein bands were detected using ECL Start Western Blotting Detection Reagent (Thermo Fisher, #32106), imaged on ImageQuant LAS 4000 (GE Healthcare Life Sciences, Marlborough, MA).

Immunofluorescence

Cells were plated on 8-well slides (Ibidi, USA, #80826), fixed in 4% PFA/PBS for 20 min and then incubated in permeabilization/blocking buffer consisting of 0.3% Triton X-100, 1% BSA, and 10% normal donkey serum in PBS for 45 minutes (0.5 mL/well of a 24-well plate). Primary antibodies (Supplementary Tables) were diluted in permeabilization/blocking buffer and incubated

overnight at 4 degrees. Next day, cells were washed 3 times with 1% BSA in PBS for 5 minutes and incubated for 1h with secondary antibody (1:200) at RT. After three washes with 1% BSA/PBS, ProLong Gold Antifade with DAPI (Thermo Fisher, #P36935) was added to the cells and cells were visualized using the EVOS microscope (Thermo Fisher).

Prostate Differentiation Reagents and Preparation

For prostate differentiation, PrEGM™ BulletKit™ (LONZA) was prepared as indicated by the kit's manufacturer with bovine pituitary extract (BPE), Human Insulin, hydrocortisone, gentamicin sulfate amphotericin-B, retinoic acid, transferrin, triiodothyronine T3, epinephrine and human EGF. SCGM™ Stromal Cell BulletKit™ (LONZA) was prepared as described by the kit's manufacturer with 5% FBS, human FGF-B, human insulin and gentamicin sulfate amphotericin-B. Prostate differentiation medium was prepared with 1:1 PrEGM:SCGM mixture and supplemented with 1X B27 (Invitrogen), Noggin (R&D systems, 100 ng/ml), EGF (R&D systems, 100 ng/ml), R-Spondin1 (R&D systems, 500 ng/ml), dihydrotestosterone (DHT, 0.3μM, Sigma), 2 mM of glutamax, 1% penicillin-streptomycin and 15 mM HEPES. All prostate differentiation experiments were performed in 4-well plates coated with matrigel. For 2D organoids, iPS cells were single cell suspended and plated at approximately $5x10^3$ cells/well with prostate differentiation medium. For 3D organoids differentiation, 6 - 8 iPSC colonies were plated with prostate differentiation medium. Prostate differentiation medium was changed every 3-4 days for 4 weeks.

Histology

3D organoids were sectioned and H/E stained by the UW-Carbone Cancer Center.

Fibroblasts isolation and culture

Primary fibroblasts were isolated from human neonatal foreskins in the UW-Skin Disease Research Center. Human primary fibroblasts were cultured in DMEM, 10% fetal bovine serum, and 1% penicillin and streptomycin.

Cloning of PSA/KLK3 promoter and GFP reporter

To construct the kallikrein-related peptidase 3/prostate specific antigen (PSA/KLK3)-promoter GFP reporter, we used as a backbone vector the PL-SIN-PGK-EiP plasmid (Addgene #21312) suitable for lentiviral production containing a PGK-GFP promoter reporter. PGK promoter was excised out by digestion with *Age*I and *Pst*I. PCR primers were designed to target human PSA/KLK3 promoter and containing the target sequences of *Age*I and *Pst*I endonucleases plus 6 nucleotide overhangs at the 3' ends forward FW5'-TTA GCA ACC GGT GTC TTG GAG TGC AAA GGA TCT A-3' and reverse RV5'-TTA GCA CTG CAG GAC AGG GTG AGG AAG ACA AC-3'. Total DNA was extracted from human fibroblasts and subjected to PCR for KLK3 promoter. PCR amplification conditions were performed under the following master mix conditions: 12.5 μL of PCR master mix (Promega, Cat.# M7502), 2.5 μL of each primer (5 μM), 1.5 μL of MgCl2 solution (25mM, Promega, Cat.# A3511) and 3 μL of DNA in 25 μL reaction. Thermal cycler conditions were 98 °C 5min, 95 °C 30 sec, 72 °C 30sec for 30 times and a final extension at 72°C for 5min. The PCR product generated was approximately 425 bp and it was prepared for TA-cloning/ligation. PL-SIN-PGK-EiP (Addgene #21312) digested with *Age*I and *Pst*I to remove the PGK-promoter. Plasmid from TA-cloning (with ligated PCR products) was also digested with *Age*I and *Pst*I to release the PSA-promoter containing the *Age*I and *Pst*I sequences to be inserted into PL-SIN-Empty-EiP plasmid. PSA-promoter containing the *Age*I and *Pst*I was

prepared for ligation with PL-SIN-Empty-EiP plasmid. Ligation was verified by endonuclease digestion with *Age*I and *Pst*I. Plasmids were then transformed into bacterial cells and stored in 30% glycerol at -80 until use. These plasmids were further used for lentiviral production of PSA/KLK3-promoter GFP-reporter.

SNP-AIMs Genetic analysis

For genetic analysis, 45 DNA samples from human neonate fibroblasts were isolated and 39 SNP-AIMs genotyped by the UW- Centre for Human Genetics of Marshfield Clinic, WI. The 45 DNAs corresponded to self-identified samples: 8 African-American, 34 European-American, 2 Hispanic-American and 1 Asian-American (45 x 39 SNP-AIMS = 1,755 x 2 chromosomes = 3,510 alleles). STRUCTURE Pritchard, Stephens and Donnelly (2000) and Falush, Stephens and Pritchard (2003), code by Pritchard, Falush and Hubisz Version 2.3.4 was used to determine the genetic ancestry admixture estimates. Burn-in period iterations (5,000) and Bayesian approach MCMC 10,000 reps after burn-in were used to detects the underlying genetic population among 45 individuals genotyped with 39 markers to compute the proportion of the genome of an individual originating from each inferred population cluster. POPGENE version 1.32 (available at http://www.ualberta.ca/~fyeh/) was used to determine genetic diversity of samples following the program's manual.

ACKNOWLEDGMENTS

This work was supported by the Department of Defense grant W81XWH-15-1-0529 and VA Merit Award 1 I01 BX002623 to V. Setaluri.

REFERENCES

Bernhardt, M., Novak, D., Assenov, Y., Orouji, E., Knappe, N., Weina, K., Reith, M., Larribere, L., Gebhardt, C., Plass, C.*, et al.* (2017). Melanoma-Derived iPCCs Show Differential Tumorigenicity and Therapy Response. Stem Cell Reports *8*, 1379-1391.

Calderon-Gierszal, E.L., and Prins, G.S. (2015). Directed Differentiation of Human Embryonic Stem Cells into Prostate Organoids In Vitro and its Perturbation by Low-Dose Bisphenol A Exposure. PLoS One *10*, e0133238.

Chua, C.W., Shibata, M., Lei, M., Toivanen, R., Barlow, L.J., Bergren, S.K., Badani, K.K., McKiernan, J.M., Benson, M.C., Hibshoosh, H.*, et al.* (2014). Single luminal epithelial progenitors can generate prostate organoids in culture. Nat Cell Biol *16*, 951-961, 951-954.

Cotter, M.P., Gern, R.W., Ho, G.Y., Chang, R.Y., and Burk, R.D. (2002). Role of family history and ethnicity on the mode and age of prostate cancer presentation. Prostate *50*, 216-221.

Deshpande, A., Yadav, S., Dao, D.Q., Wu, Z.Y., Hokanson, K.C., Cahill, M.K., Wiita, A.P., Jan, Y.N., Ullian, E.M., and Weiss, L.A. (2017). Cellular Phenotypes in Human iPSC-Derived Neurons from a Genetic Model of Autism Spectrum Disorder. Cell Rep *21*, 2678-2687.

Drost, J., Karthaus, W.R., Gao, D., Driehuis, E., Sawyers, C.L., Chen, Y., and Clevers, H. (2016). Organoid culture systems for prostate epithelial and cancer tissue. Nat Protoc *11*, 347-358.

Eggener, S.E., Badani, K., Barocas, D.A., Barrisford, G.W., Cheng, J.S., Chin, A.I., Corcoran, A., Epstein, J.I., George, A.K., Gupta, G.N.*, et al.* (2015). Gleason 6 Prostate Cancer: Translating Biology into Population Health. J Urol *194*, 626-634.

Ellwood-Yen, K., Graeber, T.G., Wongvipat, J., Iruela-Arispe, M.L., Zhang, J., Matusik, R., Thomas, G.V., and Sawyers, C.L. (2003). Myc-driven murine prostate cancer shares molecular features with human prostate tumors. Cancer Cell *4*, 223-238.

Farrell, J., Petrovics, G., McLeod, D.G., and Srivastava, S. (2013). Genetic and molecular differences in prostate carcinogenesis between African American and Caucasian American men. Int J Mol Sci *14*, 15510-15531.

Gao, D., Vela, I., Sboner, A., Iaquinta, P.J., Karthaus, W.R., Gopalan, A., Dowling, C., Wanjala, J.N., Undvall, E.A., Arora, V.K.*, et al.* (2014). Organoid cultures derived from patients with advanced prostate cancer. Cell *159*, 176-187.

Gudmundsson, J., Sulem, P., Gudbjartsson, D.F., Masson, G., Agnarsson, B.A., Benediktsdottir, K.R., Sigurdsson, A., Magnusson, O.T., Gudjonsson, S.A., Magnusdottir, D.N.*, et al.* (2012). A study based on whole-genome sequencing yields a rare variant at 8q24 associated with prostate cancer. Nat Genet *44*, 1326-1329.

Hay, I., and Wass, J. (2009). Clinical Endocrine Oncology (John Wiley & Sons).

Hoffman, R.M., Gilliland, F.D., Eley, J.W., Harlan, L.C., Stephenson, R.A., Stanford, J.L., Albertson, P.C., Hamilton, A.S., Hunt, W.C., and Potosky, A.L. (2001). Racial and ethnic differences in advanced-stage prostate cancer: the Prostate Cancer Outcomes Study. J Natl Cancer Inst *93*, 388-395.

Hou, P., Li, Y., Zhang, X., Liu, C., Guan, J., Li, H., Zhao, T., Ye, J., Yang, W., Liu, K.*, et al.* (2013). Pluripotent stem cells induced from mouse somatic cells by small-molecule compounds. Science *341*, 651-654.

Huang, Y., Hamana, T., Liu, J., Wang, C., An, L., You, P., Chang, J.Y., Xu, J., McKeehan, W.L., and Wang, F. (2015). Prostate Sphere-forming Stem Cells Are Derived from the P63-expressing Basal Compartment. J Biol Chem *290*, 17745-17752.

Moad, M., Pal, D., Hepburn, A.C., Williamson, S.C., Wilson, L., Lako, M., Armstrong, L., Hayward, S.W., Franco, O.E., Cates, J.M.*, et al.* (2013). A novel model of urinary tract

differentiation, tissue regeneration, and disease: reprogramming human prostate and bladder cells into induced pluripotent stem cells. Eur Urol *64*, 753-761.

Mordukhovich, I., Reiter, P.L., Backes, D.M., Family, L., McCullough, L.E., O'Brien, K.M., Razzaghi, H., and Olshan, A.F. (2011). A review of African American-white differences in risk factors for cancer: prostate cancer. Cancer Causes Control *22*, 341-357.

Mozayani, A., and Raymon, L. (2011). Handbook of Drug Interactions: A Clinical and Forensic Guide. (Springer Science & Business Media).

Mulholland, D.J., Tran, L.M., Li, Y., Cai, H., Morim, A., Wang, S., Plaisier, S., Garraway, I.P., Huang, J., Graeber, T.G.*, et al.* (2011). Cell autonomous role of PTEN in regulating castration-resistant prostate cancer growth. Cancer Cell *19*, 792-804.

Ohta, S., Imaizumi, Y., Okada, Y., Akamatsu, W., Kuwahara, R., Ohyama, M., Amagai, M., Matsuzaki, Y., Yamanaka, S., Okano, H.*, et al.* (2011). Generation of human melanocytes from induced pluripotent stem cells. PLoS One *6*, e16182.

Olumi, A.F., Grossfeld, G.D., Hayward, S.W., Carroll, P.R., Tlsty, T.D., and Cunha, G.R. (1999). Carcinoma-associated fibroblasts direct tumor progression of initiated human prostatic epithelium. Cancer Res *59*, 5002-5011.

Raabe, E.H., Lim, K.S., Kim, J.M., Meeker, A., Mao, X.G., Nikkhah, G., Maciaczyk, J., Kahlert, U., Jain, D., Bar, E.*, et al.* (2011). BRAF activation induces transformation and then senescence in human neural stem cells: a pilocytic astrocytoma model. Clin Cancer Res *17*, 3590-3599.

Ricks-Santi, L.J., Apprey, V., Mason, T., Wilson, B., Abbas, M., Hernandez, W., Hooker, S., Doura, M., Bonney, G., Dunston, G.*, et al.* (2012). Identification of genetic risk associated with prostate cancer using ancestry informative markers. Prostate Cancer Prostatic Dis *15*, 359-364.

Shinozawa, T., Nakamura, K., Shoji, M., Morita, M., Kimura, M., Furukawa, H., Ueda, H., Shiramoto, M., Matsuguma, K., Kaji, Y., *et al.* (2017). Recapitulation of Clinical Individual Susceptibility to Drug-Induced QT Prolongation in Healthy Subjects Using iPSC-Derived Cardiomyocytes. Stem Cell Reports *8*, 226-234.

Taylor, R.A., Cowin, P.A., Cunha, G.R., Pera, M., Trounson, A.O., Pedersen, J., and Risbridger, G.P. (2006). Formation of human prostate tissue from embryonic stem cells. Nat Methods *3*, 179-181.

Thompson, I., Tangen, C., Tolcher, A., Crawford, E., Eisenberger, M., and Moinpour, C. (2001). Association of African-American ethnic background with survival in men with metastatic prostate cancer. J Natl Cancer Inst *93*, 219-225.

Yang, R., Jiang, M., Kumar, S.M., Xu, T., Wang, F., Xiang, L., and Xu, X. (2011). Generation of melanocytes from induced pluripotent stem cells. J Invest Dermatol *131*, 2458-2466.

Zabierowski, S.E., Baubet, V., Himes, B., Li, L., Fukunaga-Kalabis, M., Patel, S., McDaid, R., Guerra, M., Gimotty, P., Dahmane, N., *et al.* (2011). Direct reprogramming of melanocytes to neural crest stem-like cells by one defined factor. Stem Cells *29*, 1752-1762.

Zhao, H., Sun, N., Young, S.R., Nolley, R., Santos, J., Wu, J.C., and Peehl, D.M. (2013). Induced pluripotency of human prostatic epithelial cells. PLoS One *8*, e64503.

Zullig, L.L., Jackson, G.L., Dorn, R.A., Provenzale, D.T., McNeil, R., Thomas, C.M., and Kelley, M.J. (2012). Cancer incidence among patients of the U.S. Veterans Affairs Health Care System. Mil Med *177*, 693-701.

FIGURE LEGENDS

Figure 1. Protocols for iPSC reprogramming and prostate differentiation approaches (**A**) iPSC reprogramming from human fibroblasts. (**B**) Feeder inductive co-culture prostate differentiation method. (**C**) Prostate stepwise differentiation (**D**) Prostate direct differentiation.

Figure 2. Prostate direct differentiation (**A**) Protocol for direct prostate differentiation. (**B**) Micrographs of iPS cell differentiation into 2D (**top panels**) and 3D (**bottom panels**) prostate organoids from day 1 to 3 weeks. (**C**) 2D (**top panels**) and 3D (**bottom panels**) Prostate organoids at 4 weeks. (**D**) Time-lapse of prostaspheres release from acinar-like structures.

Figure 3. Prostate differentiation of iPS cells into prostate organoids with PSA-GFP reporter. (**A**) Housekeeping PGK-GFP and PSA-GFP reporters' expression in iPS cells after 4 weeks of transduction. (**B**) Housekeeping PGK-GFP and PSA-GFP reporters expression in 22Rv1 prostate carcinoma cells after 3 days of transduction. (**C**) Prostate differentiation of iPSC expressing PSA-GFP reporter from 1-3 weeks. (**D**) PSA-GFP reporter expression and immunofluorescence co-staining of endogenous PSA (**top panels**) and AR (**bottom panels)** after 4 weeks.

Figure 4. Protocol for genetic selection for iPSC reprogramming and prostate differentiation of African- and European-American fibroblasts. (**A**) General protocol for genetic selection, reprogramming and prostate differentiation. (**B**) Genetic analysis of 39 SNP-AIM's and individual admixture for fibroblasts selection. (**C**) Reprogramming efficiency of African- and European-American derived fibroblasts by number of colonies (**top panels**), size of colonies (**middle panels**) and percentage of alkaline phosphatase expression of clonies (**bottom panels**). (D) Western blot analysis of reprogramming factors during reprogramming of African- and European-American genetically selected fibroblasts at day 1 and at passage 3.

Figure 5. Three germ embryonic differentiation of African- and European American iPSC. (**A**) Ectoderm differentiation and immunofluorescence staining of ectoderm markers SOX1 and OTX2. (**B**) Mesoderm differentiation and immunofluorescence staining of mesoderm markers HAND1 and Brachyury. (**C**) Endoderm differentiation and immunofluorescence of endoderm markers GATA-4 and SOX17.

Figure 6. Expression of Stem cell markers and embryoid body formation in African- and European-American iPSC. (**A**) Co-expression of E-cadherin with OCT4. (**B**) Co-expression of SSEA-4 and OCT4. (**C**) Embryoid body formation of iPSC clones.

Figure 7. Prostate differentiation of African-, European-American and 22Rv1-derived iPSC. (**A**) Phase contrast micrographs of prostate differentiation at 4 weeks. (**B**) Prostate differentiation with PSA-GFP reporter and endogenous expression of AR by immunofluorescence staining.

Supplementary Figure 1. Generation and characterization of iPS cells. (**A**) Representative scanned well of 6-well plates with iPSC colonies in bright field and expression of Alkaline phosphatase live staining. (**B**) Quantification of total and AP-positive colonies. (**C**) Western blots analysis of reprogramming factors expression during iPSC reprogramming at day 1, day 21 and at passage 3. (**D**) Immunifluorescence of stem cell markers expression in iPSC colonies. (**E**) Immunolfuoresence staining of three-germ differentiated iPS cells into ectoderm, mesoderm and endoderm. (**F**) Embryoid bodies generated from iPSC.

Supplementary Figure 2. Feeder Inductive prostate differentiation. (**A**) Protocol for Feeder inductive differentiation. (**B**) Phase contrast micrographs of prostate differentiation from days 1 to 25. (**C-D**) Immunofluoresce staining of organoids for PSA, AR and p63 expression.

Supplementary Figure 3. Stepwise prostate differentiation. (**A**) Protocol for prostate stepwise differentiation. (**B**) Endoderm and prostate fate differentiation steps. (**C**) Endoderm differentiation and immunofluorescence staining of SOX17 expression. (**D**) Prostate stepwise differentiation from 1 to 4 weeks.

Supplementary Figure 4. 2D direct prostate organoid differentiation. (**A**) Prostate direct differentiation of iPS cells with PGK-GFP housekeeping control from day 3 to 3 weeks. (**B**) Immunofluorescence staining of prostate 2D organoids for prostate markers PSA, AR, p63, NKX3.1 and CK18, 2 weeks after differentiation. **Top right** picture highlights in white dashed lines area with enriched prostate differentiation of acinar-like structures expressing PSA. Also, red dashed lines highlight area with no prostate morphogenesis not expressing PSA but showing DAPI staining. **(C)** Immunoflourescence of prostate 2D organoids with prostate markers. Prostate-related markers PSA, AR, p63, NKX3.1, Vimentin, Cytokeratin 5 (CK5), Laminin, HOXB13, Cytokeratin 18 (CK18), prostate specific membrane antigen (PSMA) and FOXA1 are expressed by 2D organoids 4 weeks after differentiation.

Supplementary Figure 5. Immunoflourescence of prostate 3D organoids, prostatspheres and H/E. (**A**) Prostate-related markers PSA, AR, p63, NKX3.1, Vimentin and Cytokeratin 18 (CK18) are expressed by 3D organoids 4 weeks after differentiation. (**B**) Prostate-related markers PSA, AR, p63, NKX3.1 and Cytokeratin 18 (CK18) expression by prostasphere-like cells 4 weeks after differentiation. (**C**) H/E staining of 3D organoid longitudinal sections (**left panels**), cross sections (**middle panels**) and prostasphere-like cells (**right panels**).

Supplementary Figure 6. Genetic Analysis with POPGENE, individual admixture estimates and karyotypes (A) Genetic distance UPGMA dendrogram of 45 DNA samples analyzed with 39 SNP-AIMs. (**B**) Genetic distance UPGMA dendrogram of selected African- and European-American fibroblasts. (**C**) Individual gene admixture ancestral estimates with STRUCTURE for K=2, K=3 and K=4 of 2 African- and 2 European-American samples selected for prostate differentiation. Chromosomal analysis of iPSC selected for prostate differentiation show normal karyotypes in all clones used for prostate differentiation.

Supplementary Figure 7. Generation of iPSC from 22Rv1 cells and prostate differentiation. (**A**) Parental 22Rv1 prostate carcinoma cells (**left**) and 22Rv1-derived iPS cells (**right**). (**B**) Differentiation of 22Rv1-derived iPSC in prostate differentiation medium from day 3 to 3 weeks. PGK-GFP housekeeping reporter was used as control. (**C**) Prostate differentiation of 22Rv1-derived iPSC in prostate differentiation medium from 1 to 3 weeks. PSA-GFP reporter was used to verify the specificity of prostate differentiation.

List of antibodies.

			CONCENTRATION	
Marker	**Company**	**Cat. #**	**WB**	**IF**
OCT4	Cell Signaling	2840	1:1000	1:50
SOX2	R&D Systems	MAB2018	N.A.	1:50
NANOG	Cell Signaling	4903	1:1000	N.A.
GAPDH	Proteintech	60004-1-Ig	1:3000	N.A.

Media, supplements and recombinant proteins used in these studies.

Media/Supplement	**Company**	**Cat. #**
Knockout(tm) Sr;	Thermo Fisher	10828028
DMEM	Thermo Fisher	11995065
DMEM/F-12	Thermo Fisher	11320033
Glutamax	Thermo Fisher	35050061
Knockout(tm) D-mem;	Thermo Fisher	10829018
Matrigel	Corning	356231
bFGF	R&D Systems	233-FB-025
Noggin	R&D Systems	6057-NG-025
LIF	Thermo Fisher	PHC9484
NEAA	Thermo Fisher	11140050
Antibiotics	Thermo Fisher	15140122
Versene	Thermo Fisher	15040066

List of Chemicals and reagents used in these studies.

Protein/Chemical	**Company**	**Cat. #**
Y-27632	AdipoGen	AG-CR1-3564
Valproic Acid	Selleckchem	S1168
CHIR99021	Selleckchem	S1263
RepSox	Selleckchem	S7223
Tranylcypromine	Selleckchem	S4246
Forskolin	Selleckchem	S2449
PD0325901	Selleckchem	S1036
2-Mercaptoethanol	Sigma	M7522

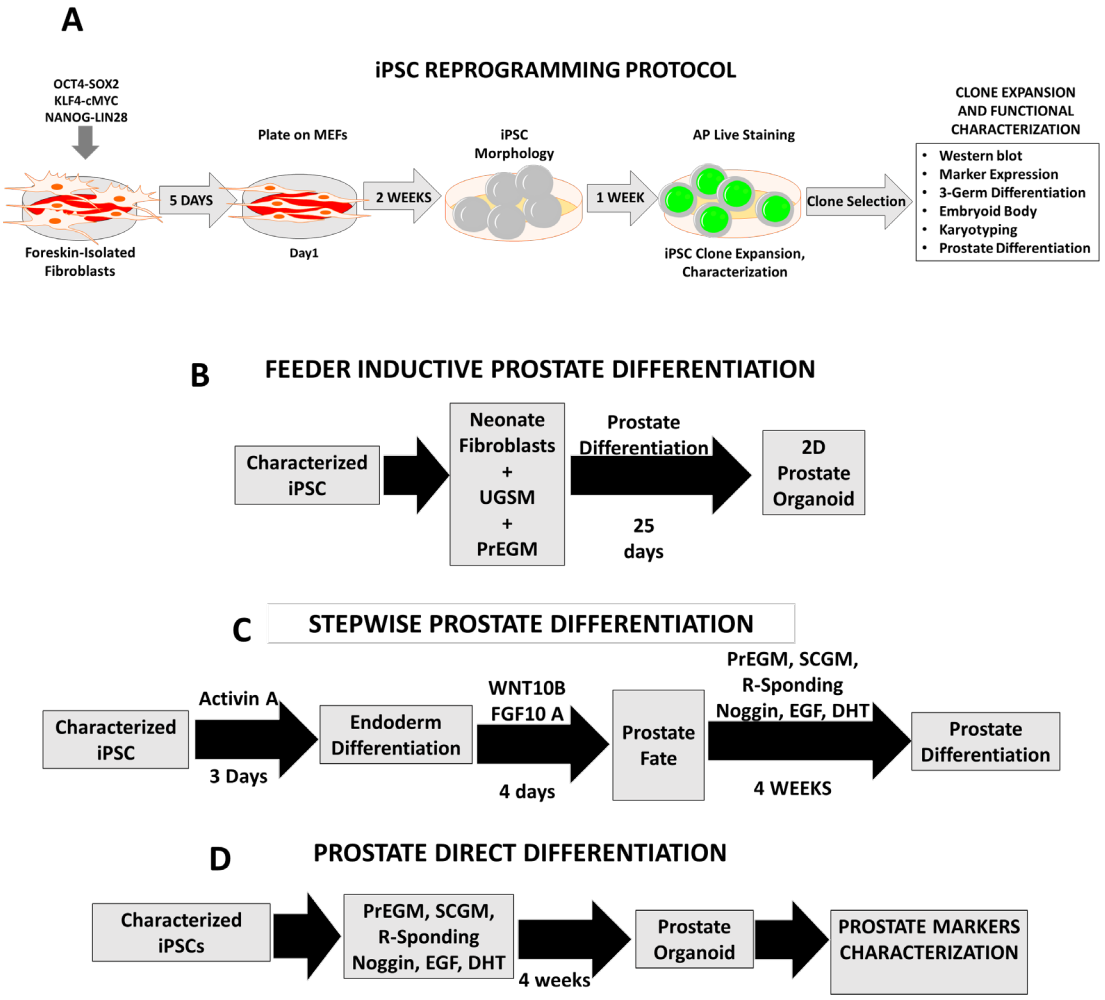
A
iPSC REPROGRAMMING PROTOCOL
OCT4-SOX2
KLF4-cMYC
NANOG-LIN28
Foreskin-Isolated Fibroblasts
5 DAYS
Plate on MEFs
Day1
2 WEEKS
iPSC Morphology
1 WEEK
AP Live Staining
iPSC Clone Expansion, Characterization
Clone Selection
CLONE EXPANSION AND FUNCTIONAL CHARACTERIZATION
Western blot
Marker Expression
3-Germ Differentiation
Embryoid Body
Karyotyping
Prostate Differentiation
B
FEEDER INDUCTIVE PROSTATE DIFFERENTIATION
Characterized iPSC
Neonate Fibroblasts + UGSM + PrEGM
Prostate Differentiation
25 days
2D Prostate Organoid
C
STEPWISE PROSTATE DIFFERENTIATION
Characterized iPSC
Activin A
3 Days
Endoderm Differentiation
WNT10B
FGF10 A
4 days
Prostate Fate
PrEGM, SCGM, R-Sponding Noggin, EGF, DHT
4 WEEKS
Prostate Differentiation
D
PROSTATE DIRECT DIFFERENTIATION
Characterized iPSCs
PrEGM, SCGM, R-Sponding Noggin, EGF, DHT
4 weeks
Prostate Organoid
PROSTATE MARKERS CHARACTERIZATION

FIGURE 1

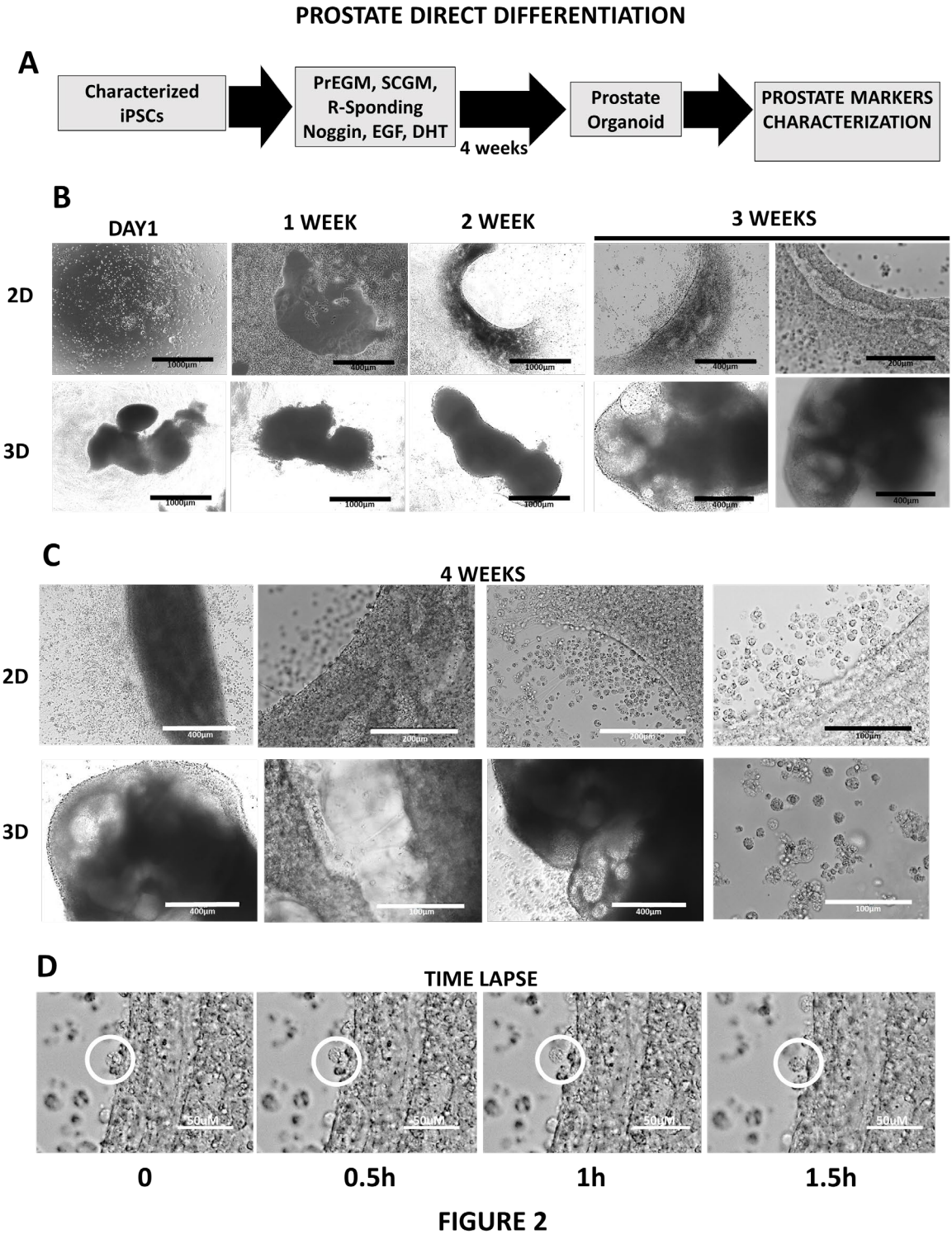
PROSTATE DIRECT DIFFERENTIATION
A
Characterized iPSCs
PrEGM, SCGM, R-Sponding Noggin, EGF, DHT
4 weeks
Prostate Organoid
PROSTATE MARKERS CHARACTERIZATION
B
DAY1
1 WEEK
2 WEEK
3 WEEKS
2D
3D
C
4 WEEKS
2D
3D
D
TIME LAPSE
0
0.5h
1h
1.5h

FIGURE 2

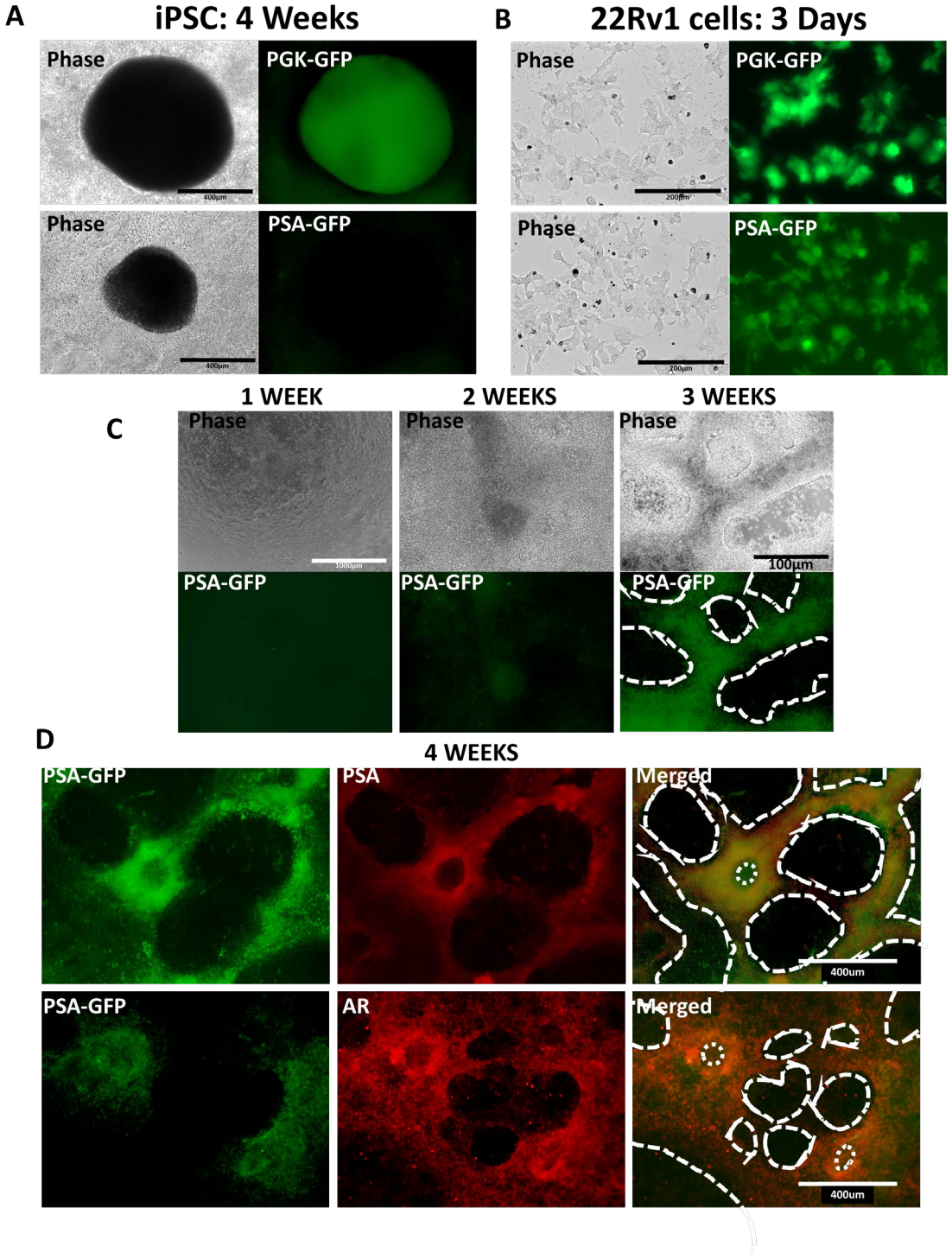
A
iPSC: 4 Weeks
Phase
PGK-GFP
Phase
PSA-GFP
B
22Rv1 cells: 3 Days
Phase
PGK-GFP
Phase
PSA-GFP
C
1 WEEK
2 WEEKS
3 WEEKS
Phase
Phase
Phase
PSA-GFP
PSA-GFP
PSA-GFP
100µm
D
4 WEEKS
PSA-GFP
PSA
Merged
400um
PSA-GFP
AR
Merged
400um

FIGURE 3

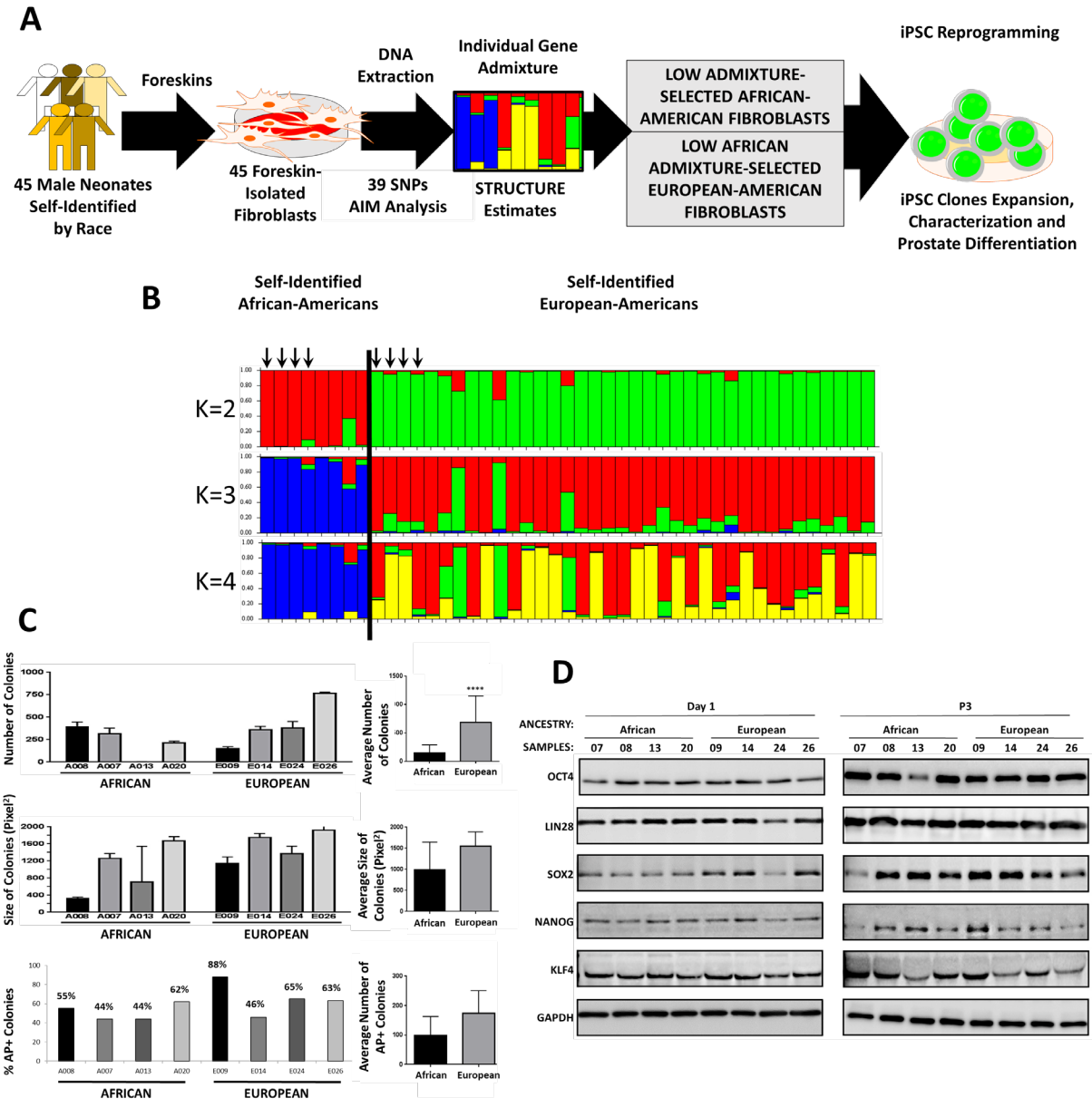
A
Foreskins
45 Male Neonates Self-Identified by Race
45 Foreskin-Isolated Fibroblasts
DNA Extraction
39 SNPs AIM Analysis
Individual Gene Admixture
STRUCTURE Estimates
LOW ADMIXTURE-SELECTED AFRICAN-AMERICAN FIBROBLASTS
LOW AFRICAN ADMIXTURE-SELECTED EUROPEAN-AMERICAN FIBROBLASTS
iPSC Reprogramming
iPSC Clones Expansion, Characterization and Prostate Differentiation
B
Self-Identified African-Americans
Self-Identified European-Americans
K=2
K=3
K=4
C
Number of Colonies
Average Number of Colonies
Size of Colonies (Pixel²)
Average Size of Colonies (Pixel²)
% AP+ Colonies
Average Number of AP+ Colonies
A008 A007 A013 A020 E009 E014 E024 E026
AFRICAN
EUROPEAN
African
European
55% 44% 44% 62% 88% 46% 65% 63%
D
Day 1
P3
ANCESTRY:
SAMPLES:
07 08 13 20 09 14 24 26
OCT4
LIN28
SOX2
NANOG
KLF4
GAPDH

FIGURE 4

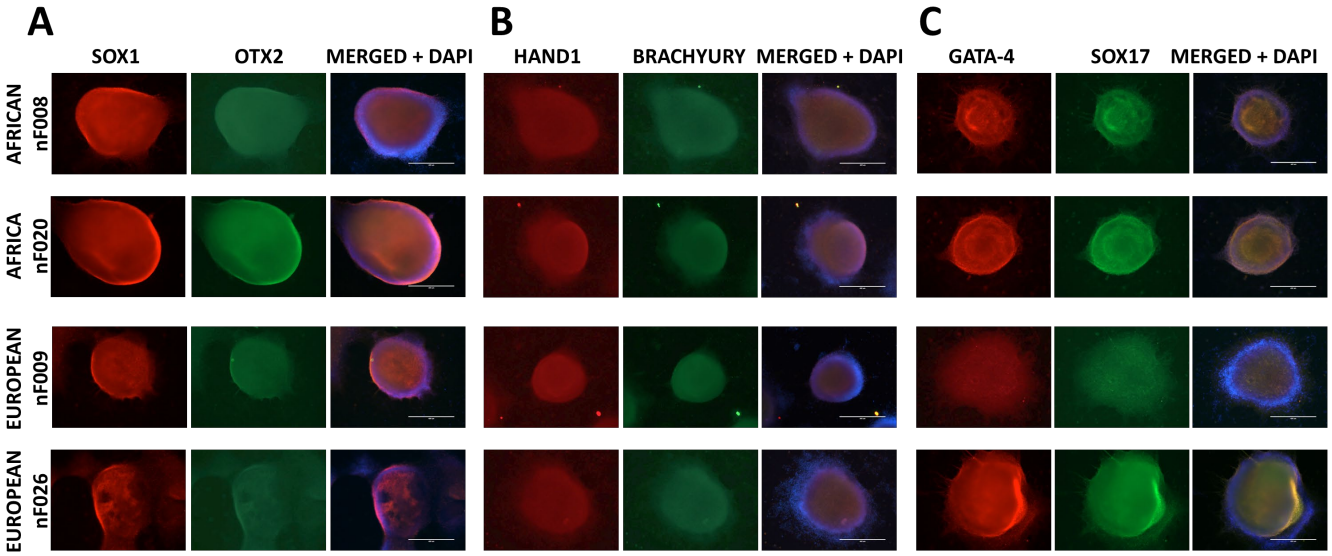
A
SOX1
OTX2
MERGED + DAPI
B
HAND1
BRACHYURY
MERGED + DAPI
C
GATA-4
SOX17
MERGED + DAPI
AFRICAN nF008
AFRICA nF020
EUROPEAN nF009
EUROPEAN nF026

FIGURE 5

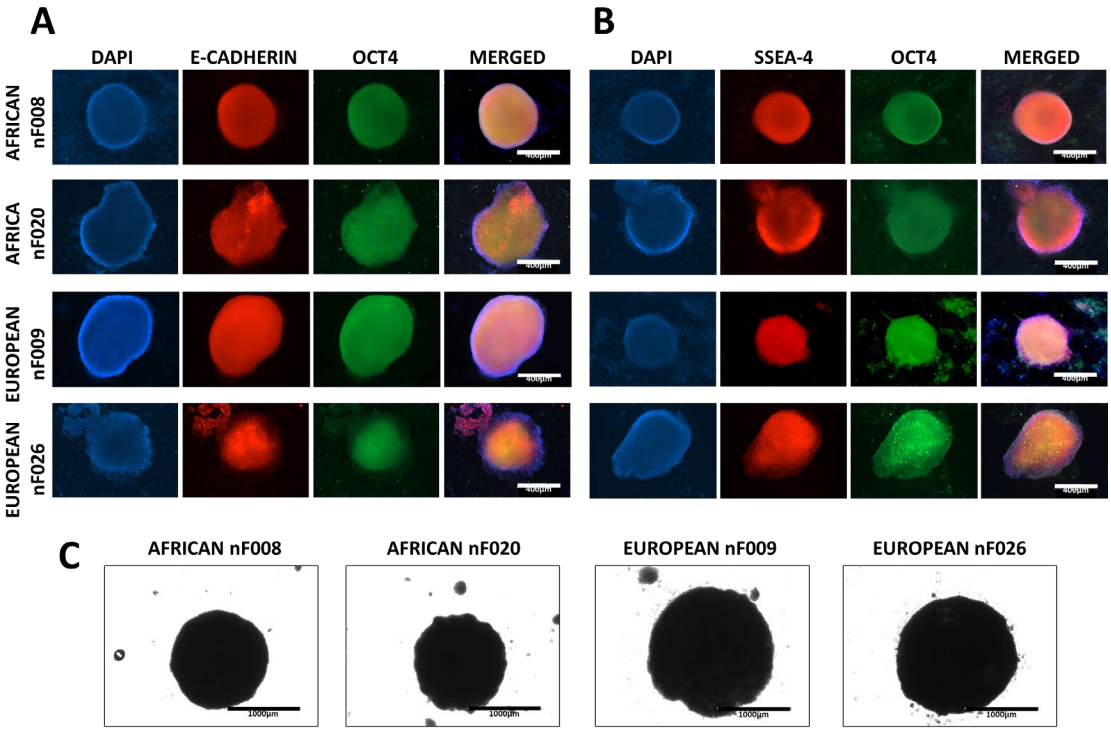
A
DAPI
E-CADHERIN
OCT4
MERGED
AFRICAN nF008
AFRICA nF020
EUROPEAN nF009
EUROPEAN nF026
B
DAPI
SSEA-4
OCT4
MERGED
C
AFRICAN nF008
AFRICAN nF020
EUROPEAN nF009
EUROPEAN nF026

FIGURE 6

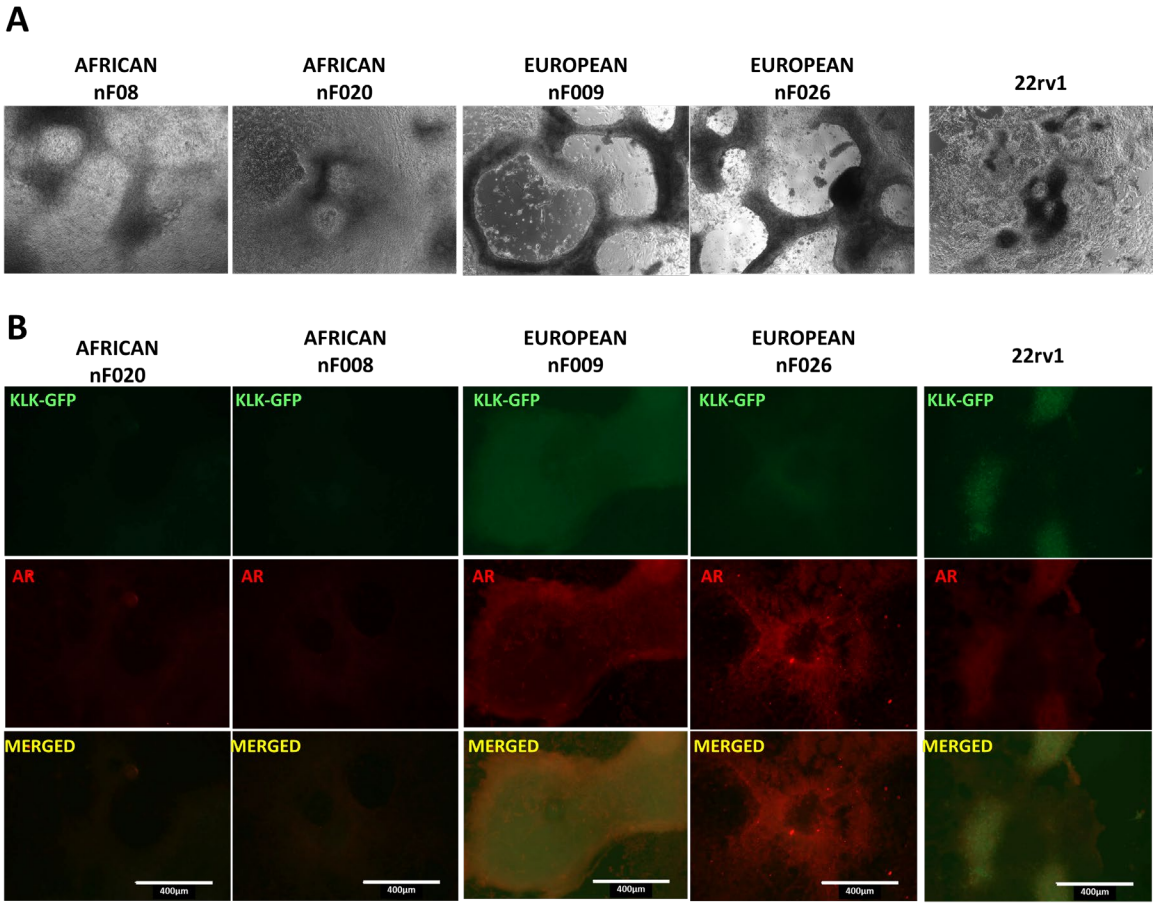
A
AFRICAN
nF08
AFRICAN
nF020
EUROPEAN
nF009
EUROPEAN
nF026
22rv1
B
AFRICAN
nF020
AFRICAN
nF008
EUROPEAN
nF009
EUROPEAN
nF026
22rv1
KLK-GFP
AR
MERGED
400µm

FIGURE 7

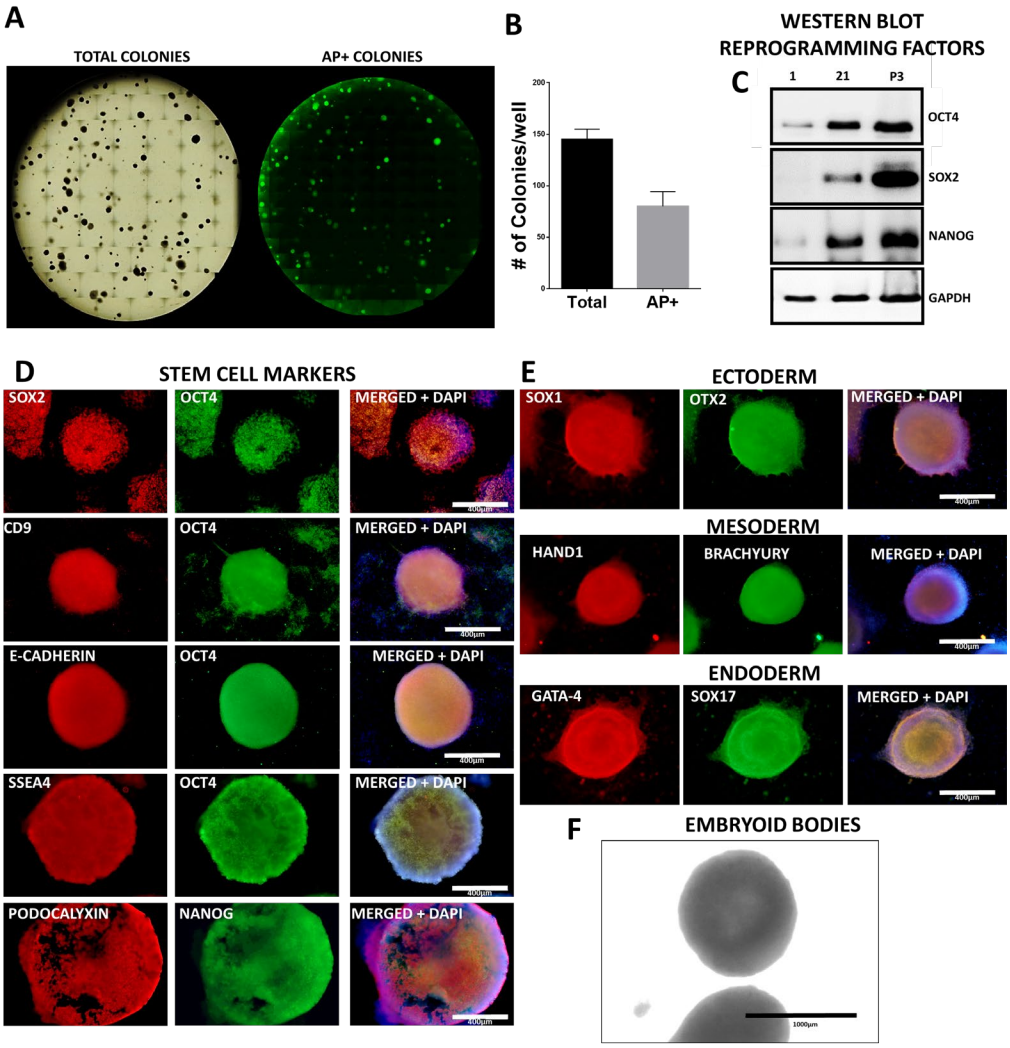

SUPPLEMENTARY FIGURE 1

FEEDER INDUCTIVE PROSTATE DIFFERENTIATION

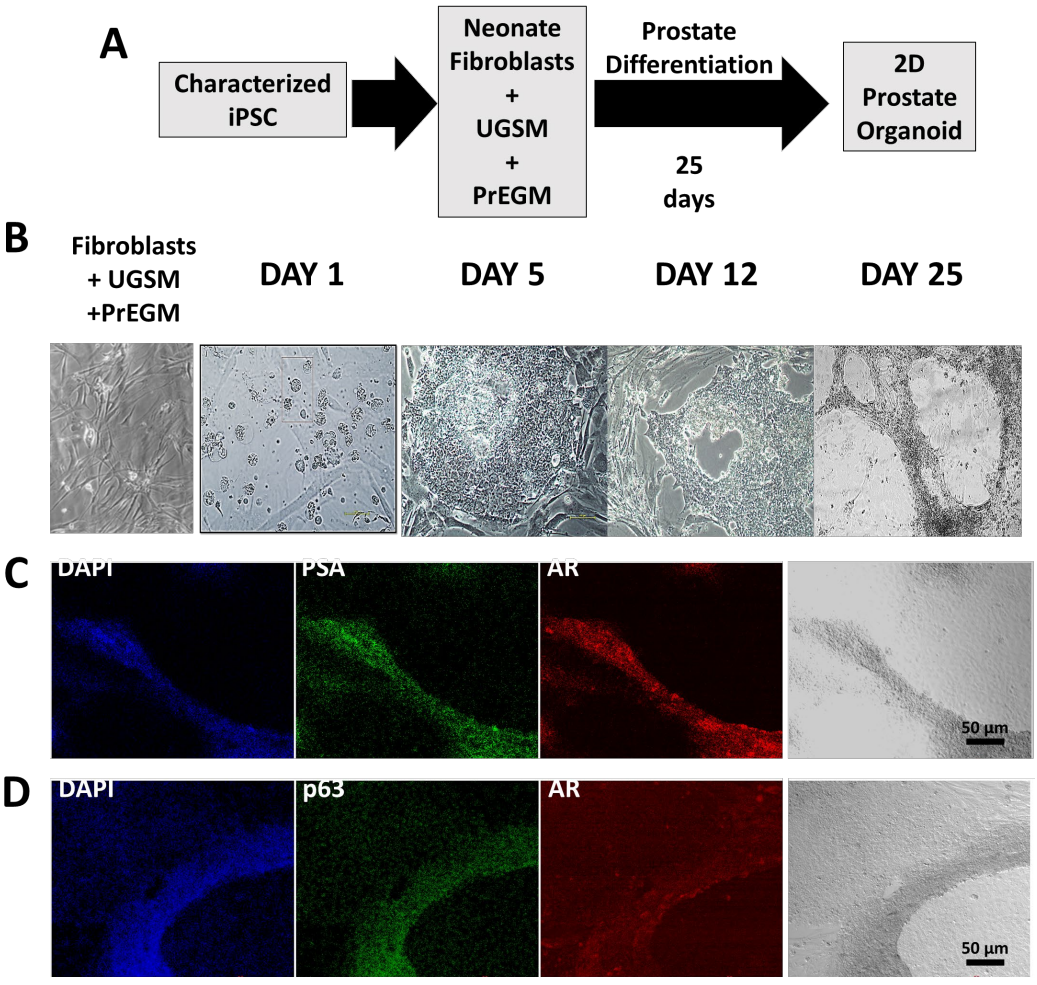

SUPPLEMENTARY FIGURE 2

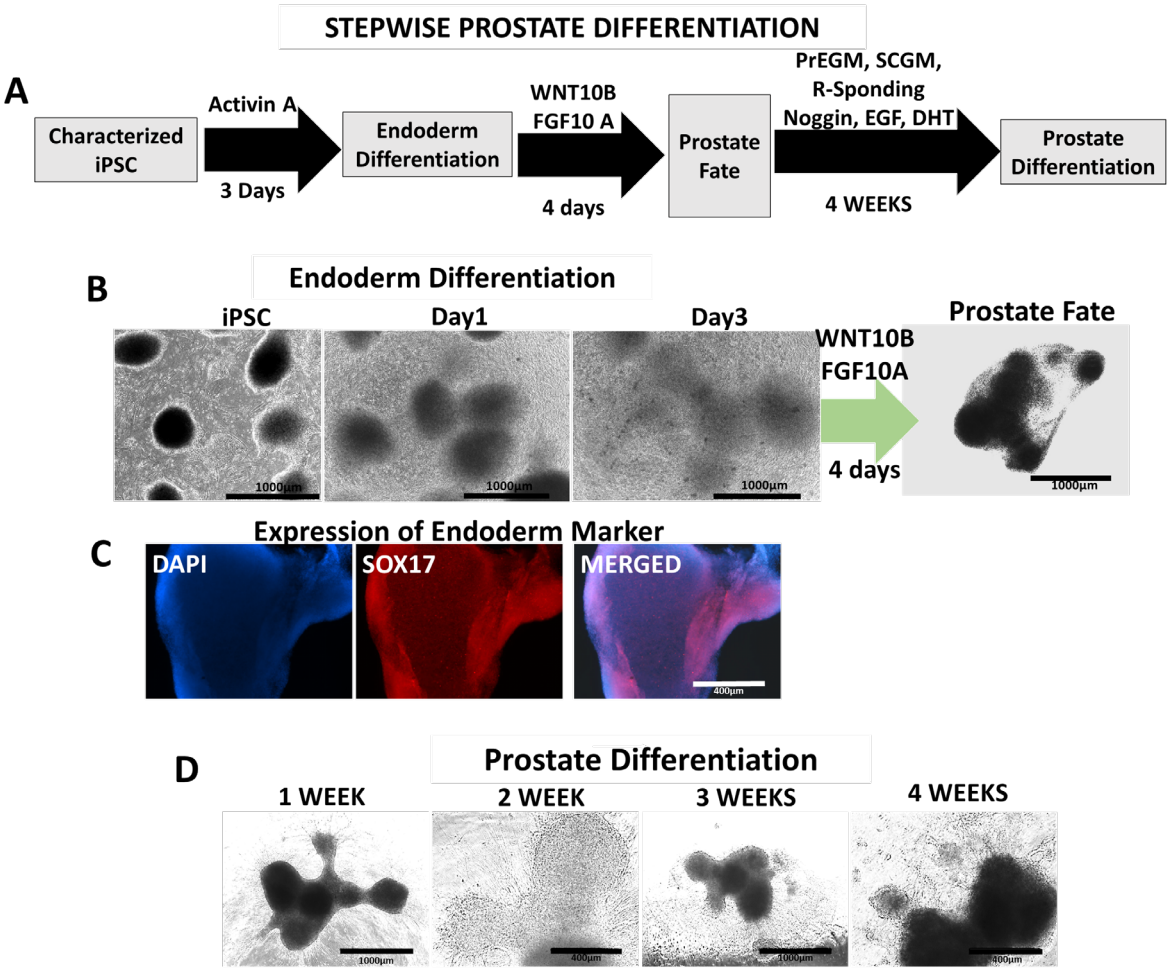

SUPPLEMENTARY FIGURE 3

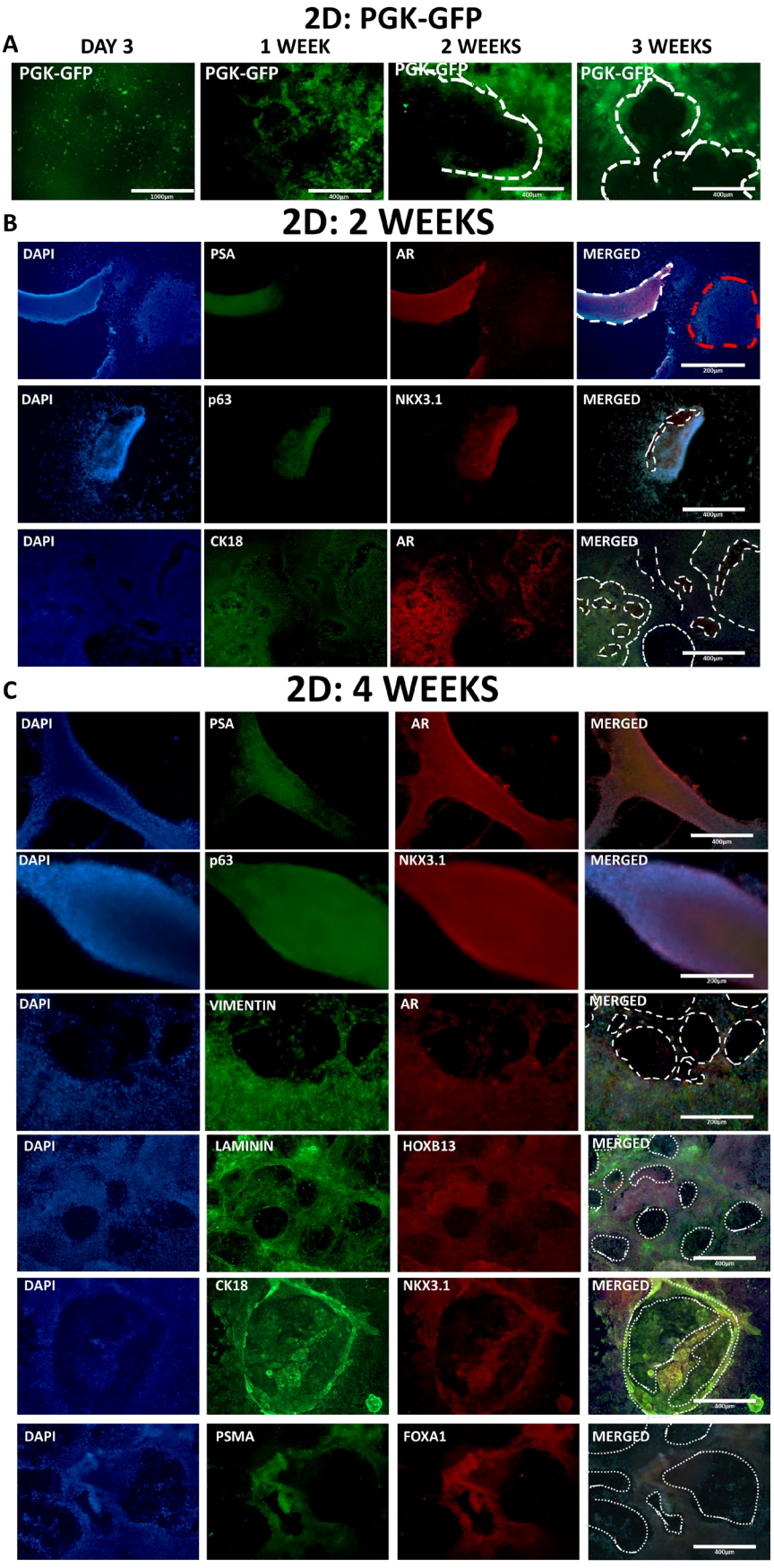

SUPPLEMENTARY FIGURE 4

3D: 4WEEKS

A

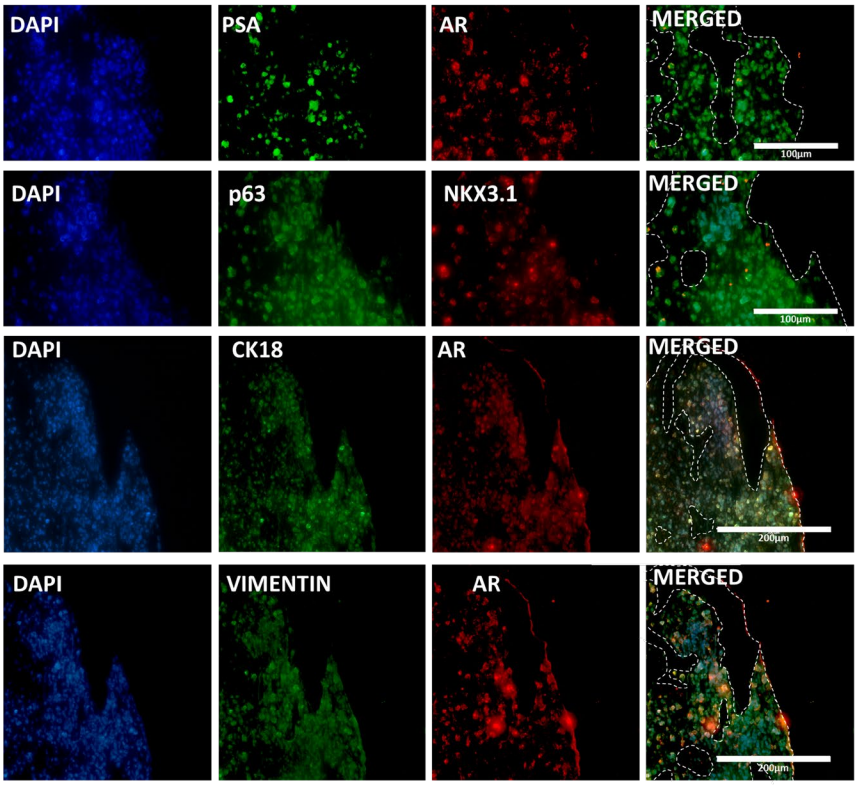

B

PROSTASPHERES: 3D, 4 WEEKS

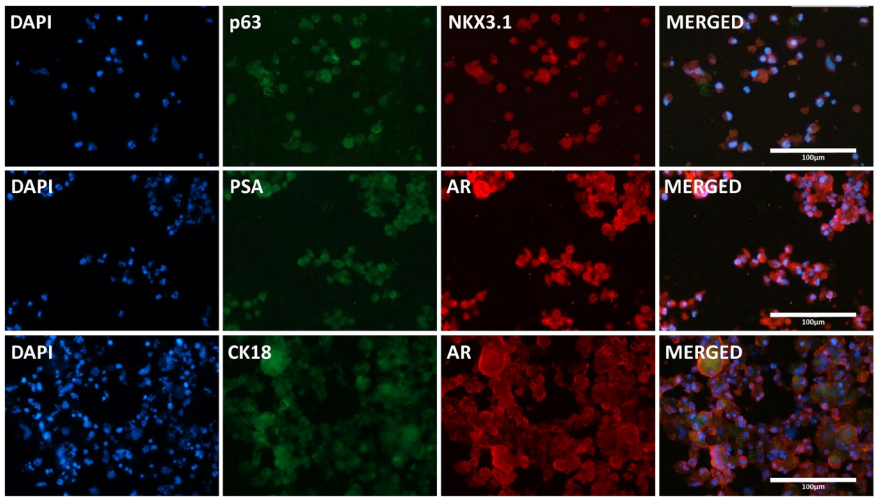

C

HISTOLOGY OF 3D ORGANOID

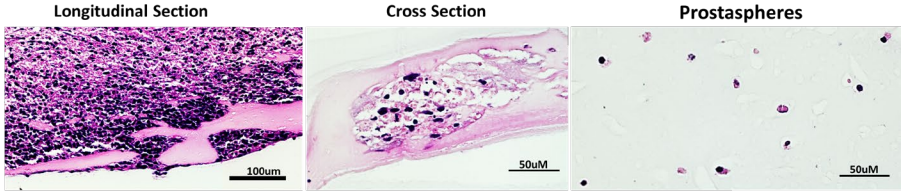

SUPPLEMENTARY FIGURE 5

GENETIC ANALYSIS: POPGENE

A

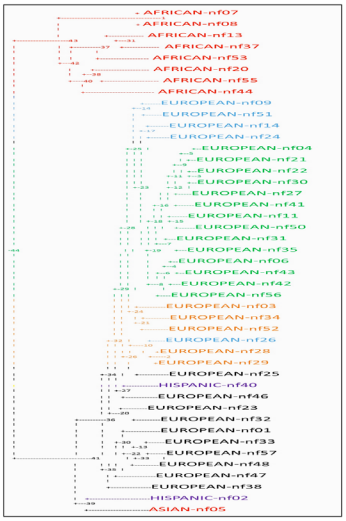

B

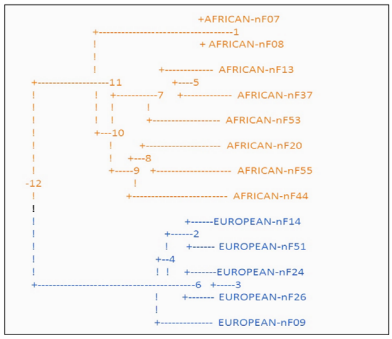

C **Inferred Ancestry of Samples and Chromosomal Analysis**

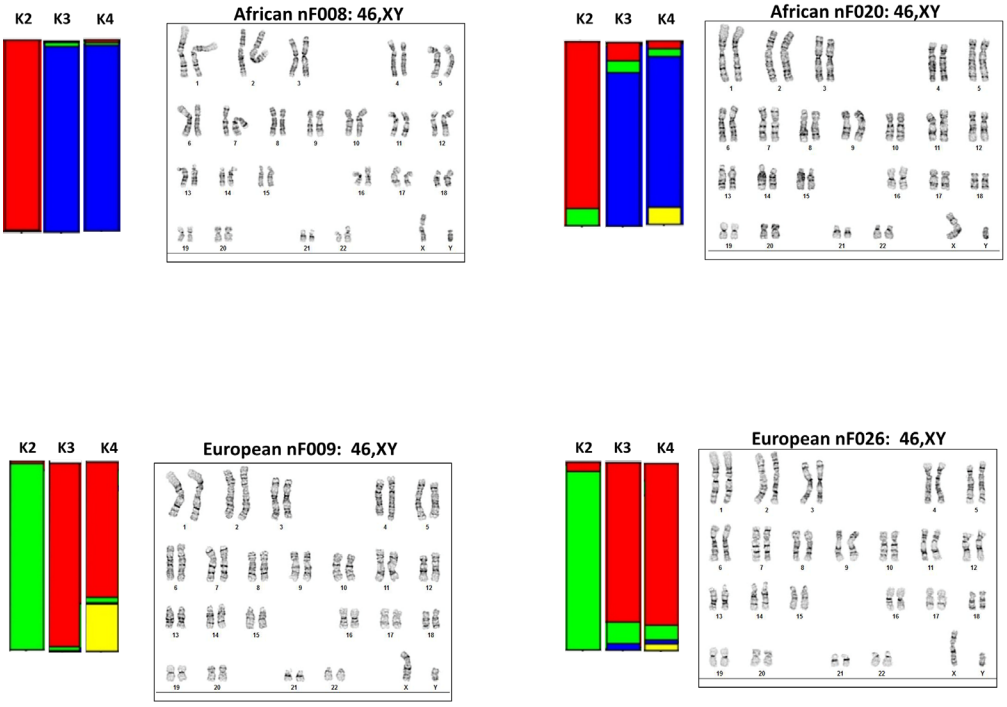

SUPPLEMENTARY FIGURE 6

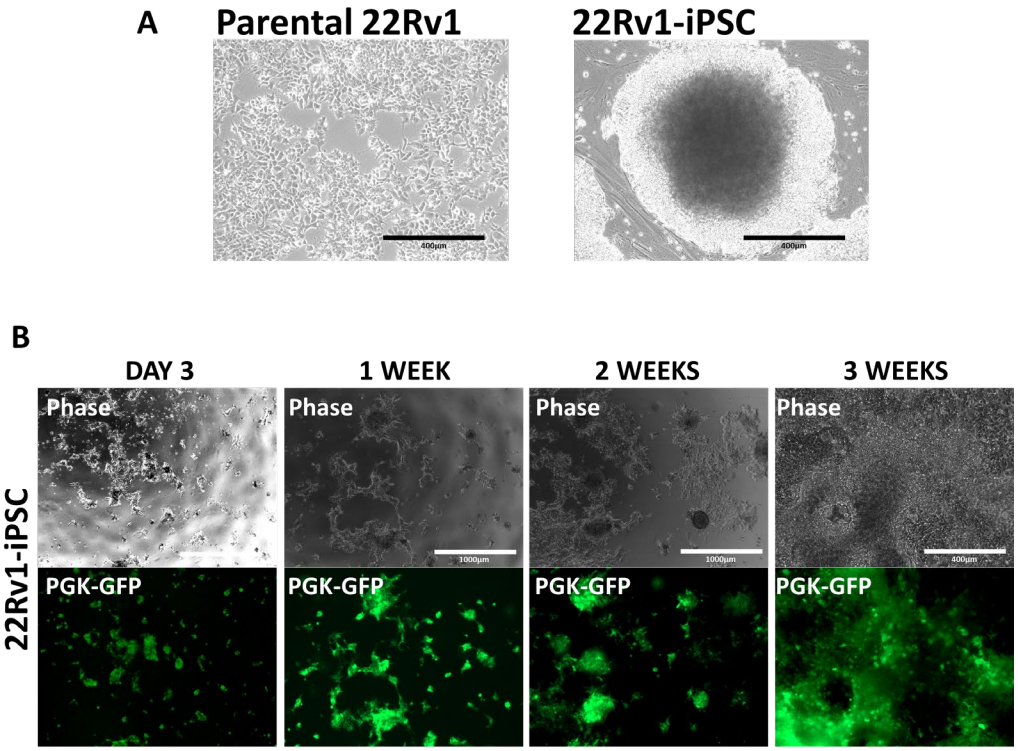

SUPPLEMENTARY FIGURE 7

Stem Cell Reports
Article

OPEN ACCESS

Melanoma Progression Inhibits Pluripotency and Differentiation of Melanoma-Derived iPSCs Produces Cells with Neural-like Mixed Dysplastic Phenotype

Edgardo Castro-Pérez,[1] Carlos I. Rodríguez,[1,4] Dareen Mikheil,[1] Shakir Siddique,[1] Alexandra McCarthy,[1] Michael A. Newton,[3] and Vijayasaradhi Setaluri[1,2,*]

[1]Department of Dermatology, University of Wisconsin School of Medicine and Public Health, Madison, WI 53706, USA
[2]William S. Middleton Memorial Veterans Hospital, Madison, WI 53705, USA
[3]Department of Statistics, Department of Biostatistics and Medical Informatics, University of Wisconsin-Madison, Madison, WI 53706, USA
[4]Present address: Department of Pathology, University of California-San Francisco, 513 Parnassus Avenue, San Francisco, CA 94143, USA
*Correspondence: setaluri@wisc.edu
https://doi.org/10.1016/j.stemcr.2019.05.018

SUMMARY

Melanomas are known to exhibit phenotypic plasticity. However, the role cellular plasticity plays in melanoma tumor progression and drug resistance is not fully understood. Here, we used reprogramming of melanocytes and melanoma cells to induced pluripotent stem cell (iPSCs) to investigate the relationship between cellular plasticity and melanoma progression and mitogen-activated protein kinase (MAPK) inhibitor resistance. We found that melanocyte reprogramming is prevented by the expression of oncogenic BRAF, and in melanoma cells harboring oncogenic BRAF and sensitive to MAPK inhibitors, reprogramming can be restored by inhibition of the activated oncogenic pathway. Our data also suggest that melanoma tumor progression acts as a barrier to reprogramming. Under conditions that promote melanocytic differentiation of fibroblast- and melanocyte-derived iPSCs, melanoma-derived iPSCs exhibited neural cell-like dysplasia and increased MAPK inhibitor resistance. These data suggest that iPSC-like reprogramming and drug resistance of differentiated cells can serve as a model to understand melanoma cell plasticity-dependent mechanisms in recurrence of aggressive drug-resistant melanoma.

INTRODUCTION

Melanoma is the most lethal form of skin disease. Current treatment modalities of metastatic melanoma with mitogen-activated protein kinase inhibitors (MAPKi) and immunotherapy are highly effective in the short term. Unfortunately, development of therapy resistance and recurrence of aggressive therapy-resistant tumors remains a major challenge. Resistance to MAPKi and aggressive recurrence have been associated with melanoma stem cells and stem cell pathways (Roesch et al., 2010). However, the relationship between melanoma plasticity and intrinsic and/or acquired MAPKi drug resistance are not well understood. Tumor cell-derived induced pluripotent stem cells (iPSCs) have been employed as model to study cancer cell plasticity in relation to the tissue/cell of tumor origin and differential response to therapy (Chao et al., 2017; Suknuntha et al., 2015). Attempts have been made to reprogram a limited number of melanoma cell lines into iPSCs (Bernhardt et al., 2017). However, systematic efforts to understand the plasticity of melanoma cells and their ability to generate iPSC-like cells have not been described. It is known, for instance, that cellular and molecular barriers, such as senescence and oncogenic mutations can either repress or enhance reprogramming of cells to iPSCs (Banito et al., 2009; Liu et al., 2015; Mosteiro et al., 2016). Much progress has been made in identifying mutations in melanoma that activate oncogenes, such as *BRAF*, *NRAS*, and *KIT*, and inactivate tumor suppressor genes, such as *PTEN*, *CDKN2A*, and *TP53* (Hodis et al., 2012). The effect of these mutations on the plasticity of the malignant melanocytes and their ability to be reprogrammed is not well understood. Plasticity of cancers including melanoma to differentiate and transdifferentiate has been shown to influence tumor progression and drug sensitivity (Kemper et al., 2014; Roesch et al., 2016; Tsoi et al., 2018). Therefore, understanding the plasticity of malignant melanocytes, including their ability to generate pluripotent cells and differentiate might shed light on mechanisms of melanoma tumor progression and drug resistance. Such an approach was previously employed to understand drug resistance of chronic and acute myeloid leukemia (Chao et al., 2017; Suknuntha et al., 2015).

Here, we describe studies on reprogramming of melanocytes and primary and metastatic melanoma cells into iPSC-like cells and their ability to retain melanocytic differentiation. We show that (1) compared with skin fibroblasts and melanocytes, reprogramming of melanoma cells to iPSCs is less efficient, and metastatic melanoma cells are more resistant to reprogramming than primary melanoma cells derived from the same patient, (2) expression of $BRAF^{V600E}$ inhibits reprogramming of melanocytes, and inhibition of $BRAF^{V600E}$ facilitates reprogramming of $BRAF^{V600E}$ mutant, BRAF inhibitor-sensitive metastatic melanoma cells, (3) although melanoma-derived iPSCs

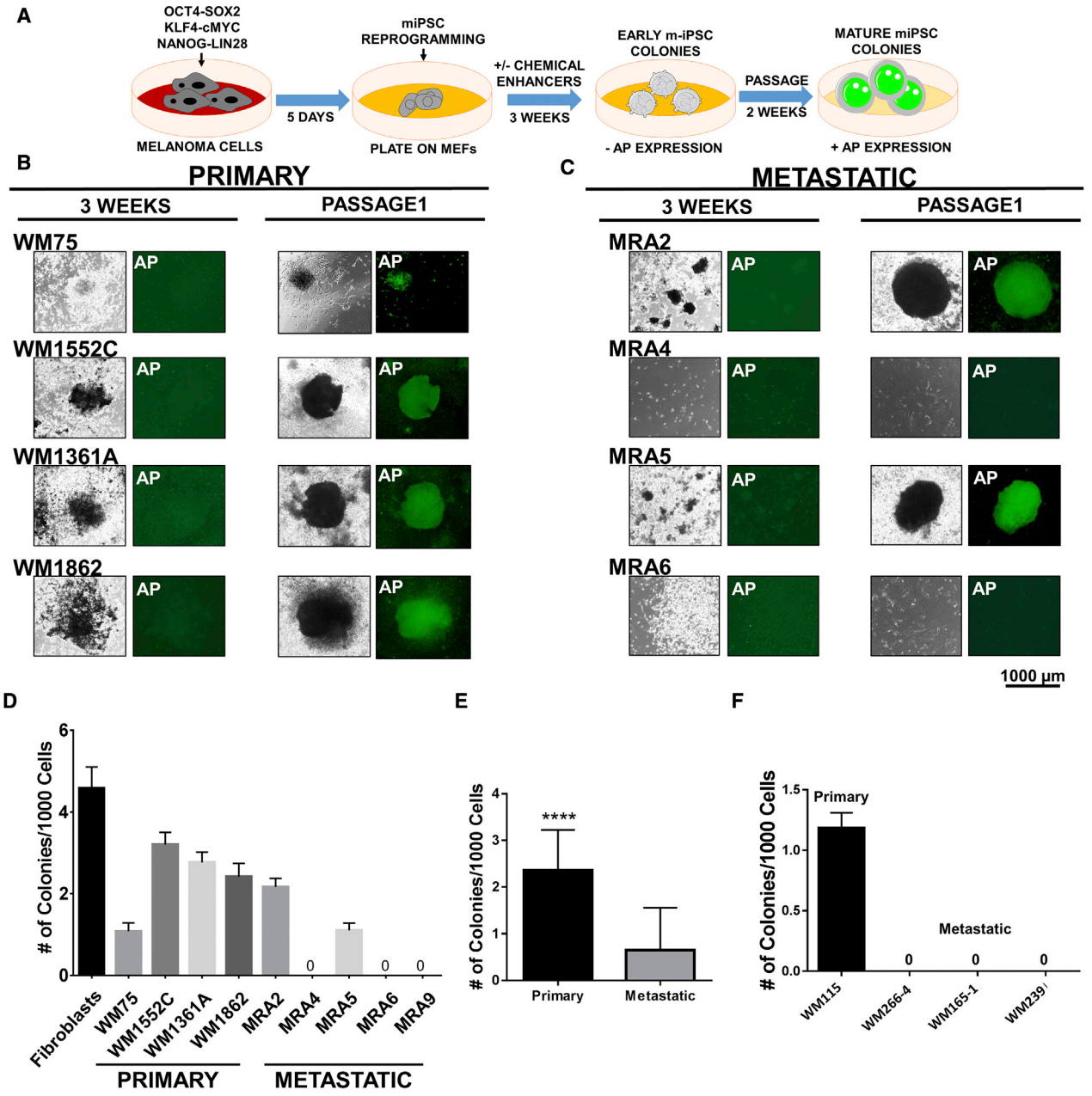

(legend on next page)

(miPSCs) are able to differentiate into cells of the three germ layers, they failed to (re)differentiate into melanocytes, but displayed a neuronal-like dysplastic phenotype *in vitro* and *in vivo*, and (4) miPSC-differentiated cells exhibit increased resistance to MAPKi. We propose that iPSC reprogramming of melanoma cells and differentiation of miPSCs can serve as a model to understand the mechanisms of recurrence of aggressive MAPKi-resistant tumors.

RESULTS

Melanoma Cells Exhibit Resistance to Reprogramming to iPSCs

First, we asked whether melanoma cells retain the plasticity to be reprogrammed to iPSC-like cells. To test this, we transduced four primary melanoma cell lines WM75, WM1552C, WM1361A, and WM1862, and five patient-derived early passage (less than 30 passages) metastatic melanoma cell lines MRA2, MRA4, MRA5, MRA6, and MRA9 (Table S1) with lentiviruses for reprogramming factors, OCT4-SOX2, NANOG-LIN28, and KLF4-cMYC, and cultured them in reprogramming medium on mouse embryonic fibroblast (MEF) feeders (Figure 1A). As controls, we identically performed reprogramming of human neonatal foreskin-derived fibroblasts and melanocytes. After 1 week, transduced fibroblasts and melanocytes, but not melanoma cells, produced granular colonies, which are early indicators of iPSC induction.

We asked whether addition of chemical agents that are known to enhance reprogramming could improve the reprograming of melanoma cells (Hou et al., 2013). These chemical agents include valproic acid (VPA), an HDAC inhibitor; CHIR-99021, a GSK-3α/β inhibitor, forskolin (FSK), an activator of adenylyl cyclase/cAMP pathway, tranylcypromine (TCP), a histone lysine-specific demethylase 1 inhibitor; and RepSox, an inhibitor of the TGF-βR-1/ALK5 pathway. After an additional 2 weeks of culture containing these compounds, fibroblasts and melanocytes generated colonies (Figure S1A). At this time (3 weeks from induction), all primary melanoma cell lines also generated iPSC-like colonies without the addition of chemicals (data not shown), but the presence of chemical boosters enhanced their ability to form such colonies. In contrast, among the metastatic melanoma cell lines, only MRA2 and MRA5 generated colonies. However, neither primary nor metastatic miPSCs exhibited alkaline phosphatase (AP) expression (Figures 1B and 1C, left panels), in contrast to the strong AP activity in fibroblast- and melanocyte-derived iPSC colonies (Figure S1A). Metastatic cells did not exhibit reprogramming in the absence of chemical enhancers (data not shown). These data suggest that malignant melanocytes, specifically metastatic melanoma cells, are resistant (less plastic) to reprogramming into iPSC-like state compared with normal melanocytes.

After first passage, miPSC colonies expressed AP and were comparable with fibroblast-iPSCs (Figures 1B and 1C, right panels). We quantitated the reprogramming efficiency by counting the colonies generated after first passage (no. of colonies/1,000 cells plated). As shown in Figures 1D and 1E, primary melanoma cell lines generated significantly higher number of iPSC-like colonies than metastatic melanoma cell lines. We verified the time course expression of the reprogramming factors by western blotting. Data in Figure 1G show that melanoma cell lines, including those that did not generate iPSC colonies, showed expression of the reprogramming factors before culture on MEF, demonstrating that failure to generate iPSCs is not due to the lack of expression of the reprogramming factors.

Loss of Plasticity Is Associated with Melanoma Tumor Progression

To test whether the loss of plasticity of metastatic cells for reprogramming to stem cell state is related to melanoma tumor progression, we performed reprogramming of a set of primary and metastatic melanoma cell lines derived from the same patient. WM115 is a vertical growth phase primary melanoma cell line and WM266-4, WM165-1, and WM239A are cell lines derived from lymph node metastatic lesions in the same patient (Herlyn et al., 1985). This matched set of primary and metastatic cell lines were

Figure 1. Reprogramming of Primary and Metastatic Melanoma Cells into miPSCs

(A) Schematic of the protocol for reprogramming melanoma cells to miPSCs.

(B and C) Reprograming progress of primary (B) and metastatic (C) cells at 3 weeks and passage 1 and expression of AP at each time point. All data shown are for colonies generated using pluripotency enhancing agents.

(D) Quantification of miPSC colony formation shown as number of colonies/1,000 plated cells. Data (mean ± SD; n = 6 replicate wells for each cell line) from a representative experiment ($n \geq 3$) are shown.

(E) Aggregate number of miPSC colonies generated from primary and metastatic melanoma cell lines. Pooled data for one experiment with four primary and five metastatic melanoma cell lines (n = 6 replicate wells for each cell line) are shown. Student's t test, ****$p < 0.0001$.

(F) Reprogramming of primary and metastatic cell lines established from the same patient. Data (mean ± SD; n = 6 replicate wells for each cell line) from one experiment are shown.

(G) Western blot analysis of reprogramming factors OCT4, NANOG, and c-Myc during reprogramming: parental cells baseline, nontransduced control (C), 1 and 5 days after transduction; and miPSCs at passage 3. GAPDH shows equal loading.

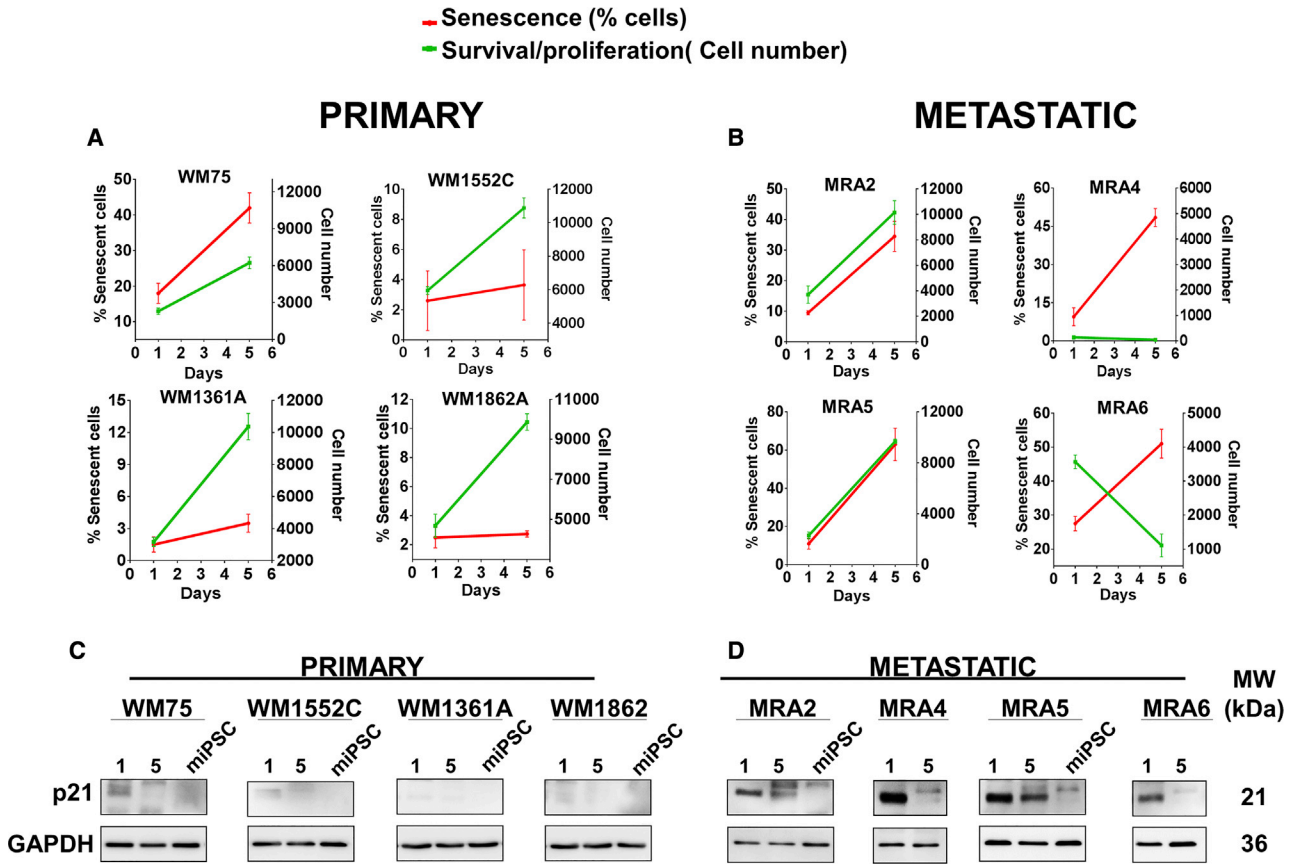

Figure 2. Effect of Transduction with Reprogramming Factors on Senescence and Cell Proliferation

(A and B) Primary (A) and metastatic (B) melanoma cells senescence (red lines) and survival/proliferation (green lines). Data (mean ± SD; n = 3 replicate wells/cell line for each time point) are shown. Approximately 5,000 cells/well of 24-well plates were seeded and transduced with reprogramming factor lentiviruses (day 0) and all wells were scanned using an EVOS FL Auto microscope, and cell number and percent SA-β-gal-stained cells were estimated using ImageJ analysis of the scanned images.

(C and D) Western blot analysis of p21 expression at 1 and 5 days after transduction in primary (C) and metastatic cells (D) and at miPSC stage. GAPDH shows equal loading.

subjected to iPSC reprogramming (Figures 1F and S1B). After 2 weeks in passage 1, primary cell line WM115, but none of the three metastatic lines, generated iPSC-like colonies. Even addition of chemical enhancers did not improve the reprogramming of the matched metastatic cells suggesting that loss of plasticity for reprogramming to iPSC-like state is associated with melanoma tumor progression.

Senescence and Cell Death Are Inversely Related with Reprogramming

We asked which factors might be responsible for the limited plasticity of metastatic melanoma cells. Senescence and cell death has been reported to influence the efficiency of reprogramming of cells to iPSCs *in vitro* and *in vivo* (Banito et al., 2009; Mosteiro et al., 2016). We asked if senescence induction on reprogramming could be a barrier for iPSC generation by metastatic melanoma cells. We evaluated the effect of transduction with the reprogramming factors on senescence and proliferation of melanoma cells. We scanned the wells (using an EVOS FL Auto microscope) on days 1 and 5 posttransduction with the reprogramming factors, and estimated cell number and percent senescent cells (senescence-associated β-galactosidase [SA-β-gal] stained) in each well (ImageJ analysis of acquired microscope images) (Figures 2A, 2B, and S2). Data showed that metastatic melanoma cells lines MRA4 and MRA6 transduced with the reprogramming factors failed to survive, suggesting that decreased cell survival affected their reprogramming. Quantitation of SA-β-gal staining showed that there was little or no induction of senescence in most primary melanoma cells, whereas transduction with the reprogramming factors induced senescence in metastatic melanoma cells. Activation of senescence was confirmed

by expression of p21 (Figures 2C and 2D), a commonly used marker to evaluate senescence during iPSC reprogramming *in vitro* and *in vivo* (Banito et al., 2009; Mosteiro et al., 2016). There was higher expression of the senescence marker p21 in metastatic than in primary cells (Figures 2C and 2D) and it remained relatively high up to 5 days. When miPSCs were generated, p21 expression was not detected in primary- or metastatic-derived miPSCs. In primary melanoma cells, p21 expression was not significantly altered on transduction. Importantly, double staining for SA-β-gal and reprogramming factor OCT4 showed that the SA-β-gal-positive senescent cells had no expression of the reprogramming factor OCT4 (Figures S2C and S2D, arrows), whereas cells with low/no SA-β-gal staining exhibited high OCT expression. These data show mutually exclusive expression of the reprogramming factors and the senescence marker, thus correlating with reprogramming efficiency.

Expression of Oncogenic BRAF^{V600E} Inhibits Reprogramming

In melanocytes, mutations in BRAF lead to the activation of oncogene-induced senescence (Dhomen et al., 2009; Michaloglou et al., 2005). In addition, oncogene activation such as *TP53* has been reported to act as a barrier to reprogramming to pluripotent cells (Liu et al., 2015). We noted that BRAF^{V600E} mutant melanoma cell lines MRA5 and MRA6 showed low efficiency or no reprogramming to iPSCs (Figure 1). Therefore, we sought to evaluate the effect of expression of oncogenic BRAF^{V600E} on melanocyte plasticity. We transduced normal human melanocytes with BRAF^{V600E}-GFP, empty vector-GFP, or NOTCH intracellular active domain (NICD-GFP) lentiviruses followed (after 1–2 weeks) by lentiviruses for reprogramming. As shown in Figure 3, while empty vector-transduced melanocytes efficiently generated iPSC colonies, BRAF^{V600E}-transduced melanocytes did not produce iPSC colonies even in the presence of chemical inducers. NICD-expressing melanocytes formed iPSC colonies, suggesting that the effect of BRAF^{V600E} on inhibition of reprogramming is highly specific and not due to a nonspecific overexpression of a signaling protein.

Expression of Stem Cell Markers in miPSCs

To characterize the iPSC-like cells generated from melanoma cells (miPSCs), we verified the co-expression of reprogramming factors OCT4 and SOX2 with stem cell surface markers SSEA4 (stage-specific embryonic antigen-4) and CDH1 (E-cadherin) (Figures S3A–S3C). Double staining of OCT4 and SOX2 showed that expression of these factors was consistent with live-cell AP staining (Figures 1B and 1C) and expression of reprogramming factors determined by western blots (Figure 1G). An exception to this observation was WM115, which showed weak expression of OCT4 and SOX2, and also weak AP activity (Figure S1B). E-Cadherin expression was higher in WM1862- and MRA2-derived miPSCs than most cells. Primary melanoma WM115, WM1862, and metastatic MRA2-derived miPSCs had higher expression of surface marker SSE4 than miPSCs derived from other cells.

Embryoid Body Formation by miPSCs

To further characterize the stem cell features of miPSCs, we performed embryoid body (EB) formation assays by the hanging drop method for up to 3 weeks (Figure S3D). WM115-, WM1862-, and MRA2-derived miPSCs, but not WM1552C-, WM1361A-, and MRA5-derived miPSCs formed EBs. The ability to form EBs appeared to correlate with strong expression of stem cell surface markers SSEA4 and E-cadherin, which are stem cell surface markers involved in cell-cell contacts necessary for efficient EB formation (Choi et al., 2014). Accordingly, EB-forming WM1862 and MRA2 miPSCs showed strong expression of both SSEA4 and E-cadherin, similar to fibroblast-derived iPSCs, whereas WM1552C miPSCs showed weak expression of E-cadherin and SSEA4; MRA5 miPSCs, on the other hand, expressed E-cadherin but not SSEA4. An exception to this pattern was WM115 miPSCs, which, despite showing low expression of AP, expressed SSEA4 but not E-cadherin and produced small EBs. Importantly, however, the ability of melanoma-iPSCs to form EBs does not seem to be the limiting factor for their differentiation into three germ layers (Figure 4), melanocytes (Figure 5C) and neural cells (Figure S6).

miPSCs Differentiate into Three Germ Layers

Pluripotency of miPSCs was assessed using *in vitro* differentiation assays and immunofluorescence staining for early markers specific for the three germ layers ectoderm, mesoderm, and endoderm (Deshpande et al., 2017; Shinozawa et al., 2017). Differentiation of miPSCs to ectoderm was verified by OTX2 expression, to mesoderm by the expression of BRACHYURY, and to endoderm by the expression of SOX17. Data in Figure 4 show that all miPSCs were able to differentiate into precursors of the three germ layers.

miPSCs Do Not Differentiate into Melanocytes but Show Neural-like Dysplasia

We next asked whether miPSCs can differentiate back to melanocyte/melanocyte-like cells. First, we validated the protocol and conditions for melanocyte differentiation using fibroblast- and melanocyte-derived iPSCs. As expected, when cultured in melanocyte differentiation medium, both fibroblast- and melanocyte-derived iPSCs generated pigmented cells (Figures 5A and 5B). Immunofluorescence

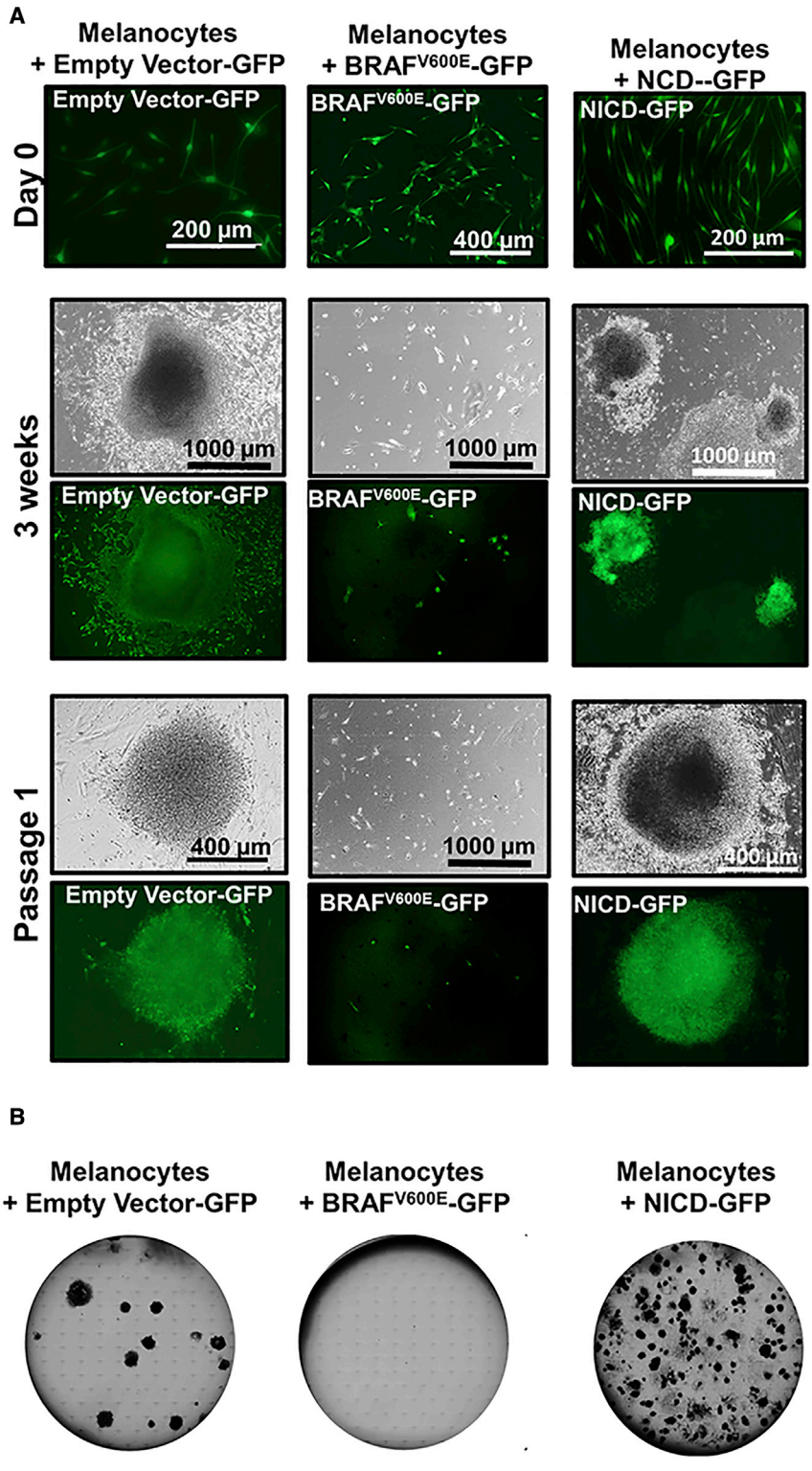

Figure 3. Effect of BRAF^{V600E} Expression on Reprogramming

(A) Top panels (day 0), from left to right, show melanocytes transduced with empty vector-GFP (control), BRAF^{V600}-GFP, or NICD-GFP lentiviruses. Middle panels (3 weeks), show colony formation in empty vector-GFP and NICD-GFP cells. Bottom panels (passage 1), show miPSC colony maturation of empty vector-GFP transduced and NCID-GFP-expressing cells. BRAF^{V600}-GFP-expressing cells did not exhibit reprogramming.

(B) Representative images of colonies (passage 1) growing for 2 weeks in six-well plates (n = 3 replicate wells) from one experiment are shown.

staining showed that these cells differentiated from fibroblast-derived iPSCs expressed MITF and SOX10, but did not express TUJ1, the neuronal marker neuronal tubulin β-III (TUBB) (Figure 5D).

In contrast, miPSCs cultured in melanocyte differentiation medium, did not generate cells with melanocytic features, but dysplastic cells with neural-like features (Figure 5A), and co-expressed melanocyte marker MITF

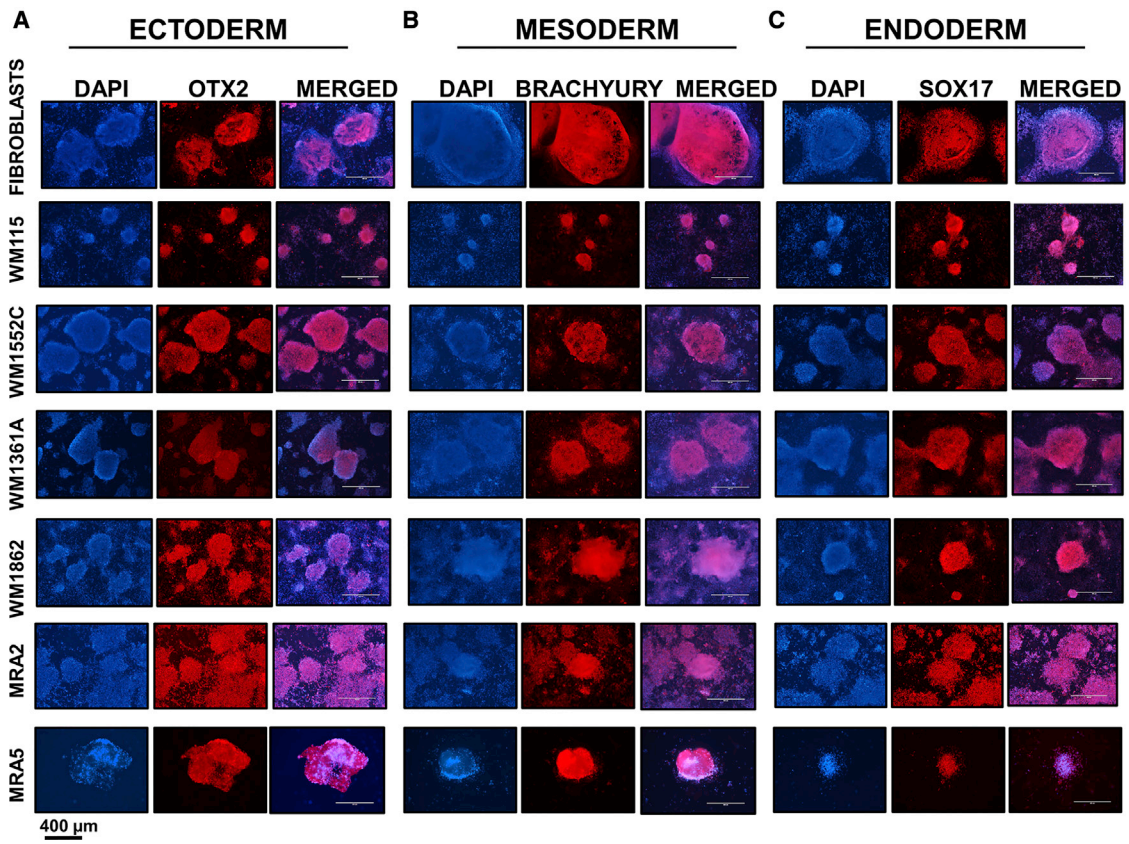

Figure 4. Differentiation of Fibroblast-iPSCs and miPSCs to Precursors of Three Germ Layers

(A) Ectoderm differentiation and expression of ectoderm marker OTX2.

(B) Mesoderm differentiation and expression of mesoderm marker BRACHYURY.

(C) Endoderm differentiation and expression of endoderm marker SOX17.

with neural markers TUBB3, MAP2, and GFAP (Figures 5E and 5F). Unlike fibroblast- and melanocyte-iPSC-differentiated cells in melanocyte differentiation medium, none of melanoma-iPSCs showed either melanocyte morphology or pigmentation. Although the parental metastatic melanoma MRA2 cells were pigmented, they lost pigment after iPSC reprogramming and did not recover pigmentation. Importantly, cells differentiated in melanocyte differentiation medium no longer displayed iPSC morphology or expression of reprogramming factors (Figure S4A).

To further evaluate melanocyte/neural differentiation, we determined the expression of melanocyte markers SOX10 and MITF; and neuronal markers TUBB3 and MAP2 in parental and melanoma-iPSC-differentiated (miPSC differentiated) in melanocyte differentiation medium. Interestingly, most parental melanoma cell lines and miPSC-differentiated cells expressed relatively low levels of melanocyte markers MITF and SOX10 (Figures S4B and S5A). The pigmented MRA2 parental cells showed the strongest expression of melanocyte markers, but differentiated cells exhibited weak expression of these melanocyte markers. In contrast, neural markers in parental and miPSC-differentiated cells exhibited stronger expression than melanocyte markers (Figures S4C and S5B). Cells differentiated from MRA2-miPSCs showed relatively weak expression of TUBB3 and MAP2, but expression of these markers was strong in cells with neural-like dysplastic morphology (Figures S4C and S5B, arrows).

In view of the neural-like dysplasia exhibited by cells differentiated from miPSCs, we sought to also evaluate the ability of these cells to differentiate along neuronal lineage. We performed neuronal differentiation of fibroblast- and melanocyte-derived iPSCs and found that they generated neuronal-like cells that express neuronal markers (Figures 5D and S6). When cultured in neuronal differentiation medium, melanoma-iPSCs were able to differentiate into cells with neuronal-like morphology and expressed terminal neuronal differentiation markers TUBB3, SYN1 (Synapsin 1), and MAP2 (Figure S6), whereas MRA2-derived miPSCs even expressed the glial

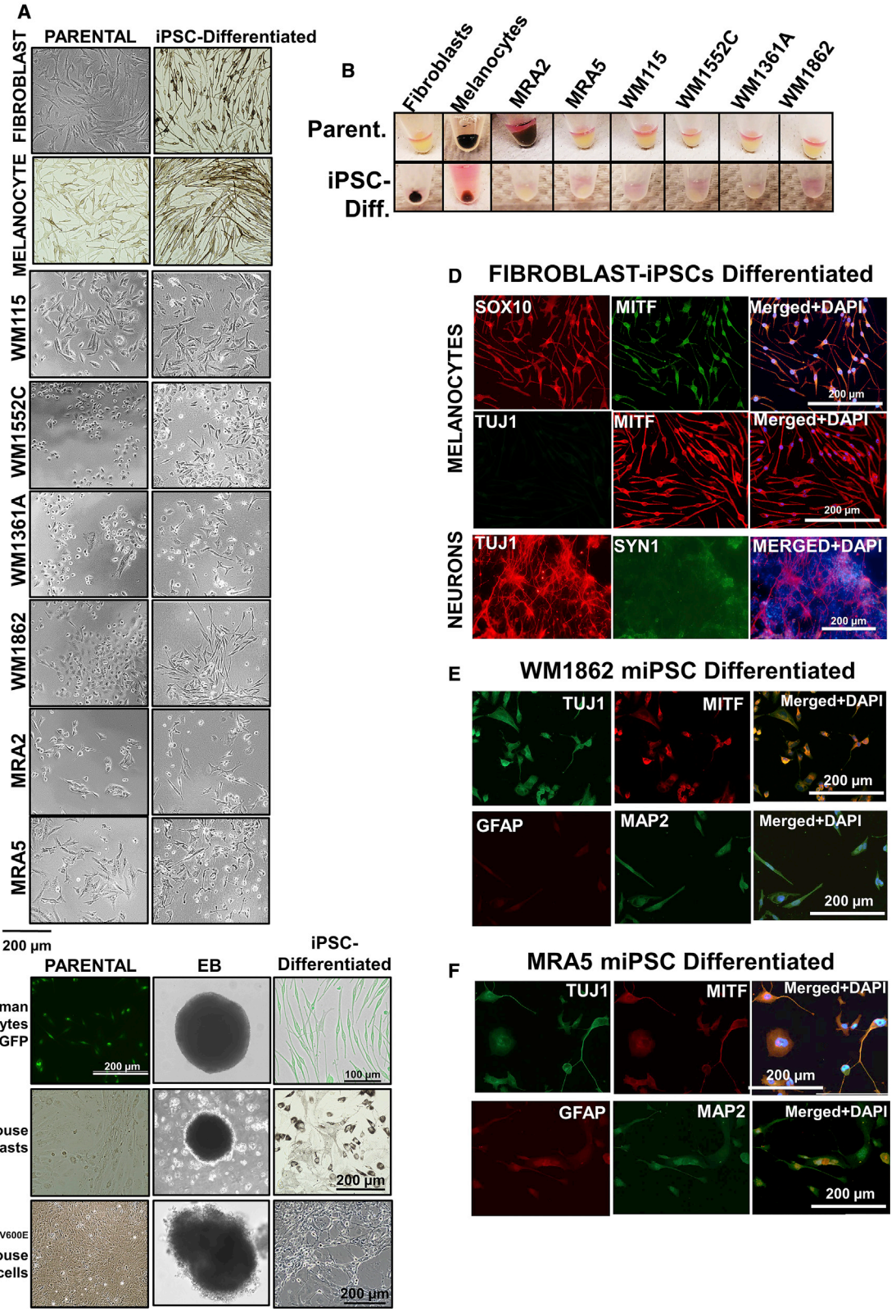

(legend on next page)

marker GFAP (Figure S6B). These data show that neuronal-directed differentiation of fibroblast-, melanocyte-, and melanoma-iPSCs generates cells with neural-like features.

We asked if neural-like dysplastic features of melanoma cells are related to their origin from cells of the neural crest/neuro-ectodermal lineage. To address this, we transduced human melanocytes with NICD-GFP and subjected these NICD-expressing cells to iPSC reprogramming. NOTCH is a neural crest marker that plays a crucial role in the development of brain and neuronal cells, and it has been implicated in melanoma and other cancers (Pinnix et al., 2009; Raafat et al., 2004; Zagouras et al., 1995). In addition, expression of NICD has been reported to induce neural crest-like reprogramming in melanocytes (Zabierowski et al., 2011a). Results showed that NICD-expressing melanocytes formed iPSC colonies that express NICD-GFP (Figure 3). NICD-expressing iPSC colonies were then subjected to EB formation and subsequently to melanocyte differentiation. Interestingly, iPSC-expressing NICD-GFP formed melanocyte-like cells (Figure 5C, top panels). These data show that NICD expression and neural crest-like state (induced by NICD) did not block reprogramming of melanocytes or (re)differentiation along melanocytic lineage in melanocyte differentiation medium.

Melanoma cells accumulate multiple mutations that may cause dysplasia and transdifferentiation (Bhat et al., 2006; Maddodi et al., 2010). We asked if neural-like dysplasia of miPSCs might also be related with oncogenic mutations. To address this question we focused on primary melanoma cells harboring $BRAF^{V600E}/Pten^{-/-}$ genotypes. We used cells isolated and cultured from $BRAF^{V600E}/Pten^{-/-}$ mouse melanoma tumors (Dankort et al., 2009) to perform iPSC reprogramming and melanocyte differentiation. As a control, we also reprogrammed mouse fibroblasts into iPSCs. Results showed that both $BRAF^{V600E}/Pten^{-/-}$ primary tumor cells and mouse fibroblasts were able to readily generate iPSC colonies and both cells formed EBs (Figure 5C, middle and bottom panels; Figure S7). EBs were subjected to melanocyte differentiation. Results showed that mouse fibroblast-iPSC produced pigmented cells with mouse melanocyte-like morphology. However, $BRAF^{V600E}/Pten^{-/-}$ mouse tumor cell-derived iPSC-generated amelanotic cells with neural-like dysplastic morphology (Figure 5C, bottom panels). These data suggest that neural-like dysplasia of melanoma-iPSCs is related to malignant transformation and activation of BRAF and loss of Pten is sufficient to block melanocyte differentiation.

miPSC-Differentiated Cells Retain Tumorigenicity and Exhibit Neural-like Dysplasia *In Vivo*

Melanocytes derived from human iPSCs, when transplanted on to nude mouse skin, produce pigmented melanocytic aggregates and express melanocyte markers (Kawakami et al., 2018). We asked whether miPSC-differentiated cells in melanocyte medium (miPSC differentiated) retain tumorigenicity and whether mouse skin environment *in vivo* induces melanocytic differentiation. For this, we selected primary WM1862 and metastatic MRA2 cell line-derived miPSCs differentiated in melanocyte medium. Both primary WM1862 and metastatic MRA2 miPSC-differentiated cells formed amelanotic tumors (Figure S5C). Western blot analysis of tumor lysates for melanocyte differentiation markers (MITF, SOX10, TYR, TYRP1, and TYRP2), neural/neural crest markers (NOTCH/NICD, PAX3, TUBB3, MAP2, and GFAP), and melanoma stem cell markers (SOX9, ALDH1, and CD271) showed a pattern of expression consistent with that observed by immunofluorescence analyses. We compared the expression of these markers in parental melanoma cells, miPSC-differentiated cells *in vitro* and tumors derived *in vivo* from miPSC-differentiated cells. Parental primary melanoma cell line WM1862 and WM1862-miPSC-differentiated cells showed weak or no expression of melanocyte markers *in vitro*, but a weak induction of these markers was noted in tumors *in vivo* (Figure S5D). Parental metastatic melanoma MRA2 cells showed strong expression of melanocyte markers TYR, TYRP1, TYRP2, and MART1 but weak expression of MITF and SOX10. However, the expression of a subset of these markers was extinguished in MRA2-miPSC-differentiated cells both *in vitro* and *in vivo*. These data suggest that miPSC-differentiated cells fail to express melanocyte markers, even when present in the cutaneous environment.

Figure 5. Melanocyte Differentiation of Fibroblast-iPSCs, Melanocyte-iPSCs, and Melanoma-iPSCs

(A) Morphology of parental and iPSCs induced to differentiate in melanocyte medium. Top–bottom: cells differentiated from fibroblast-iPSCs, melanocyte-iPSCs, and primary melanoma-iPSCs: WM115, WM1552C, WM1361A, and WM1862; and metastatic iPSCs: MRA2 and MRA5.

(B) Cell pellets from parental melanoma and miPSC-differentiated cells.

(C) Reprogramming of human melanocytes expressing NICD-GFP, mouse fibroblasts, and $BRAF^{V600}/Pten^{-/-}$ mouse tumor cells, EB formation, and melanocyte differentiation.

(D) Immunofluorescence staining of cells differentiated from fibroblast-iPSCs in melanocyte differentiation medium (top panels) and neuronal differentiation medium (bottom panels) with melanocytic markers SOX10 and MITF, and neuronal markers, TUJ1 and SYN1.

(E and F) Immunofluorescence of cells differentiated from primary WM1862 (E) and metastatic MRA5 (F) melanoma miPSCs in melanocyte differentiation medium with melanocytic marker MITF and neural markers GFAP and MAP2.

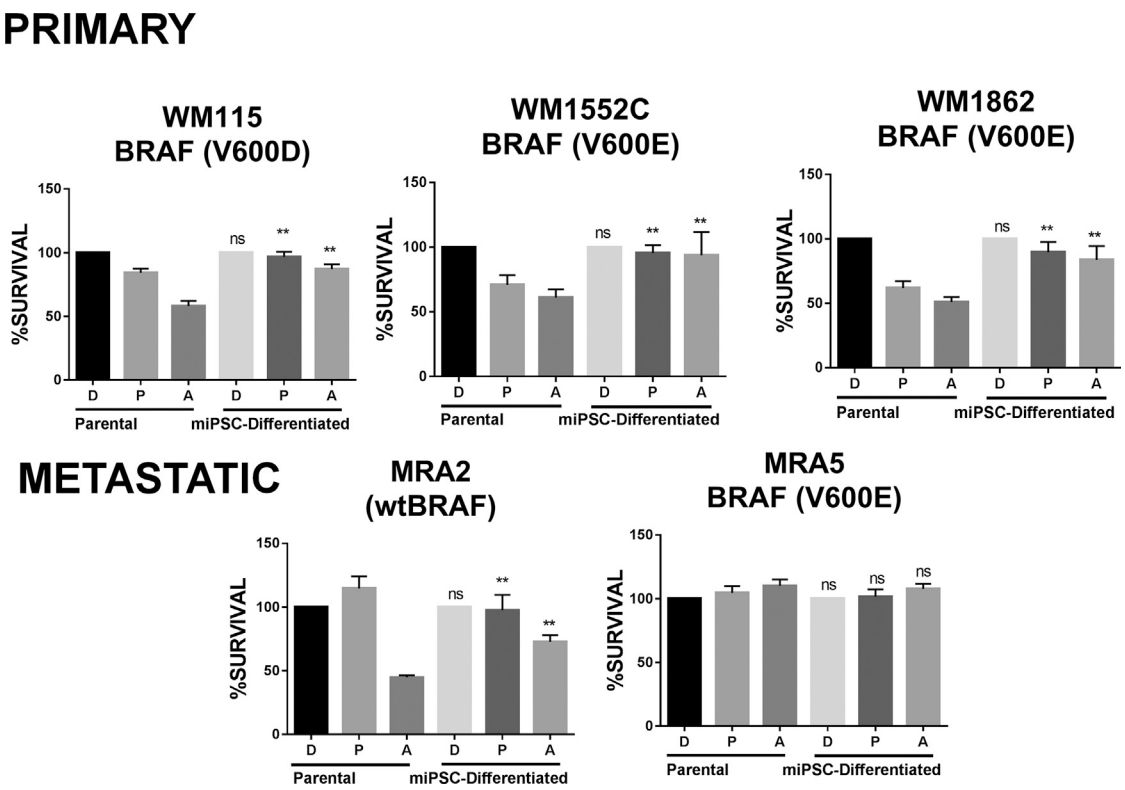

Figure 6. Acquired MAPKi Resistance in Melanoma-iPSC Differentiated Cells

Melanoma cells (parental) were reprogrammed into melanoma-iPSCs (miPSCs) and embryoid bodies generated and allowed to differentiate in melanocyte medium (miPSC differentiated). The sensitivity of parental melanoma cells and miPSC-differentiated cells to MAPKi (at previously determined half maximal inhibitory concentrations) was evaluated. Survival of each parental melanoma cell line and miPSC-differentiated cells treated with DMSO (D), PLX4032 (P) (0.5 μM), or AZD6244 (A) (0.5 μM) 72 h was estimated by MTT assay. Data (mean ± SD; n = 6–8 replicate wells/cell line) from one experiment are shown. Employing two-factor linear regression (factors cell line and parental versus induced), we tested contrasts between parental and induced cells for each drug and cell line. $^{**}p < 10^{-4}$ for all contrasts, except for MRA5 (ns, not significant).

Both primary WM1862 and metastatic MRA2 cells showed a highly similar pattern of expression of neural markers. NICD was present in WM1862 parental and WM1862-miPSC-differentiated cells and MRA2-miPSC-differentiated cells. PAX3 was present in tumors produced by both cell lines. Both cell lines retained the neuronal markers TUBB3 and MAP2 under all conditions. In MRA2 cells, TUBB3 was detected in parental pigmented cells and the miPSC-differentiated cells *in vivo* (tumor) but not *in vitro* (Figure S5B). GFAP expression was induced in tumors derived from both WM1862 and MRA2 miPSC-differentiated cells.

Skin stem cell marker SOX9 and melanoma stem cell markers ALDH1 and CD271 were present only *in vivo* (tumors). These data suggest that miPSC-derived cells display mixed dysplastic features of neural crest-, neural-, melanocyte-, and melanoma stem cell-like differentiation. However, while weak expression of melanocyte markers is retained, strong expression of neural crest, neural, and melanoma/stem cell markers are retained throughout the reprogramming and differentiation.

miPSC-Differentiated Cells Exhibit Acquired Resistance to MAPK Inhibition

Next, we asked whether $BRAF^{V600E}$ mutant miPSC-differentiated cells retain sensitivity to BRAFi PLX4032/vemurafenib and MEKi AZD6244/selumetinib. Based on the half maximal inhibitory concentration of the parental metastatic MRA5 and MRA6 melanoma cell lines (Rodríguez et al., 2017), we evaluated whether miPSC-differentiated cells are also sensitive to concentration of MAPKi inhibitors that kill parental cells. As shown in Figure 6, both primary and metastatic melanoma parental cells were sensitive to MEKi AZD6244 and parental cells with $BRAF^{V600E}$ mutation were sensitive to killing by PLX4032. However, miPSC differentiated in melanocyte medium (miPSC differentiated) showed resistance to killing. MRA5 is intrinsically resistant to both drugs and MRA5-miPSC-differentiated

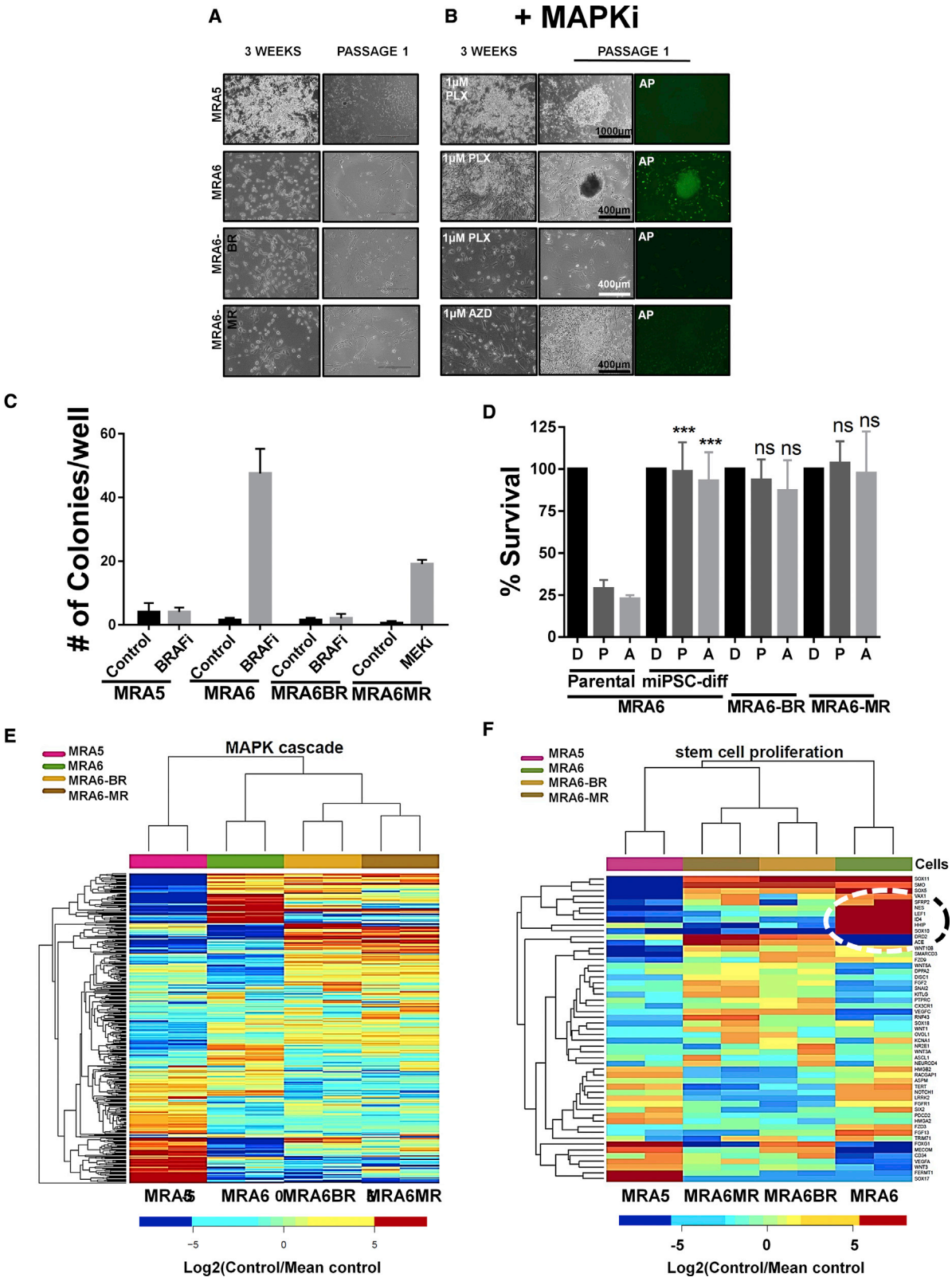

(legend on next page)

cells remain resistant to both inhibitors similar to the parental MRA5 cells.

Resistance to MAPK Inhibitors Correlates with Loss of Plasticity for Reprogramming

We investigated whether MAPKi resistance is related to reprogramming to the iPSC-like state. We selected two $BRAF^{V600E}$ melanoma cell lines—MRA5 shows intrinsic resistance to both BRAFi and MEKi, and MRA6 is sensitive to both drugs. We also generated two MAPKi-resistant cell lines from MRA6: MRA6BR and MRA6MR, which are resistant, respectively, to BRAFi and MEKi (Rodríguez et al., 2017). Data showed that addition of BRAFi during reprogramming significantly increased the efficiency of reprogramming of BRAFi-sensitive MRA6 cells to iPSC-like cells (Figures 7A–7C). In contrast, intrinsically MAPKi-resistant MRA5 and MRA6BR cells that acquired resistance to BRAFi did not yield iPSC colonies even in the presence of BRAFi. Although MEKi also enhanced the plasticity of MAR6MR cells into stem cell state, the colonies did not exhibit iPSC-like morphology or express the stem cell marker AP and did not survive beyond passage 2. These results suggest that treatment of $BRAF^{V600E}$ mutant melanoma with BRAFi can enhance their plasticity to activate pluripotent stem cell-like state, whereas $BRAF^{V600E}$ mutant melanomas that are intrinsically resistant or have acquired resistance to BRAFi are refractory to the effects of BRAFi on their plasticity. MRA6-derived miPSC-differentiated cells in melanocyte differentiation medium did not generate melanocytes and showed acquired resistance to both BRAFi and MEKi, similar to MRA6BR and MRA6MR cells, respectively (Figure 7D).

Acquired resistance to MAPKi and recurrence of highly aggressive melanoma are known to be associated with stem cell pathways (Roesch et al., 2010). We asked whether the difference in plasticity (to reprogramming to the iPSC-like state) between MAPKi-sensitive and -resistant cells could be related to differences in the elaboration of oncogenic MAPK and stem cell pathway gene expression programs. Whole transcriptome RNA sequencing analysis showed that gene expression profiles for MAPKi-resistant and MAPKi-sensitive cells were distinct. Figures 7E and 7F show that stem cell proliferation and MAPK cascade genes are the most significantly differentially expressed genes. MAPKi-sensitive MRA6 cells show higher expression levels of stem cell proliferation genes including SOX10, HHIP, ID4, and LEF1, genes related to growth and development including TGFA, GFRA1, and FGF13 compared with MAPKi-resistant cells (Figures 7E and 7F). These data suggest that oncogenic MAPK signaling restricts the plasticity of melanoma cells (for iPSC-like reprogramming) and that this inhibitory effect can be overcome by inhibition of the MAPK pathway.

DISCUSSION

In this study we investigated the plasticity of melanocytes and melanoma cells for reprogramming to iPSCs and differentiation into melanocytes. We show that expression of oncogenic $BRAF^{V600E}$ inhibits the plasticity of melanocytes and that pharmacological inhibition of $BRAF^{V600E}$ promotes the reprogramming of melanoma cells. These observations are consistent with previous reports that showed that oncogene c-Jun inhibited reprogramming of somatic cells (Liu et al., 2015).

Limited plasticity of melanoma cells to iPSC reprogramming appears to correlate with tumor progression. Reprogramming of genetically matched primary and metastatic melanoma cells from the same patient showed that metastatic cells are more resistant to reprogramming, suggesting that accumulated mutations in melanoma cells during tumor progression inhibit plasticity (Bozic et al., 2010). We noted that metastatic cells refractory to reprogramming also exhibited high senescence and limited survival and proliferation on iPSC reprogramming, consistent with

Figure 7. Resistance to MAPKi Inhibits Reprogramming of $BRAF^{V600E}$ Mutant Cells

(A) Morphology of BRAF mutant cells during reprogramming. Intrinsically MAPKi-resistant MRA5, MAPKi-sensitive MRA6, cells with acquired resistance to BRAFi (MRA6BR), and MEKi (MRA6MR) at 3 weeks post-iPSC induction and at passage 1 in the absence of MAPKi.

(B) Reprogramming in the absence or presence of BRAFi (for MRA5, MRA6, and MRA6BR) and MEKi (for MRA6MR).

(C) Quantitation of iPSC reprogramming shows number of colonies generated. Data (mean ± SD; n = 6 replicate well/cell line) from one experiment are shown.

(D) miPSC-differentiated cells from MAPKi-sensitive MRA6 cells show acquired resistance to BRAFi and MEKi. Survival (MTT assays) of MRA6 (MAPKi sensitive) parental melanoma cells, MRA6-miPSC-differentiated cells in melanocyte medium, MRA6BR and MRA6MR treated with DMSO (D), PLX4032 (P, 0.5 μM), or AZD6244 (A, 0.5 μM) for 72 h. Data (mean ± SD; n = 6–8 replicate wells/cell line) shown are from one experiment. Student's t test for parental versus differentiated (D versus D, ns, not significant; P versus P, ***p = 0.0006; A versus A, ***p = 0.0010). No significant difference was noted in MRA6-miPSC-differentiated cells compared with MRA6BR and MRA6MR cell lines.

(E and F) RNA sequencing differential expression data for genes in $BRAF^{V600E}$ mutant MAPKi-resistant (MRA5, MRA6BR, and MRA6MR) and MAPKi-sensitive (MRA6) cells. (E) MAPK Cascade (GO: 0000165) 177 genes with highest marginal variance. (F) Stem Cell Proliferation (GO: 0072089) top 24 genes with highest marginal variance.

previous reports that showed that senescence and proliferation affected reprogramming *in vitro* an *in vivo* (Banito et al., 2009; Mosteiro et al., 2016). A limitation of these studies is that these cell lines used were propagated in culture. However, freshly isolated cells from primary melanoma tumors are often difficult to acquire due to the size of the excised lesions and medico-legal requirements of diagnostic pathology.

miPSCs exhibited stem cell-like features including expression of stem cell markers and ability to differentiate into three germ layers. More interestingly, miPSCs were more amenable to differentiate along neural dysplastic lineages than melanocytic lineage both *in vitro* and *in vivo*. Dedifferentiation is thought to be a hallmark of melanocytic neoplasms, which often resemble various stages of their embryonic development. Dedifferentiation also appears to influence the sensitivity of melanocytic neoplasms to drugs (Tsoi et al., 2018). Cutaneous melanocytic neoplasms are also known to acquire variable characteristics of neural and other neural crest derivatives (Fang et al., 2001; Iyengar and Singh, 2010). Skin stem cells also express neural crest markers and exhibit similarities with melanoma cells including self-renewal and differentiation into multiple neural crest lineages (Zabierowski et al., 2011b).

Expression of active NOTCH (NICD) was shown to be sufficient to reprogram melanocytes into neural crest-like state (Zabierowski et al., 2011a). Our data show that expression of NICD did not block iPSC reprogramming of melanocytes and their ability to redifferentiate to melanocytes. These data suggest that lack of melanocyte differentiation and patterns of neural crest- and neural-like dysplasia of melanoma-iPSCs could not be explained by their origin from neural crest lineage but may be related to de-differentiation/transdifferentiation of melanocytes during malignant transformation. Resetting of melanoma cells by iPSC reprogramming, however, does not restore the melanocytic program disrupted by oncogenic mutations but generates neural-like dysplasia. Consistent with this notion, we previously reported that expression of oncogenic $BRAF^{V600E}$ induces the expression of neuronal marker MAP2 in melanoma cells (Bhat et al., 2006; Maddodi et al., 2010). Another possibility, however, is that different oncogenic mutations might induce different patterns of plasticity such as neuronal, glial, or neural crest lineages. For example, neuronal differentiation from MRA2-miPSCs, which harbor wild-type BRAF but loss of PTEN showed neural-like dysplasia with strong expression of glial cell marker GFAP in neural-directed differentiation. Intriguingly, glial cell precursors from cutaneous innervation were reported to serve as a source of melanocytes in the skin (Adameyko et al., 2009).

Furthermore, the different patterns of lineage marker expression of miPSC-differentiated cells could also be related to clinical and histological subtypes of cutaneous melanoma. Detailed clinical and histopathological studies have grouped melanocytic neoplasms into distinct categories based on association with chronic sun damage and their anatomical location; however, it is not known whether these histologically distinct lesions all arise from melanocytes at the same stage in the melanocytic lineage differentiation, i.e., skin-resident precursors with neural crest-like features, melanocyte stem cells, melanoblasts, or terminally differentiated melanocyte (Grichnik et al., 2014; Kulesa et al., 2006; Yu et al., 2010). Recent studies employing $BRAF^{V600E}$ models of mouse melanoma showed that UVB-induced melanocytic neoplasms can originate in the hair-bearing skin from melanocyte stem cells (Moon et al., 2017), whereas non-UV-induced lesions arise in the interfollicular tail from mature differentiated pigment producing melanocytes, but not from dormant amelanotic melanocytes or melanocyte stem cells from the hair follicle bulge (Köhler et al., 2017). These *in vivo* mouse models, although elegant and powerful, have limitations when extrapolated to human melanocytic neoplasms. For example, they are limited to $BRAF^{V600E}$-driven melanomas and do not fully recapitulate the characteristic subtypes and spectrum of histological presentations in human melanomas. In this context, our observations on the differences in plasticity of primary and metastatic human melanoma cells suggest iPSC reprogramming of melanoma cells is a useful model to understand the origin and progression of melanocytic neoplasms. It is of interest to investigate whether the plasticity of miPSCs to differentiate to neural-like dysplastic cells reflects the cell of origin, i.e., differentiated melanocytes and melanocytic stem cells versus precursors of neural crest-derived melanocytic precursors (Yu et al., 2010).

Resistance to BRAFi and MEKi appears to limit the plasticity of melanoma cells into stem cell state. Although cells sensitive to BRAFi expressed higher levels of stem cell proliferation and growth/development-related genes than MAPKi-resistant cells, constitutive activation of the MAPK pathway appears to block reprogramming of MAPKi-sensitive cells, whereas plasticity for reprogramming is unlocked on inhibition of oncogenic BRAF. However, once cells acquire MAPKi resistance, expression of stem cell marker expression is diminished and the cells are less susceptible to reprogramming. BRAFi did not restore plasticity in the MAPKi-resistant cells. In addition, cells differentiated from melanoma-iPSCs in melanocyte differentiation medium exhibited decreased sensitivity to BRAFi and MEKi. Our results are consistent with published data (Bernhardt et al., 2017) and suggest that miPSC-differentiated cells are less dependent on MAPK signaling for survival and proliferation.

Reprogramming of melanoma cells into a stem cell state facilitated by BRAFi (PLX4032) in cells sensitive to BRAFi

could serve as a novel strategy to uncover mechanisms of acquired resistance related to cellular plasticity. After reprogramming and differentiation in melanocyte differentiation medium, sensitive cells become resistance to BRAFi. BRAFi-sensitive cells exhibit a stem cell expression signature with oncogenic MAPK cascade, but are not able to reprogram unless BRAFi is added during reprogramming. We suggest that, in patients with melanoma, BRAFi might modulate the expression of stem cell genes involved in melanoma plasticity, transdifferentiation, and acquired resistance through stem cell pathways, and such genes might be targets for overcoming therapy resistance.

EXPERIMENTAL PROCEDURES

Cell Culture

Primary fibroblasts and melanocytes were isolated from human neonatal foreskins in the UW-Skin Disease Research Center. All primary and metastatic cells of the WM series were obtained from Rockland Immunochemicals (Limerick, PA). MRA series of metastatic melanoma cell lines were established and genotyped for BRAF and RAs mutations at UW-Madison by Dr. Mark Albertini. Human primary fibroblasts, all melanoma cells, and mouse tumor cells were cultured in DMEM, 10% fetal bovine serum (FBS), and 1% penicillin and streptomycin (PenStrep). Human melanocytes were cultured in 254 basal media containing HMGS2. MEFs were obtained from WiCell Research Institute and plated following their protocol recommendations. All cells were cultured in a humid incubator at 37°C with 5% CO_2 and regularly tested for mycoplasma. Isolation and use of human cells was approved by appropriate institutional review committees.

Reprogramming of iPSCs and AP Live Staining

Five days after… transduction with three reprogramming lentiviruses, cells were plated on six-well plates with MEF feeders (WiCell Research Institute) with stem cell reprogramming medium (KO DMEM, 20% KOSR, 1% GlutaMAX, 1% NEAA, 1% PenStrep, 10 ng/mL basic fibroblast growth factor [bFGF], 2×10^{-4} M of 2-mercaptoethanol) at a density of 2×10^4 cells per well of six-well plates. A cocktail of up to five chemicals was used for reprogramming melanoma cells including FSK (10 μM), VPA (500 μM), CHIR99021 (10 μM), RepSox (5 μM), and TCP (5 μM). Medium was replaced every 3–4 days for 3 weeks. After 3 weeks, colonies were passaged using Versene on fresh MEFs every 2 weeks with maintenance stem cell medium, which is the same as reprogramming but supplemented with 4 ng/mL bFGF, CHIR99021 (3 μM), and PD0325901 (1 μM). AP live staining (Thermo Fisher Scientific, no. A14353) was performed after 3 weeks of reprogramming and after 2 weeks in passage 1 according to the manufacturer's protocol.

EB Formation, and Melanocyte and Neuronal Differentiation

EBs and melanocyte differentiation were performed as reported (Ohta et al., 2011; Yang et al., 2011) with modifications. Neuronal differentiation was performed essentially as reported (Bernhardt et al., 2017) (Supplemental Experimental Procedures).

MTT Assays

miPSC-differentiated cells were first expanded in DMEM, 10% FBS, and 1% PenStrep for 2 weeks and passed at least 5 times. For MTT assays, 4,000 cells/well were plated on 96-well plates with DMEM, 10% FBS, and 1% PenStrep and incubated at 37°C overnight, and, the next day, medium was replaced with medium containing 0.5 μM of PLX4032 or AZD6244 inhibitors for 72 h. The absorbance was read at 540 nm after adding 20 μL of a 5-mg/mL MTT dye solution at 37°C for 45 min.

RNA Sequencing and Transcriptome Analysis

Cells were plated on six-well plates and, after 24 h, RNA samples were collected and purified using the miRNeasy Mini Kit (no. 217004, QIAGEN). Samples were then sent for sequencing at Sanford Burnham Prebys Medical Discovery Institute, Orlando, FL. Transcriptome data were deposited at NCBI (accession no. GEO: GSE110179). Data were analyzed as described in Supplemental Experimental Procedures using RSEM (Li et al., 2010) for abundance estimation and EBSeq (Leng et al., 2013) for differential expression analysis.

Statistical Analysis

Statistical analyses were performed using GraphPad Prism 7 and R. Student's unpaired t test was performed for significance studies with a 95% confidence interval ($p < 0.05$). For the data on drug resistance of miPSCs, we employed two-factor linear regression (factors cell line and parental versus induced) and we tested contrasts between parental and induced cells for each drug and cell line.

SUPPLEMENTAL INFORMATION

Supplemental Information can be found online at https://doi.org/10.1016/j.stemcr.2019.05.018.

AUTHOR CONTRIBUTIONS

V.S. and E.C.-P. designed the study. E.C.-P performed all the experiments. C.I.R. characterized the MRA cell lines and generated MAPKi-resistant cells. D.M. produced BRAF(V600E) and NICD lentiviruses and contributed to mouse melanoma cell line experiments. S.S. and A.M. assisted E.C.-P. with cell culture experiments, microscopy, and ImageJ. M.A.N. performed statistical analyses. V.S. and E.C.-P. wrote the manuscript with input from M.A.N.

ACKNOWLEDGMENTS

This work was supported in part by Department of Defense grant W81XWH-15-1-0529 and VA Merit Award 1 I01 BX002623 and NIH/NIAMS grant P30AR066524 to V.S. M.A.N. was supported in part by the Biostatistics Shared Resource of the UWCCC, P30CA014520-41. We thank Dr. Igor Slukvin for critical reading of the manuscript and comments and suggestions.

Received: July 31, 2018
Revised: May 16, 2019
Accepted: May 17, 2019
Published: June 20, 2019

REFERENCES

Adameyko, I., Lallemend, F., Aquino, J.B., Pereira, J.A., Topilko, P., Müller, T., Fritz, N., Beljajeva, A., Mochii, M., Liste, I., et al. (2009). Schwann cell precursors from nerve innervation are a cellular origin of melanocytes in skin. Cell *139*, 366–379.

Banito, A., Rashid, S.T., Acosta, J.C., Li, S., Pereira, C.F., Geti, I., Pinho, S., Silva, J.C., Azuara, V., Walsh, M., et al. (2009). Senescence impairs successful reprogramming to pluripotent stem cells. Genes Dev. *23*, 2134–2139.

Bernhardt, M., Novak, D., Assenov, Y., Orouji, E., Knappe, N., Weina, K., Reith, M., Larribere, L., Gebhardt, C., Plass, C., et al. (2017). Melanoma-derived iPCCs show differential tumorigenicity and therapy response. Stem Cell Reports *8*, 1379–1391.

Bhat, K.M., Maddodi, N., Shashikant, C., and Setaluri, V. (2006). Transcriptional regulation of human MAP2 gene in melanoma: role of neuronal bHLH factors and Notch1 signaling. Nucleic Acids Res. *34*, 3819–3832.

Bozic, I., Antal, T., Ohtsuki, H., Carter, H., Kim, D., Chen, S., Karchin, R., Kinzler, K.W., Vogelstein, B., and Nowak, M.A. (2010). Accumulation of driver and passenger mutations during tumor progression. Proc. Natl. Acad. Sci. U S A *107*, 18545–18550.

Chao, M.P., Gentles, A.J., Chatterjee, S., Lan, F., Reinisch, A., Corces, M.R., Xavy, S., Shen, J., Haag, D., Chanda, S., et al. (2017). Human AML-iPSCs reacquire leukemic properties after differentiation and model clonal variation of disease. Cell Stem Cell *20*, 329–344.e7.

Choi, H.S., Kim, W.T., and Ryu, C.J. (2014). Antibody approaches to prepare clinically transplantable cells from human embryonic stem cells: identification of human embryonic stem cell surface markers by monoclonal antibodies. Biotechnol. J. *9*, 915–920.

Dankort, D., Curley, D.P., Cartlidge, R.A., Nelson, B., Karnezis, A.N., Damsky, W.E., You, M.J., DePinho, R.A., McMahon, M., and Bosenberg, M. (2009). Braf(V600E) cooperates with Pten loss to induce metastatic melanoma. Nat. Genet. *41*, 544–552.

Deshpande, A., Yadav, S., Dao, D.Q., Wu, Z.Y., Hokanson, K.C., Cahill, M.K., Wiita, A.P., Jan, Y.N., Ullian, E.M., and Weiss, L.A. (2017). Cellular phenotypes in human iPSC-derived neurons from a genetic model of autism spectrum disorder. Cell Rep. *21*, 2678–2687.

Dhomen, N., Reis-Filho, J.S., da Rocha Dias, S., Hayward, R., Savage, K., Delmas, V., Larue, L., Pritchard, C., and Marais, R. (2009). Oncogenic Braf induces melanocyte senescence and melanoma in mice. Cancer Cell *15*, 294–303.

Fang, D., Hallman, J., Sangha, N., Kute, T.E., Hammarback, J.A., White, W.L., and Setaluri, V. (2001). Expression of microtubule-associated protein 2 in benign and malignant melanocytes: implications for differentiation and progression of cutaneous melanoma. Am. J. Pathol. *158*, 2107–2115.

Grichnik, J.M., Ross, A.L., Schneider, S.L., Sanchez, M.I., Eller, M.S., and Hatzistergos, K.E. (2014). How, and from which cell sources, do nevi really develop? Exp. Dermatol. *23*, 310–313.

Herlyn, M., Balaban, G., Bennicelli, J., Guerry, D., Halaban, R., Herlyn, D., Elder, D.E., Maul, G.G., Steplewski, Z., and Nowell, P.C. (1985). Primary melanoma cells of the vertical growth phase: similarities to metastatic cells. J. Natl. Cancer Inst. *74*, 283–289.

Hodis, E., Watson, I.R., Kryukov, G.V., Arold, S.T., Imielinski, M., Theurillat, J.P., Nickerson, E., Auclair, D., Li, L., Place, C., et al. (2012). A landscape of driver mutations in melanoma. Cell *150*, 251–263.

Hou, P., Li, Y., Zhang, X., Liu, C., Guan, J., Li, H., Zhao, T., Ye, J., Yang, W., Liu, K., et al. (2013). Pluripotent stem cells induced from mouse somatic cells by small-molecule compounds. Science *341*, 651–654.

Iyengar, B., and Singh, A.V. (2010). Patterns of neural differentiation in melanomas. J. Biomed. Sci. *17*, 87.

Kawakami, T., Okano, T., Takeuchi, S., Osumi, K., Soma, Y., Itoh, M., Hirobe, T., and Jimbow, K. (2018). Approach for the derivation of melanocytes from induced pluripotent stem cells. J. Invest. Dermatol. *138*, 150–158.

Kemper, K., de Goeje, P.L., Peeper, D.S., and van Amerongen, R. (2014). Phenotype switching: tumor cell plasticity as a resistance mechanism and target for therapy. Cancer Res. *74*, 5937–5941.

Köhler, C., Nittner, D., Rambow, F., Radaelli, E., Stanchi, F., Vandamme, N., Baggiolini, A., Sommer, L., Berx, G., van den Oord, J.J., et al. (2017). Mouse cutaneous melanoma induced by mutant BRaf arises from expansion and dedifferentiation of mature pigmented melanocytes. Cell Stem Cell *21*, 679–693.e6.

Kulesa, P.M., Kasemeier-Kulesa, J.C., Teddy, J.M., Margaryan, N.V., Seftor, E.A., Seftor, R.E., and Hendrix, M.J. (2006). Reprogramming metastatic melanoma cells to assume a neural crest cell-like phenotype in an embryonic microenvironment. Proc. Natl. Acad. Sci. U S A *103*, 3752–3757.

Leng, N., Dawson, J.A., Thomson, J.A., Ruotti, V., Rissman, A.I., Smits, B.M., Haag, J.D., Gould, M.N., Stewart, R.M., and Kendziorski, C. (2013). EBSeq: an empirical Bayes hierarchical model for inference in RNA-seq experiments. Bioinformatics *29*, 1035–1043.

Li, B., Ruotti, V., Stewart, R.M., Thomson, J.A., and Dewey, C.N. (2010). RNA-Seq gene expression estimation with read mapping uncertainty. Bioinformatics *26*, 493–500.

Liu, J., Han, Q., Peng, T., Peng, M., Wei, B., Li, D., Wang, X., Yu, S., Yang, J., Cao, S., et al. (2015). The oncogene c-Jun impedes somatic cell reprogramming. Nat. Cell Biol. *17*, 856–867.

Maddodi, N., Bhat, K.M., Devi, S., Zhang, S.C., and Setaluri, V. (2010). Oncogenic BRAFV600E induces expression of neuronal differentiation marker MAP2 in melanoma cells by promoter demethylation and down-regulation of transcription repressor HES1. J. Biol. Chem. *285*, 242–254.

Michaloglou, C., Vredeveld, L.C., Soengas, M.S., Denoyelle, C., Kuilman, T., van der Horst, C.M., Majoor, D.M., Shay, J.W., Mooi, W.J., and Peeper, D.S. (2005). BRAFE600-associated senescence-like cell cycle arrest of human naevi. Nature *436*, 720–724.

Moon, H., Donahue, L.R., Choi, E., Scumpia, P.O., Lowry, W.E., Grenier, J.K., Zhu, J., and White, A.C. (2017). Melanocyte stem

cell activation and translocation initiate cutaneous melanoma in response to UV exposure. Cell Stem Cell *21*, 665–678.e6.

Mosteiro, L., Pantoja, C., Alcazar, N., Marión, R.M., Chondronasiou, D., Rovira, M., Fernandez-Marcos, P.J., Muñoz-Martin, M., Blanco-Aparicio, C., Pastor, J., et al. (2016). Tissue damage and senescence provide critical signals for cellular reprogramming in vivo. Science *354*. https://doi.org/10.1126/science.aaf4445.

Ohta, S., Imaizumi, Y., Okada, Y., Akamatsu, W., Kuwahara, R., Ohyama, M., Amagai, M., Matsuzaki, Y., Yamanaka, S., Okano, H., et al. (2011). Generation of human melanocytes from induced pluripotent stem cells. PLoS One *6*, e16182.

Pinnix, C.C., Lee, J.T., Liu, Z.J., McDaid, R., Balint, K., Beverly, L.J., Brafford, P.A., Xiao, M., Himes, B., Zabierowski, S.E., et al. (2009). Active Notch1 confers a transformed phenotype to primary human melanocytes. Cancer Res. *69*, 5312–5320.

Raafat, A., Bargo, S., Anver, M.R., and Callahan, R. (2004). Mammary development and tumorigenesis in mice expressing a truncated human Notch4/Int3 intracellular domain (h-Int3sh). Oncogene *23*, 9401–9407.

Rodríguez, C.I., Castro-Pérez, E., Prabhakar, K., Block, L., Longley, B.J., Wisinski, J.A., Kimple, M.E., and Setaluri, V. (2017). EPAC-RAP1 axis-mediated switch in the response of primary and metastatic melanoma to cyclic AMP. Mol. Cancer Res. *15*, 1792–1802.

Roesch, A., Fukunaga-Kalabis, M., Schmidt, E.C., Zabierowski, S.E., Brafford, P.A., Vultur, A., Basu, D., Gimotty, P., Vogt, T., and Herlyn, M. (2010). A temporarily distinct subpopulation of slow-cycling melanoma cells is required for continuous tumor growth. Cell *141*, 583–594.

Roesch, A., Paschen, A., Landsberg, J., Helfrich, I., Becker, J.C., and Schadendorf, D. (2016). Phenotypic tumour cell plasticity as a resistance mechanism and therapeutic target in melanoma. Eur. J. Cancer *59*, 109–112.

Shinozawa, T., Nakamura, K., Shoji, M., Morita, M., Kimura, M., Furukawa, H., Ueda, H., Shiramoto, M., Matsuguma, K., Kaji, Y., et al. (2017). Recapitulation of clinical individual susceptibility to drug-induced QT prolongation in healthy subjects using iPSC-derived cardiomyocytes. Stem Cell Reports *8*, 226–234.

Suknuntha, K., Ishii, Y., Tao, L., Hu, K., McIntosh, B.E., Yang, D., Swanson, S., Stewart, R., Wang, J.Y., Thomson, J., et al. (2015). Discovery of survival factor for primitive chronic myeloid leukemia cells using induced pluripotent stem cells. Stem Cell Res. *15*, 678–693.

Tsoi, J., Robert, L., Paraiso, K., Galvan, C., Sheu, K.M., Lay, J., Wong, D.J.L., Atefi, M., Shirazi, R., Wang, X., et al. (2018). Multi-stage differentiation defines melanoma subtypes with differential vulnerability to drug-induced iron-dependent oxidative stress. Cancer Cell *33*, 890–904.e5.

Yang, R., Jiang, M., Kumar, S.M., Xu, T., Wang, F., Xiang, L., and Xu, X. (2011). Generation of melanocytes from induced pluripotent stem cells. J. Invest. Dermatol. *131*, 2458–2466.

Yu, H., Kumar, S.M., Kossenkov, A.V., Showe, L., and Xu, X. (2010). Stem cells with neural crest characteristics derived from the bulge region of cultured human hair follicles. J. Invest. Dermatol. *130*, 1227–1236.

Zabierowski, S.E., Baubet, V., Himes, B., Li, L., Fukunaga-Kalabis, M., Patel, S., McDaid, R., Guerra, M., Gimotty, P., Dahmane, N., et al. (2011a). Direct reprogramming of melanocytes to neural crest stem-like cells by one defined factor. Stem Cells *29*, 1752–1762.

Zabierowski, S.E., Fukunaga-Kalabis, M., Li, L., and Herlyn, M. (2011b). Dermis-derived stem cells: a source of epidermal melanocytes and melanoma? Pigment Cell Melanoma Res. *24*, 422–429.

Zagouras, P., Stifani, S., Blaumueller, C.M., Carcangiu, M.L., and Artavanis-Tsakonas, S. (1995). Alterations in Notch signaling in neoplastic lesions of the human cervix. Proc. Natl. Acad. Sci. U S A *92*, 6414–6418.